Prostor
kraj
čas
20

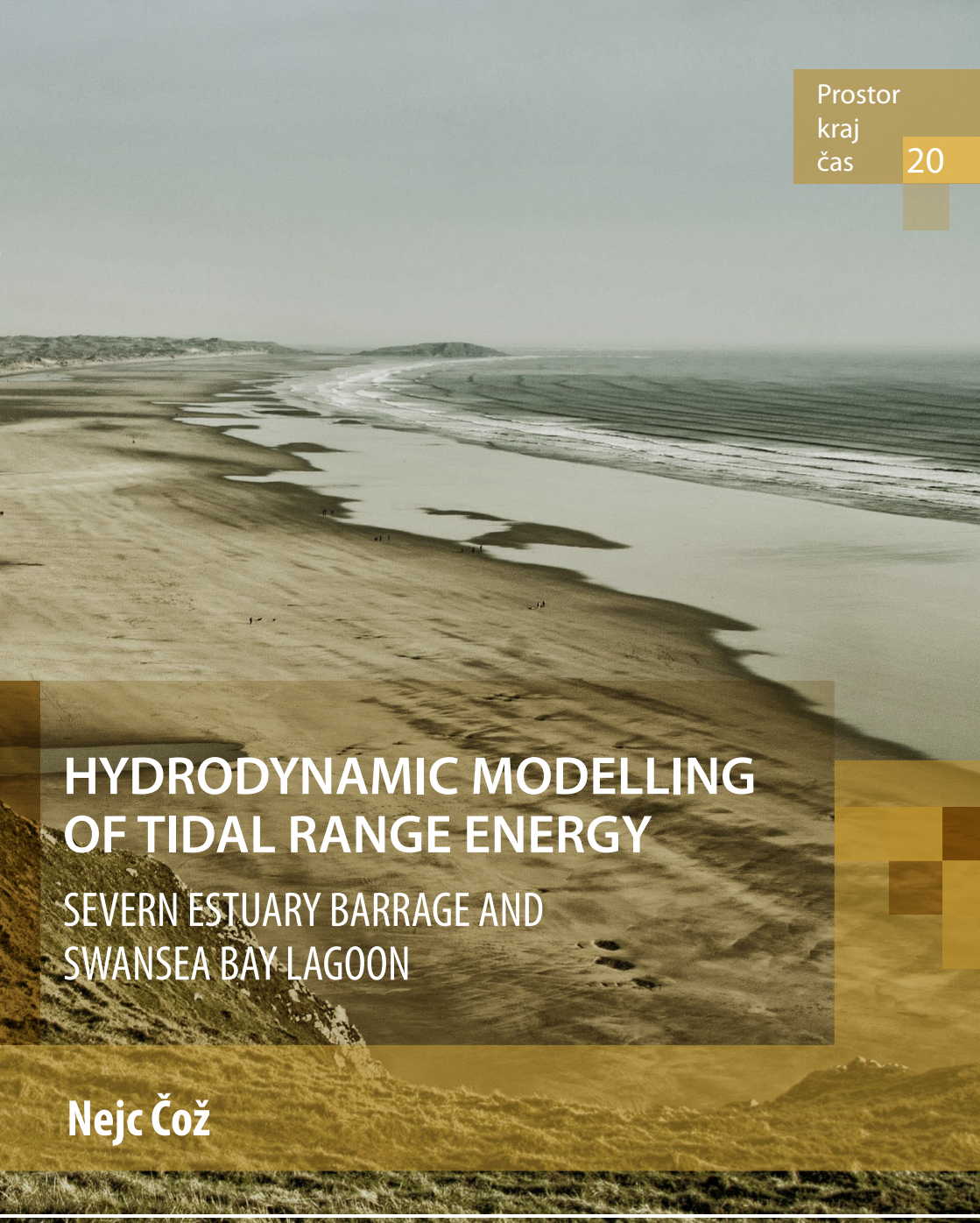

HYDRODYNAMIC MODELLING OF TIDAL RANGE ENERGY

SEVERN ESTUARY BARRAGE AND SWANSEA BAY LAGOON

Nejc Čož

HYDRODYNAMIC MODELLING OF TIDAL RANGE ENERGY: SEVERN ESTUARY BARRAGE AND SWANSEA BAY LAGOON

Nejc Čož

Ljubljana 2023

PROSTOR, KRAJ, ČAS 20

HYDRODYNAMIC MODELLING OF TIDAL RANGE ENERGY: SEVERN ESTUARY BARRAGE AND SWANSEA BAY LAGOON

Nejc Čož

Edited by: Žiga Kokalj and Nataša Gregorič Bon
Reviewed by: Gašper Rak and Nejc Bezak
Design and layout: iOK, Izven okvirjev, svetovanje in razvoj, Žiga Kokalj, s.p.

Issued by: ZRC SAZU, Institute of Anthropological and Spatial Studies
For the issuer: Ivan Šprajc
Publisher: Založba ZRC
Represented by: Oto Luthar
Editor-in-chief: Aleš Pogačnik

First edition.
Ljubljana, 2023

The cover photo is from the author's personal archive.

The author acknowledges the financial support from the Slovenian Research Agency (research core funding Earth Observation and geoinformatics (No. P2-0406) and through the call for publishing scientific monographs in 2022).

Kataložni zapis o publikaciji (CIP) pripravili v Narodni in univerzitetni knjižnici v Ljubljani.

COBISS.SI-ID 139094275
ISBN 978-961-05-0710-9 (PDF)

Nejc Čož

HYDRODYNAMIC MODELLING OF TIDAL RANGE ENERGY:

SEVERN ESTUARY BARRAGE AND SWANSEA BAY LAGOON

Založba ZRC

HYDRODYNAMIC MODELLING OF TIDAL RANGE ENERGY: SEVERN ESTUARY BARRAGE AND SWANSEA BAY LAGOON

Nejc Čož

Abstract

Hydrodynamic modelling has an important role in the development of Tidal Range Energy Structures (TRS). The aim of this research study was to develop a methodology for the simulation of TRS with Delft3D software. The study has focused on two key issues of the regional–scale hydrodynamic models. Firstly, the majority of studies before the year 2016 have ignored the conservation of momentum of the flow through the hydraulic structures. Secondly, 3D hydrostatic models have been largely underused in TRS simulations to date. The first key objective was to develop a TRS module for Delft3D software. The case study of Severn Barrage was used for validation. Direct comparisons with the past studies showed good agreement between the results, confirming the appropriateness of the developed model. The second key objective was to introduce a novel approach for the treatment of momentum transfer through hydraulic structures. This was achieved by representing the momentum of the discharged water as an additional external force in the momentum equation. The final key objective was to apply the developed method to a regional-scale model of a tidal lagoon. The Swansea Bay lagoon case study showed that momentum conservation only affected the area close to the structure. The results were found to be sensitive to the vertical velocity profile of the jet. Extending the 2D model to 3D was found to be more important for the estimation of local bed shear stress, than for predicting the velocity field. The 3D simulations did slightly improve the accuracy of the velocity field, but more importantly, they have produced a more realistic vertical velocity profile. The 3D model can capture the attachment of the jets to the bottom surface, distorting the standard logarithmic profile assumed in depth-averaged shallow water flows. In general, the 2D model with momentum conservation was found to be sufficient for analysing hydrodynamics in most cases. However, the 3D model has proved to be indispensable for accurate predictions of local-scale impacts, especially in an around the lagoon.

Key words: tidal power, hydrodynamics, Delft3D, tidal range, renewable energy, hydraulic structures, numerical modelling

HIDRODINAMIČNO MODELIRANJE ENERGIJE PLIMOVANJA: PREGRADA SEVERN BARRAGE IN ZALIV SWANSEA BAY

Nejc Čož

Izvleček

Hidrodinamično modeliranje ima pomembno vlogo pri zasnovi objektov za izkoriščanje energije plimovanja. Cilj raziskave je bil razviti metodologijo za simulacijo plimskih elektrarn (PE) s programsko opremo Delft3D. Osredotočili smo se na reševanje dveh pomanjkljivosti hidrodinamičnih modelov PE in sicer: (i) večina do sedaj objavljenih regionalnih hidrodinamičnih modelov ni upoštevala ohranitve vztrajnostnega momenta pri toku skozi hidravlične objekte; (ii) dosedanje raziskave so temeljile zgolj na 2D modelih, medtem ko je bila uporaba 3D modelov omejena na simulacije na lokalni ravni. Prvi zastavljeni cilj je bil razviti modul za simulacijo PE v modelu Delft3D. Validacija modula je bila izvedena na študiji primera pregrade Severn Barrage, kar je omogočilo neposredno primerjavo z obstoječimi rezultati v literaturi. Primerjava je pokazala dobro ujemanje rezultatov in s tem potrdila ustreznost razvitega modela. Drugi zastavljeni cilj je bil zagotoviti ohranitev momenta pri toku skozi hidravlične objekte. Razvili smo metodo, pri kateri ohranitev momenta na iztoku predstavimo kot dodatna zunanjo silo v momentni enačbi. Na koncu smo razvito metodo preizkusili na študiji primera PE v zalivu Swansea Bay. Ohranitev momenta je pomembno vplivala na simulacijo toka v neposredni bližini hidravličnih objektov, saj je tok predvsem v tem območju, močno občutljiv na vertikalno porazdelitev hitrost. Glavna prednost 3D simulacije pred 2D modelom se je pokazala pri oceni lokalnih strižnih napetosti dna, saj je ta omogočila natančnejšo napoved vertikalnega profila hitrosti. Ob iztoku iz turbine namreč pride do t.i. prilepljanja tokovnic na dno, kar popači logaritemsko obliko profila, ki je predpostavljena v 2D simulacijah toka. Na podlagi rezultatov lahko trdimo, da je za hidrodinamično simulacijo delovanja PE v večini primerov zadosten že 2D model, ki upošteva ohranitev momenta na iztoku iz hidravličnih objektov. Kljub temu pa je v primerih, kadar nas zanimajo vplivi zgolj v bližini objekta, smiselno model razširit v 3D, zlasti za napovedovanje strižnih obremenitev dna na iztoku iz hidravličnih objektov.

Ključne besede: energija plimovanja, hidrodinamika, Delft3D, plimovanje, obnovljiva energija, hidravlični objekti, numerično modeliranje

CONTENTS

1
INTRODUCTION

With increasing concern over climate change and a rapid rise of carbon dioxide concentrations in the atmosphere, the move towards renewable energy has never been more relevant. Nowadays, the concern over the future of our planet is rapidly increasing, sparking serious debates amongst the general public, experts, industry stakeholders and governments on how to mitigate the effects of climate change. "Sustainable development", "Carbon neutrality", "Low-carbon economy", "Life-cycle assessment", "Carbon footprint" and "Renewable energy" are just some of the commonly used buzzwords that repeatedly emerge from such debates. Governments and industries have finally started to invest heavily in the development of renewable energy technologies to combat these issues (REN21 2018). The signing of the historical Paris Agreement in 2015 saw 174 states and the European Union committing to contesting the climate change by adopting mitigation strategies into their own national agendas (United Nations 2016a). To date, the number of signatories has risen to 195 Parties, that together represent more than 88 per cent of global greenhouse emissions (United Nations 2016b). In 2017, the renewable power generation saw its largest annual increase ever, raising total capacity by almost 9% globally over the previous year and thereby overtaking the combined additions in coal, natural gas and nuclear power in the same year (REN21 2018). The continuous advancements in the technology, that can be attributed to the intensive academic and commercial research studies are constantly increasing the efficiency and affordability of renewable energy solutions. In general, tidal energy is considered to be a promising technology with great potential for the production of clean power (Hendry 2016). In contrast to wind and solar, tidal energy conversion is entirely predictable and can be forecasted with high accuracy and far into the future (Ellabban et al. 2014).

There are two main principles for the extraction of tidal power. Tidal stream technologies generate electricity by extracting kinetic energy from the tidal current, while tidal range technologies rely on the potential energy created by rising and falling of tides. Severn Estuary has the most significant tidal range in the UK, presenting a potential for deployment of both stream and range technologies. Due to its exceptional tidal amplitude, it is considered the most important region for the development of tidal range technologies in the country. As a result, the region has attracted a lot of commercial interest and has been frequently used in academic research for case studying the deployment of the technology.

Conceptually, Tidal Range Structures (TRS) work on the principle of creating an artificial hydraulic head difference by impounding water, which is then used to drive the turbines installed in the impoundment walls. Based on the layout of the walls, the structures can be split into barrages and lagoons. The barrages are generally very large structures that span the two banks of a large inlet or bay, creating an extensive impoundment basin on the upstream side of the wall (DECC 2010). Tidal lagoons are much smaller objects. They are created by constructing a circularly-shaped embankment that forms the impoundment basin. Due to their smaller size, they are thought to be a more environmentally friendly alternative to barrages (Angeloudis and Falconer 2017). With both types of technology being viable for deployment in the Severn Estuary, several different configurations of barrages and lagoons, including a combination of both, have been proposed so far. A proposal from Severn Tidal Power Group (STPG 1989) has been the most popular and most studied design proposal for a tidal barrage. With an embankment wall spanning between Cardiff and Weston-super-Mare, it was estimated that this scheme could generate around 17 TWh of electricity per year, supplying around 5 per cent of UK's energy requirements (Bray et al. 2016). However, due to its large size, high construction costs and uncertainties over environmental impacts, the scheme has gradually fallen out of favour. In its place, tidal lagoons have been progressively gaining more attention, which led to the formation of Tidal Lagoon Power, a company that put forward a plan for construction of six tidal lagoons in the UK (Hendry 2016). A tidal lagoon in Swansea Bay would be the first of the proposed schemes, powering around 150,000 households with a prospective 320 MW of installed capacity.

Environmental impacts are one of the main concerns regarding the TRS in the Severn Estuary (Kirby and Retière 2009). They include:

- changes in maximum and minimum water levels, which can lead to reduction of intertidal habitats and increase in flood risk in some places Xia et al. (2010b);
- interruption to fish migration and injury from impact with turbines (Dadswell and Rulifson 1994); and
- changes in sediment transport patterns due to reduced velocity of the tidal current, which can affect the marine ecosystem through stronger light penetration due to lowered levels of turbidity and concentration of suspended sediment (Ahmadian et al. 2010a; Neill et al. 2017; Cornett et al. 2013).

The physical presence of a tidal barrage or lagoon will also have an impact on society, affecting activities occurring in the area and wellbeing of local residents. This may include increased difficulty to navigate for commercial and recreational vessels due to an obstruction; collision risk; noise pollution during both construction and operation; negative effect on tourism, recreation and activities in nature (Hooper and Austen 2013). However, not all impacts are necessarily negative; potential benefits, apart from clean energy, include potential road and rail links (in the case of a barrage), increased employment, improved conditions for recreation either upstream or inside the basin, and lowering flood risk. All these factors present a complex multi-objective system that requires a sophisticated decision-making tool for impact analysis and a reliable hydrodynamic model is one of the essential elements for such investigation.

Hydrodynamic models have an important role in the development of tidal energy schemes. They play a key part in the optimisation of the design and operating procedures and provide a good base for assessment of environmental impacts (Adcock et al. 2015). Consequently, there is an incentive for constant development and improvement of numerical modelling tools to enhance the accuracy and confidence in the hydrodynamic simulation (Angeloudis et al. 2016b). The numerical models extend from simple theoretical and 0D models to sophisticated multidimensional models that often require access to high-performance computing to make them feasible for practical use (Neill et al. 2018). The most commonly used are 2D hydro-environmental models – they are flexible and robust tools for modelling the flow at a regional scale. They have been applied to the analysis of tidal barrages and lagoons by a number of authors, utilizing several different software suites, such as DIVAST (Ahmadian et al. 2010a), EFDC (Zhou et al. 2014a; Bray et al. 2016), FV2D (Ahmadian et al. 2014b) and TELEMAC (Bourban et al. 2014).

Operation of a TRS is not by default included in conventional hydrodynamic models, hence, a particular TRS module has to be developed and retrofitted into the original source code. For the model to work properly it is essential that the implemented algorithms are based on a firm theoretical background and have to include at least:

- a method to physically separate the two subdomains (impoundment basin and seaward side);
- an algorithm that determines operational stages of the power plant, i.e. controlling the gates and turbines that allow transfer of the water between the two sub-basins; and
- procedures that accurately calculate the transfer of water through sluices and turbines.

Based on the needs of an individual study, these algorithms can considerably vary in complexity from model to model. For example, a study focused on optimisation of electricity output will consider a more complex formulation of the way power generation is estimated, while a different study focusing on environmental impacts might completely ignore the power production, but would introduce a more sophisticated representation of water transfer through the hydraulic structures.

To increase accuracy of the hydrodynamic predictions, this study includes a newly developed method for transfer of momentum though hydraulic structures. Treatment of momentum is important for accurate predictions of the velocity field in the vicinity of the TRS (Angeloudis et al. 2016b). Conventional models often simplify the transfer through hydraulic structures and completely ignore the conservation of momentum. While that would be sufficient for preliminary analysis or prediction of assessment of far-field impacts, disregarding the momentum conservation generally leads to unrealistic predictions of the near-field conditions, particularly regarding the jets that form just downstream of the hydraulic structures. This can have a direct impact on phenomena associated with the velocity field, including water quality, sediment transport; and an indirect impact on predicted estimation of power production. The implementation of such procedures normally requires a full user-access to the source code, which is only possible with academic research codes or open-sourced software.

One such modelling suite is Delft3D, an open source software, which was developed by Deltares, and is already widely used across industry and academia worldwide (Deltares 2014). It includes options for both 2D depth-averaged and 3D hydrostatic simulations. The curvilinear grid allows for a more natural fit of the

computational mesh to the complex coastline and offers possibility for high resolution refinement of the grid around the areas of interest, such as around the barrage or lagoon. It integrates flow and transport modelling systems, making it very attractive for hydro-environmental analysis of coastal and estuarine environments, such as the coastal waters around the UK. The software was selected to be used in this study with an aim to build a flexible and robust modelling tool that will be used for analysis of future tidal proposals in the Severn Estuary by the Hydro-environmental Research Centre (HRC) at Cardiff University. However, the open-source nature of Delft3D, and its wide-spread use across both academia and industry, means that the developed modifications will be available for use by any interested party.

In summary, the development of renewable energy projects is crucial for decreasing the carbon footprint and is a paramount factor in the transition towards the carbon-free economy. Tidal power presents one of the largest untapped renewable resources. The sheer scale of a tidal range power plant requires a significant initial investment and faces a lengthy construction period. Hence, any uncertainties on the efficiency of the power production and worries about the environmental impacts can discourage the stakeholders and lawmakers from supporting such schemes. The assessment of TRS relies heavily on the numerical modelling of their operation and simulation of the resulting hydrodynamic conditions.

2
LITERATURE REVIEW

2.1. Renewable energy

By definition, renewable energy is energy produced from natural sources - such as sun, wind and water - that are continually replenished on a human timescale (Ellabban et al. 2014). Renewable sources represent one of the main drivers of sustainable development and are fundamental for a transition towards a carbon-neutral economy (Dincer 2000). The extraction technologies have been already known and successfully deployed for decades, however, the accelerated development and a rapid increase in capacity have exposed a number of challenges related to renewable energy. One of the biggest drawbacks is the stochastic nature of the sources; oftentimes they are weather dependent and geographically diffused, which means that their output can be predicted, but not controlled (Uqaili and Harijan 2012). There are also questions over environmental and ecological impacts; for example, projects involving wind and tidal turbines have raised concerns over an increase in animal mortality rate as well as loss of important natural habitats (Wolf et al. 2009). Nevertheless, the positives still significantly outweigh the negatives, when compared to the traditional fossil fuel based technologies.

Renewable resources provided 29.3 per cent of the electricity generated in the UK in 2017, an increase of 4.8 percentage points from the previous year (BEIS 2018). Table 1 classifies the UK's annual electricity production by a renewable resource. With a 39 per cent increase from the previous year, wind extraction has now become the primary source of renewable electricity in the country. The 50 TWh of output was achieved by an extensive increase in capacity and favourable wind conditions in 2017. Tidal energy finds itself on the other end of the spectrum – together with wave technology it produced only 4 GWh of output in 2017, making it almost negligible source in the country's renewables portfolio. Alternatively, the viability of the

technology can be represented by the capacity factor (CF), an indicator that measures the economic (not physical) efficiency of power production. The CF metric is primarily used for cost calculations of power generation schemes and can be indirectly used for illustrating the overall achievement of carbon reduction objectives (Boccard 2009). It is defined as a ratio between the net electricity generated in a selected time interval to the energy that could have been generated at continuous full-power operation during the same period.

The Digest of UK Energy Statistics (BEIS 2018) has presented the CFs for the UK's renewable energy sector for the year 2017 as a ratio between the net generated electricity and the total generating capacity, as presented in Table 1. The main reason for a low CF factor of the wave and tidal source is that the deployed technologies are still in their initial stages, with the CF expected to increase with further development of the technologies. For example, a study from (Clarke et al. 2006) showed how the CF of tidal stream turbines can be significantly increased solely by regulating and limiting the power delivered from a turbine by using a lower capacity generator. This enabled the turbines to operate at their rated capacity for longer periods of time, raising the CF from the initial 14.7 per cent to 32.5 percent, which is already much closer to ratios achieved by wind and hydropower (see Table 1).

Table 1: UK's annual electricity production from renewable sources in 2017 (BEIS 2018).

Renewable source	% increase from 2016	Output capacity [TWh]	% of total output	Capacity factor (%)
Wind	39	50	50	31.7
Bioenergy	6	31.9	32	61.5
Solar PV	11	11.5	12	10.7
Hydropower	10	5.9	6	36.5
Wave and tidal	100	0.004	< 0.01	3.0

Despite decades of development efforts, the ocean energy remains a largely untapped energy resource in the UK and worldwide. At the end of 2017, there was 529 MW of installed capacity in operation globally, of which more than 90 per cent came from only two tidal barrage facilities – Rance Tidal Power Station in France and Sihwa in South Korea (REN21 2018). The other 10 per cent are wave and tidal-stream resources. The successful deployment of MeyGen (Atlantis Resources Limited 2018) and Nova Innovation (Nova Innovation 2019) tidal stream, located off Caithness and Shetland respectively (Scotland, UK), have presented a breakthrough in commercial viability of the tidal stream technology. Both schemes are connected to the national grid, are fully-operational, and have already received a full consent and necessary

permissions for construction of additional turbines that will further increase their capacity. Although there has recently been more progress in the tidal stream energy, tidal range represents a more established technology, with the first successful tidal range project deployed more than 50 years ago.

2.1.1. Tidal Power

In literature, the terms 'Marine power', 'Ocean energy' and 'Hydropower' are often used interchangeably when referring to tidal power. Diagram in Figure 1 illustrates the relationship of tidal power with these expressions. Adjectives 'marine' and 'ocean' are synonyms that refer to the energy carried by the ocean's body of water; i.e. waves, tides, salinity gradients and temperature gradients (IRENA 2018a). Offshore wind and offshore solar farms are sometimes erroneously included in this group because they are both constructed in marine environments.

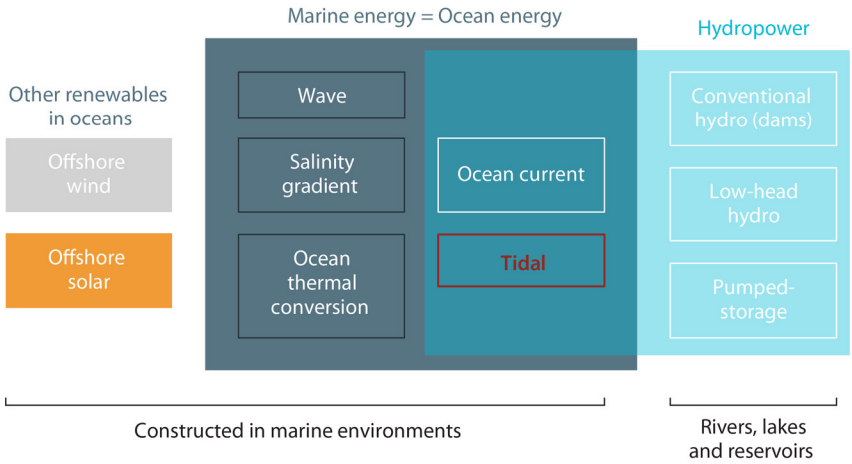

Figure 1: A diagram illustrating the overlap between marine energy and hydro-power.

However, their resource for power generation is stored in the atmosphere and the sun respectively, and not in the ocean's body of water. Hydropower relies on the extraction of energy stored in flowing water by driving the water through a hydraulic turbine (IRENA 2018b). The hydroelectric power can be generated either from the potential energy (dams, pumped-storage and tidal range) or from the kinetic energy (low-head hydro on rivers, ocean currents and tidal stream). Similarly, the terms 'energy' and 'power' are often used as synonyms, even though they technically mean different things. Energy is the capability to do work or generate power, while power

represents the rate of extracted/consumed energy per unit time, most of the times in the form of electricity. The terms are interrelated and can, therefore, be used interchangeably when describing the technology; for example, tidal power and tidal energy both refer to the technology used for harnessing the energy stored in tides.

Tidal power can be further divided into three sub-groups: tidal range, tidal stream and other innovative solutions (Figure 2). The latter represent embryonic technologies that could theoretically work but have not been yet seriously considered for practical deployment. They include proposals like tidal reefs and tidal fences – modified barrage designs that would lessen the impacts on the environment (DECC 2008), or Dynamic Tidal Power – a technology that uses a difference between the potential and kinetic energy of tides (Hulsbergen et al. 2008).

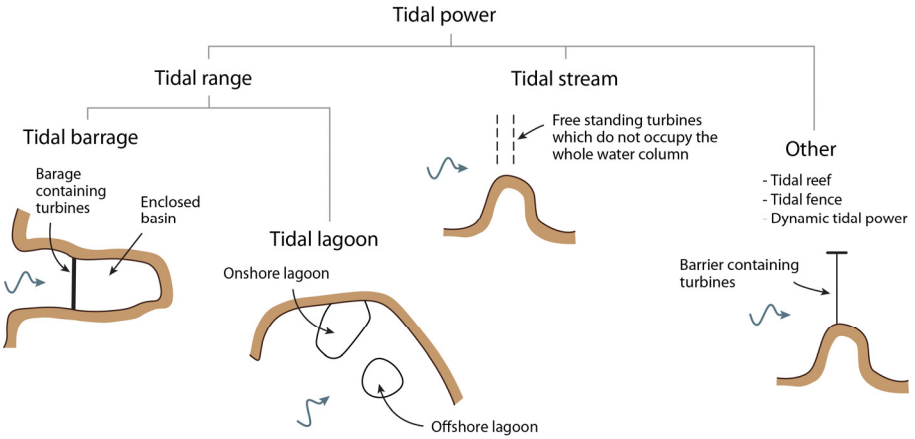

Figure 2: Classification of tidal power technologies. Adapted from Adcock et al. (2015).

Tidal range and tidal stream are the two main technological concepts for extracting energy from tides. Tidal stream takes advantage of kinetic energy stored in tidal currents. The energy is extracted through a tidal stream turbine – a device similar to a wind turbine but modified to work in an aquatic environment. Tidal range, on the other hand, relies on the potential energy stored in the tidal amplitude. This is achieved through the construction of a retention wall or an impoundment basin that is used to establish a hydraulic head difference, that drives the turbines installed in the structure's wall.

Based on the layout of the embankment, tidal range structures can be roughly split into two groups: (i) tidal barrages, and (ii) tidal lagoons (Figure 2). With tidal barrages, the embankment is constructed across an estuary or a large bay, creating a

very large retention basin (DECC 2010). Tidal lagoons usually impound a much smaller area; most commonly they are constructed in the shape of a horseshoe and attached to the coastline (Waters and Aggidis 2016a). To avoid construction in the intertidal zone, the lagoon could be instead located offshore, usually taking a more circular shape to make the construction more economical (Adcock et al. 2015).

2.1.2. Existing projects

The history of harnessing tidal energy stretches all the way back to ancient times (Charlier and Menanteau 1997). The technology known as a tidal mill was already used by the ancient Greeks. Tidal mills were simple yet effective structures, using the water wheel to generate mechanical power by harnessing tidal energy, either directly from the tidal stream or through a construction of a dam with sluices, that formed a retention basin, from which the water was released during the low tides (Charlier 2007). The two concepts essentially represent the first prototypes of the modern-type tidal stream and tidal range power plants. The technology has been used continuously throughout history, however, it was not until the 1960s when tides were for the first time used to generate electricity instead of just mechanical power.

Table 2: Overview of the operational tidal range projects as of 2018.

Power Plant	Country	Year	Capacity [MW]	Basin area [km2]	Mean tidal range [m]
La Rance	France	1966	240	22	7.9
Kislaya Guba	Russia	1968	1.7	2	2.4
Annapolis Royal	Canada	1984	20	6	6.4
Jiangxia	China	1985	3.9	2	5.0
Lake Sihwa	South Korea	2011	254	42	7.8

The first such project was successfully built in France on the Rance River estuary in 1966. Similar smaller projects followed in Russia (Kislaya Guba), Canada (Annapolis Royal Generating Station) and China (Jiangxia) in 1968, 1984 and 1985 respectively (Table 2). After that, it was not until 2011 when the next larger project was constructed; on Lake Sihwa in South Korea, a tidal range power plant was installed into an existing barrage, transforming an artificial lake into a tidal basin, making it the largest tidal range scheme by installed capacity in the world. Even though there is still a lot of unused potential for tidal generation worldwide, no new tidal range energy projects have been initiated since.

Rance Tidal Power Station, France

Figure 3: An aerial image of the Rance Tidal Power Station located in the Rance River estuary in France. Image captured from Google Earth.

The Rance Tidal Power Station is located on the estuary of the Rance River in Brittany, France (Figure 3). It is the first fully operational tidal range project in the world; opened in 1966, it has been reliably producing electricity for over 50 years (Charlier 2007). The barrage is 750 m long and extends down to a depth of 13 m, forming a 22 km^2 impoundment basin with a 184 million m^3 storage capacity (Andre 1978). The barrage houses 24 identical 10 MW bulb units, which produce a total output of 240 MW and have an annual production capacity of around 480 GWh and a capacity factor of 24 per cent (Andre 1976; Neill et al. 2018). The turbines can only generate on an ebb tide, most efficiently under a head of 10 m, and between limits of 3.4 and 16.5 m (Andre 1976). The project is considered a success, however, the concerns about the associated environmental impacts have continually been raised since the beginning of its operation. Much of the damage has been caused by the construction, effectively destroying the local marine ecosystem (Retiere 1994). However, the majority of the species have since then returned; better understanding of the biological processes in the estuaries and continuous advancements in construction techniques mean that future projects should be able to avoid similar outcomes (Kirby and Retière 2009).

Sihwa Lake Tidal Power Station, South Korea

Figure 4: An aerial image of the Sihwa Lake Tidal Power Station located in the on the western coast of the Korean Peninsula. Image captured from Google Earth.

Sihwa Lake Tidal Power Station is currently the world's largest (by capacity) and most recent tidal range structure. It is located on the western side of the Korean Peninsula (Figure 4), in the region experiencing the highest tides in the Yellow Sea (H. S. Lee 2011). The embankment was initially constructed to create a freshwater reservoir in the Kyeonggi Bay, creating a 56.5 km^2 lake, while also creating 173 km^2 of reclaimed land (Bae et al. 2010). Soon after construction, the lake was severely contaminated by the excessive inflow of polluted water. The only way to improve the water quality of the bay was to allow seawater exchange with the reservoir. The authorities saw an opportunity to turn this disaster into a positive; they constructed a tidal range power plant, that is simultaneously performing two functions:

- seawater exchange for improved water quality and
- clean power generation.

The power plant incorporates 10 bulb units with a total capacity of 254 MW and employs a flood-only operational scheme due to the limitations of the maximum water surface elevation in the lake (Cho et al. 2012). The project was considered a great success from a power generation, environmental and tourism points of view, so much so that it led South Korean government to explore further options for tidal range schemes in the region (Waters and Aggidis 2016b).

Kislaya Guba Tidal Power Station, Russia

Figure 5: An aerial image of Kislaya the Guba Tidal Power Station located in the Kislaya Guba fjord in the Barents Sea, Russia. Image captured from Google Earth.

Kislaya Guba Tidal Power Station was constructed in 1968 as a trial project by the Soviet government (Bernshtein 1972). Located in the Kislaya Guba fjord in the Barents Sea (Figure 5), it is the smallest of the existing tidal range schemes. Initially designed for just 400 kW, its installed capacity has recently grown to 1.7 MW (Neill et al. 2018). The power plant has recently celebrated 50 years of successful electricity generation, motivating the government to explore other viable sites in Russia – the White Sea reportedly holds a potential of 16 000 MW in its tidal range (Chaineux and Charlier 2008).

Annapolis Royal Generating Station, Canada

The Annapolis Royal Generating Station is a 20 MW tidal range power plant, located on the Annapolis River in Nova Scotia, Canada (Figure 6). Constructed in 1984, this scheme consists of a single Straflo turbine with a 20 MW of installed capacity, that produces 50 GWh of electricity per year. The powerplant is also used for flood defence, while the installed ship locks serve as an important transport link on the Annapolis River (Neill et al. 2018).

Figure 6: An aerial image of the Annapolis Royal Generating Station located on the Annapolis River in Nova Scotia, Canada. Image captured from Google Earth.

Figure 7: An aerial image of the Jiangxia Tidal Power Station located in the in Jiangxia Harbour, Wenling City, China. Image captured from Google Earth.

Jiangxia Tidal Power Station, China

The Jiangxia Tidal Power Station was opened in 1985 and is located in Jiangxia Harbour, Wenling City, Zhejiang Province, China (Figure 7). The power plant operates bi-directionally and houses six bulb turbines, the last of which was installed in 2007, providing an installed capacity of 3.9MW (S. Wang et al. 2011). There have been

several other tidal range proposals in Zhejiang Province that never became fully operational due to the issues with turbine construction and location-related problems (Li and Pan 2017; Du et al. 2017).

2.1.3. Tidal resource and future proposals

There are many possible locations in the UK and worldwide, that are potentially feasible for the exploitation of tidal range for power generation. The Severn Estuary and Bristol Channel have been for decades considered as one of the key locations for the deployment of the technology in the UK (Roberts 1982). Other notable sites currently undergoing feasibility studies include Bay of Fundy in Canada (Cornett et al. 2013); White Sea in Russia (Bernshtein 1972); and Mersey Estuary (Aggidis and Benzon 2013), Soloway Firth (Aggidis and Feather 2012), Morecambe Bay (Burrows et al. 2009) and North Wales Coast (Evans et al. 2004) in the UK. In addition to these larger sites, there are numerous small-scale sites of interest in South Korea, India, Australia and Brazil (Rourke et al. 2010).

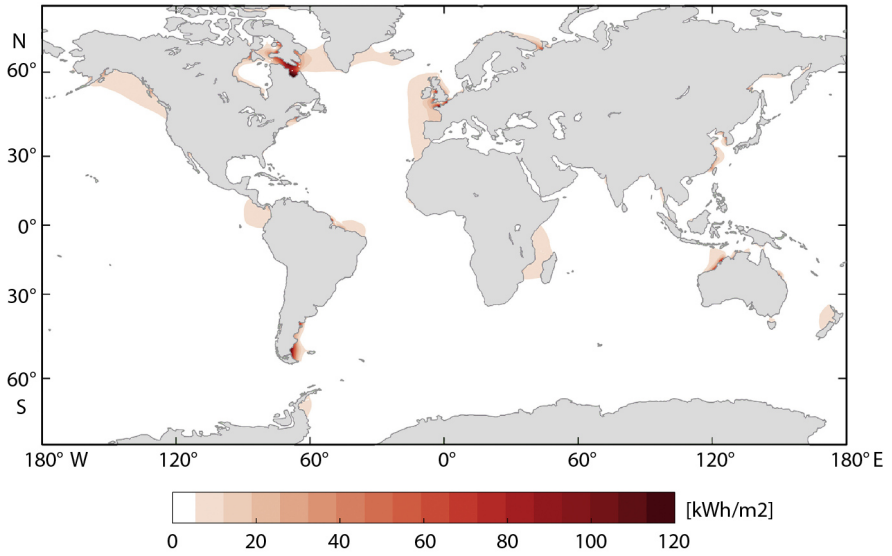

Figure 8: The global theoretical tidal range energy resource calculated as annual energy yield in kWh/m^2. Adapted from Neill et al. (2018).

Worldwide

The analysis by Neill et al. (2018) estimated the global annual theoretical tidal range resource to be around 25 880 TWh. The resource characterization was based on annual sea surface elevations and water depths at 1/16° x 1/16° global resolution and is presented on a contour map in Figure 8. The minimum acceptable annual energy yield was assumed to be 50 kWh/m^2 and maximum acceptable water depth of 30 m, constraining the potentially viable areas to coastal regions of only 11 countries (presented in the darker shades of red in Figure 8). Sorted in the order from having the most to having the least tidal range resource they include Australia, Canada, United Kingdom, France, USA, Brazil, South Korea, Argentina, Russia, India and China.

However, in practice, the technical resource could be significantly lower than the estimated theoretical yield; according to some estimations the effective resource as low as 37 per cent (Prandle 1984). In addition, some areas could be impossible to exploit due to practical difficulties with development at larger scales, or due to the socio-economic, political and environmental constraints. Sea ice presents another obstacle for northern locations including Alaska, and Hudson Bay in Canada. Considering all these restrictions, the available global annual potential energy is reduced to 5792 TWh, with 90 per cent of the resource distributed across only five countries, including Australia, Canada, UK, France and USA. For a detailed list of locations, that were identified as technically feasible, the readers are referred to the publication by Neill et al. (2018).

United Kingdom

The review paper by Neill et al. (2018) has further focused on the northwest European shelf seas and including the entirety of the British Isles and French north coast (Figure 9). This region alone contains approximately one-quarter of the global theoretical resource. Based on the criteria for the exploitable area, 53 per cent of the resource was found in UK waters, with the remaining 47 per cent found off the north coast of France. In the UK it is concentrated along the coasts of Liverpool Bay, the Severn Estuary and Bristol Channel, Wash, and southeast England (Figure 9). It has been estimated that the total UK tidal range potential could meet 10-15% of the UK's current electricity demand (DECC 2010). The most attractive region for the tidal range generation is the Severn Estuary (Figure 9, Table 3); with an exceptional tidal range of 14 m and a potential maximum installed capacity of 13.5 GW and a capacity factor of up to 20 per cent, it was estimated that it could deliver 19.7 TWh of electricity per year. For comparison, the proposed Hinkley Point C nuclear power station is

expected to provide a similar annual output, however, due to a high capacity factor in the range of 90 per cent for modern day nuclear power technologies, this could be achieved through only 3.2 GW of electricity generation capacity (BEIS 2016).

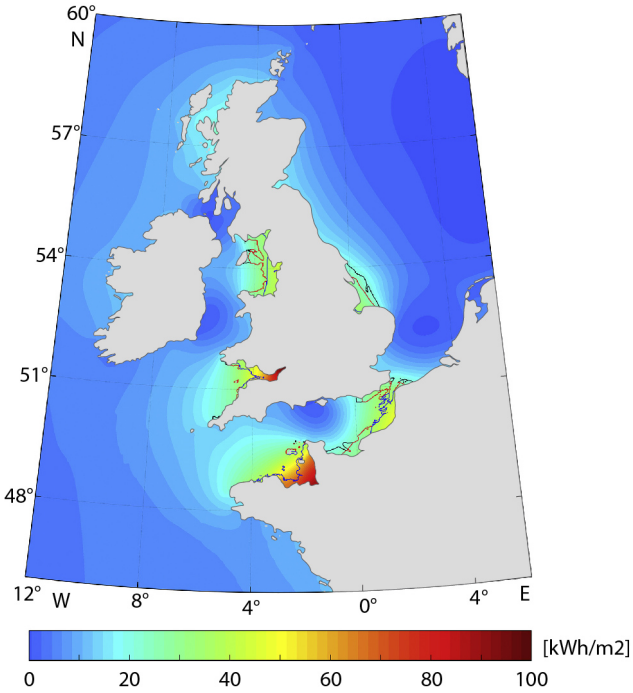

Figure 9: The theoretical tidal range energy resource over the northwest European shelf seas, calculated as annual energy yield in kWh/m^2. Areas landward of the [blue, red, black] contour lines denote regions with water depths less than 30m and where energy density exceeds 84, 60, and 50 kWh/m2, respectively. Adapted from Neill et al. (2018).

Table 3: UK Tidal range resource by region (DECC 2010).

Location	Mean tidal range [m]	Estimated max. installed capacity [MW]	Predicted annual energy output [GWh]
Severn Estuary	11	13 500	19 700
Solway Firth	5.5	7200	10 250
Morecambe Bay	6.3	3000	4630
Wash	4.45	2400	3750
Humber	4.1	1080	1650
Thames	4.2	1120	1370
Mersey	6.45	700	1320
Dee	5.95	840	1160

Following a public consultation in 2010, the Department of Energy and Climate Change (DECC) released a map of shortlisted tidal range schemes in the Severn Estuary, that are presented in Figure 10 (DECC 2010). The factors used to determine feasibility of the proposals were:

- technical risk,
- cost of construction,
- cost of produced energy,
- how the costs fit into the energy and climate change goals,
- affordability,
- environmental impact, and
- regional impact (ports, fishing and employment).

The shortlisted schemes are all based on the technology that has been already tried and tested in tidal range schemes across the world.

The projects, shortlisted in Figure 10, included three tidal barrage alternatives, as well as two different tidal lagoon proposals. The barrage proposals have since fallen out of favour and the focus has shifted more towards the lagoons. Because lagoons are significantly smaller structures, they are viewed as a more environmentally-friendly alternative to the barrages, as well as more economical and technically feasible (Hinson 2018). In 2012, a report from Crown Estates (2016) concluded that there is potential for a significant quantity of tidal lagoons in the UK, particularly on the West Coast. An ambitious plan by Tidal Lagoon Power Ltd (TLP) soon followed, with proposals for a fleet of six tidal lagoons across the country. The first is the tidal lagoon in Swansea Bay, with the others to be built in the Severn Estuary and off the English coast of the Irish Sea (Cebr 2014).

The Severn Barrage

The first proposal for a barrage in the Severn Estuary dates back to 1849 when Thomas Fulljames proposed building a barrage from Beachley to Aust with an aim to establish conditions for a large shipping harbour in the estuary (Carne 1995). The commercialization of the electricity production in the next century popularised the idea of a tidal barrage powerplant, that could harness a great capacity of electricity due to the exceptional tidal range in the estuary. In search of the most feasible solution, the barrage design went through a number of proposals. The advancements in numerical simulations contributed to even more rapid development of the proposals in recent years. Several different locations along the Severn Estuary were considered, with the UK government shortlisting three possible

layouts in a feasibility study in 2010 (DECC 2010). The possible layouts included Beachley Barrage, located just upstream of the Severn Bridge and the smallest of the selected alternatives (Figure 10-B5); Shoots Barrage, a smaller barrage located just downstream of the Second Severn Crossing (Figure 10-B4); and Brean Down to Lavernock Point Barrage, the same layout as first proposed by the Severn Tidal Power Group (STPG 1989).

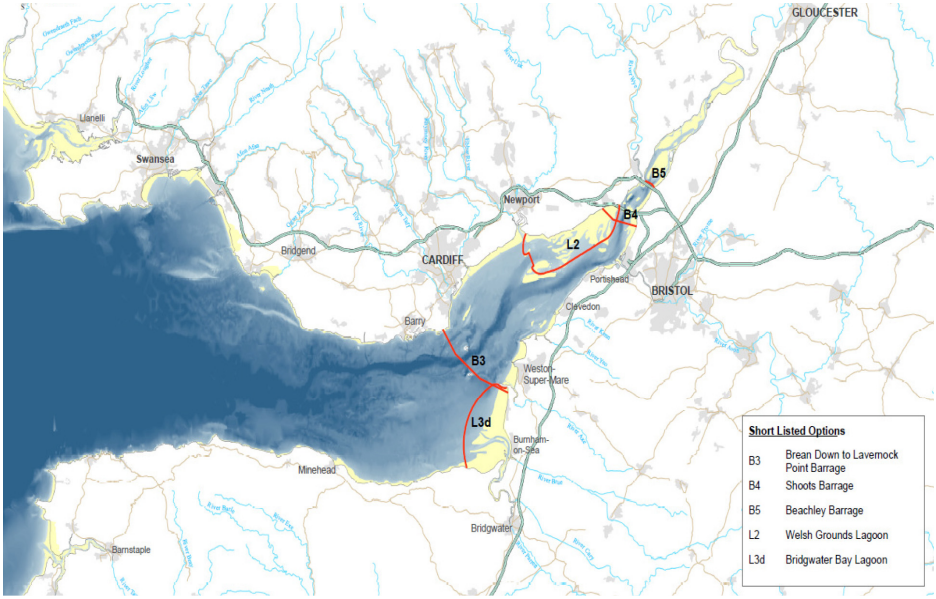

Figure 10: Map of shortlisted schemes in the Severn Estuary (DECC 2010).

The most popular and the most studied of the alternatives is the STPG design and is commonly referred to as the original Severn Barrage (Falconer et al. 2009). The proposal presented a 16.2 km long barrage, housing 216 bulb turbines for a total installed capacity of 8640 MW, generating only during the ebb tide (STPG 1989). It was predicted that such a scheme should yield between 14 and 17 TWh of electricity per year, roughly equivalent to 5 per cent of the UK's electricity demand (Bray et al. 2016). The project has been viewed as somewhat controversial, mostly because of the inevitable environmental implications of such a large-scale project, including changes in tidal range regime, potential loss of intertidal zones and reduction of tidal currents, directly and indirectly affecting the turbidity, suspended sediment concentrations and the benthic ecosystem (Kadiri et al. 2012). However, there were also noteworthy benefits to the construction of a barrage, such as reduction of flood

risk (Ahmadian et al. 2014a), opportunities for recreation and tourism, and bolstering of local industry. The Severn Barrage tidal range power plant has been considered economically unfeasible by the UK Government, however, the project has not been ruled out of future consideration, if the environmental implications could be mitigated (DTI 2003).

The Swansea Bay Lagoon

In 2011, the TLP was set up to develop, construct and operate tidal lagoon power stations, with the project in Swansea Bay being the first of the six proposed schemes in the UK (Hendry 2016). The project involves the construction of an artificial lagoon in a shape of a horseshoe, connected to the Swansea Bay coast, creating an 11.6 km^2 impoundment for the purpose of tidal power generation (Waters and Aggidis 2016a). Even though it would be considerably smaller than the proposed Severn barrage, if constructed, it would become the world's largest tidal range power plant to date. The lagoon would incorporate 16 bulb turbines for a total installed capacity of 320 MW, generating an estimated annual output of 0.5 TWh. The TLP was planning to design a lagoon-specific type of bi-directional bulb turbine, that could be standardised and easily scalable, reducing the turbine cost of future projects (Tidal Lagoon Power 2016).

One of the main environmental concerns associated with tidal lagoons is their impact on sediment dynamics (Neill et al. 2017). How the construction of a lagoon affects sediment dynamics is directly connected to the changes in the tidal hydrodynamics and will be significantly influenced by the operating mode and the design of the structure (Cornett et al. 2013). It was shown that a counter-rotating eddy may form on the sides of the jet discharged from the turbines, significantly changing local sediment transport. Inside the impoundment, the reduced velocity can lead to increased accumulation of sediments which can lead to silting of the lagoon.

The project received development consent from the Secretary of State for Energy and Climate Change in 2015 and full support from the independent review, commissioned by the UK Government, entitled the Hendry Review of Tidal Lagoons (Hendry 2016). However, the UK government has recently withdrawn its support for the project and put the project indefinitely on hold, with the main concern being the cost of electricity compared to alternatives, such as wind farms and nuclear power (Guardian Media Group 2018).

2.1.4. Advantages and disadvantages of TRS

Based on the extensive review above, it can be concluded that TRS technology has a great potential in the field of renewable energy. However, with many advantages, the TRS do not come without any negatives. Based on the contemporary research, the main advantages and disadvantages of the technology are summed up below.

Advantages:

- Renewable source: they do not depend on fossil fuels and do not produce CO_2 emissions. The source (tidal range) is renewed continuously by the gravitational pull of the Moon and Sun (Rourke et al. 2010).
- Reliable: TRSs are designed for a very long lifespan; for example, the expected lifetime of the proposed Severn Barrage is 120 years, with turbine replacement occurring only every 40 years (Kelly et al. 2012).
- Efficient: bulb turbines used in TRSs are known to have high efficiency, with peak values above 90 per cent (Waters and Aggidis 2016b)
- Low operating costs: they can virtually operate unattended (Hendry 2016).
- Flood protection: TRSs can reduce the flood risk of the impounded coastal areas (Ahmadian et al. 2014b).
- Consistent and predictable: tides can be forecasted and are therefore predictable, which also means that power generation is predictable (Neill et al. 2018).

Disadvantages:

- Location-specific: generation costs for TRSs are driven by the strength of the tidal range and the bathymetry of the site (Hendry 2016). Only 5 countries share as much as 90 per cent of the resource (Neill et al. 2018).
- Environmental impacts: can change mean water elevations and reduce maximum current velocity (Xia et al. 2010c). There are also potential negative impacts on fish, marine mammals and birds (Dadswell and Rulifson 1994).
- Uncertainty: impacts are difficult to quantify, and so governments are hesitant to proceed with large-scale development (Neill et al. 2018).
- Distance from the grid: they require construction close to the existing national grids to prevent excessive grid connection costs (Hendry 2016).
- High initial cost: the estimated construction costs are substantial; £1bn for a lagoon in Swansea Bay and £34bn for the barrage across the Severn Estuary (Waters and Aggidis 2016a).

2.2. Tidal hydrodynamics

Tidal energy is derived from the gravitational pull between the Earth's oceans and the heavenly bodies, particularly the Moon and the Sun, as well as from the centrifugal force produced by the rotation of the Earth and Moon about each other, as illustrated in Figure 11 (Rourke et al. 2010). This means that tidal phenomena are periodic, with the exact nature of periodic response varying according to the movement of the bodies and local geographical peculiarities (Hammons 1993).

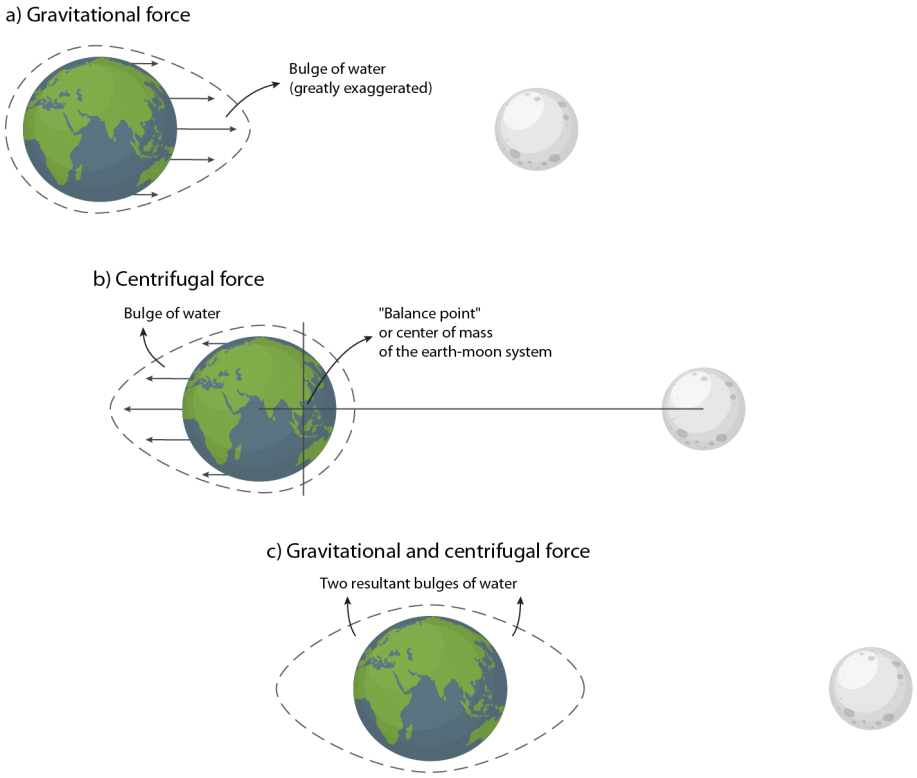

Figure 11: The effects of the Moon on the tidal range. Adapted from Rourke et al. (2010).

The contribution to the tide by the energy at a particular frequency can be described by tidal harmonic constituent. Each constituent is represented by a cosine curve and holds the information about its amplitude and phase lag. Summing up a set of various tidal constituents gives a harmonic tidal prediction that can be used by numerical models. The nomenclature for naming the constituents is a combination of a capital letter (or Greek letter in some cases) and a subscript number, which explain the source of the constituent and an approximate number of cycles per day respectively. For example, the most common constituents are M_2 and S_2 which present the influence of the Moon with 1.9323 tidal cycles per day and Sun with exactly 2 tidal cycles per day, both greatly contributing to the semidiurnal tidal activity (Parker 2007). Because of the elliptical orbit of the Moon and Earth the amplitude of the semidiurnal tide varies through the lunar month (29.5 days), with the tidal range being greatest at the full moon or new moon (spring tides) and lowest at half-moon (neap tides). Other major tidal constituents include N_2 and L_2 with a slightly higher and lower period than M_2 respectively, and diurnal constituents K_1, O_1, P_1, Q_1, and S_1, with periods of 23.93, 25.82, 24.07, 26.87, and 24.00 hours (Wolanski and Elliott 2016).

Figure 12 illustrates two different extremes of an idealised tidal wave propagating in the shallow waters. If the wave enters an endless river, it will propagate up the river as a progressive wave (Figure 12a). Both crest and trough of the wave, i.e. high and low tide, move progressively up the reach, with the maximum flood current occurring at the same time as high water. If the width of the river was to decrease, moving upstream, the amplitude will increase due to the funnelling effect, as the same amount of water is being forced through a smaller cross-section. If this river is closed-off at exactly one quarter of a tidal wavelength, the tidal wave will be reflected at the closed end, superimposing the incoming and outgoing waves into a standing wave (Figure 12b). In this case, high water would occur at the same time everywhere on one side of the node and the tidal range would increase due to the superposition of the amplitude. If the tidal basin has the right combination of length and depth, where the natural period is exactly the same as the tidal period, its tidal range will be amplified even further due to the resonance of the tidal waves (Parker 2007).

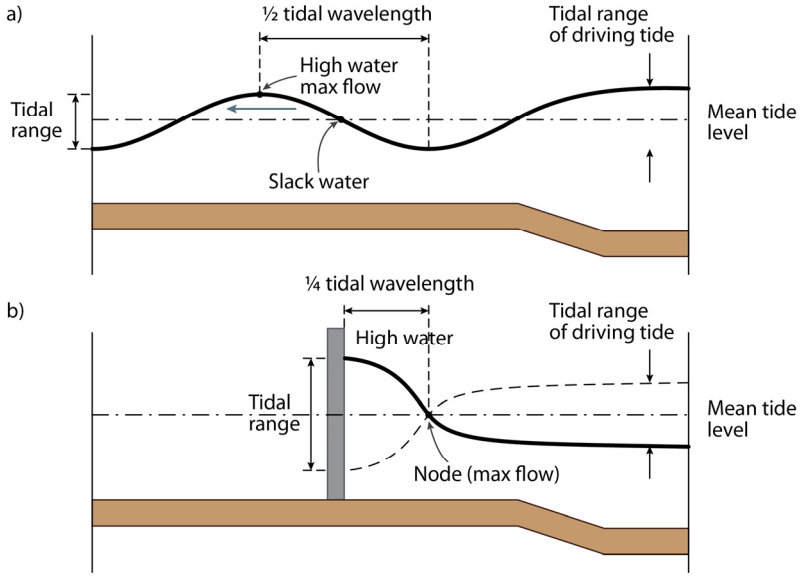

Figure 12: Difference in tidal range of shallow waters between (a) the progressive and (b) standing waves, shown for an idealized frictionless tide Adapted from Parker (2007).

This is also the case in Severn Estuary, where the tidal range is driven by two main mechanisms: (i) a funnelling effect at the upper reaches of the channel due to the wedge-shaped geometry and (ii) the quarter wavelength resonance of the channel with the incident North Atlantic tidal wave (Gao and Adcock 2015). The typical mean spring tide at the mouth of Severn River is 12.2 m, with the high spring tidal range at approximately 14 m (Liang et al. 2014). In oceanography, the cotidal charts are used to signify locations that are in phase with one another. To view the cotidal chart for UK, please refer to figures on page 52 in Neill and Hashemi (2018) and figure on page 7 in Uncles (2010). The entire Severn Estuary experiences a similar tidal phase, which means that water levels rise and fall almost uniformly across the whole domain. These unique characteristics can make the Severn Estuary challenging to represent in a hydrodynamic simulation; careful attention must be paid to the selection of appropriate boundary conditions, especially when including the tidal range energy devices (Adcock et al. 2011).

2.3. Numerical modelling of tidal range structures

The main purpose of the hydrodynamic simulations is to provide valuable insight into resource assessment, the quantification of the potential impacts, and minimization of any detrimental effects through design optimisation (Neill et al. 2018). Hydrodynamic models provide time-series approximations of the state variables, such as water surface elevation and current velocity, which makes them useful tools for the study of potential impacts of the TRS. For the simulations to work properly and achieve a high level of reliability, a wide range of multi-scale processes must be included, either by simulating them directly or by providing parameterized approximations. This includes tidal, fluvial and wave dynamics, sediment transport and water quality, as well as the implementation of hydraulic structures, impoundment walls and operational algorithms of the tidal range power plants. The assessment of TRS schemes relies on the development of the numerical tools that can simulate their operation over time. A great number of computational studies on the design and performance has been published to-date. They range from simplified preliminary studies to more complex and detailed investigations of the technology, that often require high-performance computing capabilities for practical application.

2.3.1. The multi-scale modelling approach

A review paper by Adcock et al. (2015) presents the idea of the multi-scale nature of hydrodynamic models. Depending on the motivation and needs, different levels of sophistication are incorporated into the model, and often the scales of a model will overlap. An example of that can be seen in studies by Ahmadian et al. (2010a; 2014a) and Kadiri et al. (2012) where a coupled 1D-2D model is used to achieve higher efficiency and accuracy of sediment transport and water quality. Based on the scale and level of sophistication we can split the models roughly into four different groups: global-, regional-, local- and subgrid-scale models.

2.3.2. Regional-scale models

The majority of hydrodynamic studies of TRS are made on the regional scale. The flow complexities that occur on this level require us to use at least 2D if not 3D numerical models. They usually employ grids with the cell sizes ranging from as small as tens of meters to as large as several kilometres. A number of studies have applied 2D models to investigate the operation and environmental impacts of different TRS schemes. Falconer et al. (2009), Xia et al. (2010c), Kadiri et al. (2012), Ahmadian et al. (2014a)

and Zhou et al. (2014b) have all used various numerical models for the analysis of the proposed Severn barrage in the Severn estuary. In all cases, the models have proved useful for a variety of studies, such as; investigation of regional hydrodynamics, sediment transport and water quality, optimisation of power generation efficiency and coastal flood risk assessment. Regional-scale models were also used on many tidal lagoon projects in the UK; Swansea Bay lagoon (Angeloudis et al. 2016b), North Wales lagoons (Angeloudis et al. 2016a; Ahmadian et al. 2010b) and Cardiff lagoon (Xia et al. 2010b; Angeloudis and Falconer 2017) to name just a few.

2.3.3. Global-scale and far-field models

Global-scale models usually refer to the atmospheric and ocean models that cover a large part or even the entire of the Earth's globe. In tidal range modelling, such models are used to assess the open boundary problem that can occur due to the operation of large schemes, e.g. a tidal barrage in an estuary (Adcock et al. 2011). The impacts on the flow conditions can be potentiality so far-reaching that they have a noticeable effect on the open boundary if the domain is too small (i.e. regional-scale). To evaluate far-field impacts in such cases, we need to expand regional models to a global scale. Such models employ a coarser numerical grid to cover an area where open boundary extends far away from the original location to a point where impacts of TRS on boundaries becomes negligible. In the case of the UK, it means going as far as the edge of the continental shelf, so they are commonly known as continental shelf models (CSM). Examples can be found in studies by Zhou et al. (2014a) and Bray et al. (2016) where the open-source EFDC model was used to develop a CSM for the Severn barrage. A comprehensive study on the potential of renewable energy extraction in the UK has been conducted by Bourban et al. (2014). They have employed a two-dimensional TELEMAC code to model an area that covers all of UK coastal waters, the North Sea and extends offshore slightly beyond the northern European continental shelf.

2.3.4. Local-scale models

All the studies mentioned above are interested in large-scale hydrodynamic conditions but not so much on the local details. For studying flow on a local scale, i.e. in the vicinity of a barrage or a lagoon, a more detailed model with a denser mesh has to be employed. Typically, these models focus on the performance efficiency of the turbines or local scour due to the accelerated flow through a turbine. For example, an experimental study by Jeffcoate et al. (2013; 2017) assessed the shear

stress of the bed downstream of a tidal barrage due to a three-dimensional nature of the flow conditions created by flow through turbines.

2.3.5. Subgrid-scale models

Studies on the subgrid-scale are looking at the representation of important small-scale physical processes that occur at length-scales that cannot be adequately resolved on a computational mesh. They are mostly concerned with the flow through the turbine itself and use more complex computational models, such as full 3D RANS simulation and large-eddy simulation (LES) (Wilhelm et al. 2016a).

The simulations presented in this study cover different spatial scales. In the first case study, an extensive continental shelf model of the Severn barrage was constructed for far-field analysis on a large-scale, while the second case study focused on a regional-scale model of the Severn Estuary for the Swansea Bay lagoon project. The developed methodology is robust enough to be applied to any case, regardless of the size of the domain and the resolution of the grid. At the same time, it is almost impossible to put one model into a single category. Take the Swansea Bay lagoon model as an example - its domain is covering a relatively broad area of the Severn Estuary and Bristol Channel, but the flexibility of the curvilinear grid allows for a more refined resolution in the areas of interest (such as close to the structure). The inclusion of the lagoon and the focus on the treatment of the flow through the hydraulic structures causes the model overlap between the regional and local scale. This illustrates the challenges associated with TRS modelling, where the border between different scales often becomes fuzzy (Neill et al. 2018). The case studies presented in this book try to address the significance of the multi-scale approach to the modelling and its appropriateness for the analysis of the TRS projects.

2.3.6. Evolution of numerical modelling of the Severn barrage

A great number of studies on hydrodynamic modelling of the Severn barrage have been published over the course of the last 10 years. In this section, when referring to the Severn barrage, we focus exclusively on the so-called Cardiff-Weston layout of the barrage, which is the largest scheme considered to be potentially feasible by the Department of Energy and Climate Change (DECC 2010). During this period, we have seen the Severn barrage model evolve through a series of refinements and optimisations. The model was implemented into a number of software programmes,

ranging from purely research codes such as DIVAST to more sophisticated open-source software suites such as EFDC and Delft3D.

A detailed study on the numerical modelling of the Severn barrage was first published by Xia et al. (2008; 2010a). The model employed a TVD finite volume scheme, based on a triangular unstructured grid, a method that is commonly used for simulation of estuarine hydrodynamics. The barrage was modelled through the domain decomposition technique with special treatment of the internal boundary in the location of turbines and sluice gates. This initial model used a simplified representation of the turbines; they were modelled using an orifice equation, which is inadequate for the representation of turbines, as it provides inaccurate flow rates and consequently gives erroneous estimates of power production. With an ebb-only generation scheme, it predicted mean power output of 2 GW over a typical mean spring tidal cycle, a decrease of a maximum water level upstream of the barrage by 0.5-1.5 m, and a significant decrease of the maximum tidal currents in the main channel.

The same model was also used in a study that investigated two alternative TRS projects in the Severn Estuary – the Fleming Lagoon and the Shoots Barrage (Xia et al. 2010b). Both alternatives were considered because of the smaller size, therefore reducing the ecological footprint of the project. The study concluded that the Fleming Lagoon would have little influence on the hydrodynamic processes in the estuary, while both barrages (Severn and Shoots) induced much more significant environmental impacts, such as a marked reduction in the water body exchange and the permanent flooding of some intertidal zones in the impounded basin area. The reported power output over a typical spring tidal cycle was 31.1 GWh, 5.6 GWh and 5.1 GWh for the Cardiff-Weston barrage, Shoots Barrage and Fleming lagoon respectively. In addition to a greater yield of produced power, the Severn barrage would also contribute to some positive hydrodynamic effects, especially with regard to the flood risk reduction.

In a study by Falconer et al. (2009) the above model was refined by replacing the orifice equation with a hill chart. A hill chart is a manufacturing characteristic of a turbine and it relates the specific discharge and power production efficiency to the instantaneous head difference across the turbine, thereby more accurately predicting the turbine flow rate and power output. The refinements resulted in a reduction of the power output from 31.1 GWh to a more realistic 24.2 GWh over a mean spring tidal cycle. A further study by Xia et al. (2010b) used the same model to investigate the impact of different operating modes on water elevations and power

output. Three different schemes were considered – ebb-only, flood-only and two-way generation. Flood generation produced the least electricity, while ebb and two-way predicted similar outputs. Two-way generation also raised concerns over increased flood risk and environmental impacts due to a reduced tidal range upstream of the barrage, making it less favourable of the two options.

The estimation of power output was further improved by Xia et al. (2012), where the simulation was extended over a full neap-spring tidal cycle, to include the neap-spring variation in tidal range. An extrapolation of the results over the whole year resulted in the estimated tidal energy output ranging between 13 and 16 TWh per annum, which is similar to 15.6 TWh per annum reported in DECC (2010). The study showed that more detailed information on the barrage and turbine parameters will result in more accurate predictions, indicating also that the power output from the Severn Barrage could be increased with technological advances in the sluice gate and turbine performance. The model was also used to investigate the role of the barrage in the future coastal flood risk in the estuary (Xia et al. 2011). Different seaward boundary scenarios were used, simulating the rise of the water surface elevation due to climate change. The results indicated that the construction of the barrage would help mitigate the impacts of the sea level rise by reducing the maximum water elevation upstream of the barrage.

Similar conclusions were presented in another study that investigated the impacts of Severn barrage on the sea level rise (Ahmadian et al. 2014b). To reduce uncertainties arising from the treatment of the open boundary and increase the accuracy of the model, a cascade of three one-way nested models was employed to dynamically downscale the hydrodynamic processes from a global (ocean and atmospheric) model, through a regional (Irish Sea model), to a local coastal scale (Severn Estuary) model. The results showed that the barrage would reduce flood risk and showed no significant change in the electricity output due to the sea level rise.

The Severn barrage was also studied using DIVAST (Depth-Integrated Velocities and Solute Transport), a 2D hydro-environmental numerical model developed at Hydro-environmental Research Centre (HRC) in Cardiff University. In the study by Ahmadian et al. (2010a) DIVAST was dynamically linked with a 1D model, to Simulate the sediment transport and water quality indicator processes. 1D model covered the meandering upstream reach of the Severn Estuary, while the rest of the estuary together with the Bristol Channel fell into the 2D domain. Results showed that changes in tidal currents due to the construction of a barrage correspond to the reduction in suspended sediment levels, leading to a reduction in the concentration

levels of faecal bacteria and increased light penetration within the water column. This raised concerns from an ecological point of view, as the changes will also affect the benthic biodiversity of the estuary. The same model was later used to compare between ebb-only and two-way operational scheme (Ahmadian et al. 2014a). Results showed a larger decrease in the suspended sediment levels in the case of an ebb-only generation scheme, favouring the two-way operational scheme due to the smaller impacts on the environment.

EFDC (Environmental Fluid Dynamics Code) is another hydrodynamic modelling suite that was used to model the Severn barrage. EFDC is an open-source code developed and supported by the engineering company Dynamic Solutions-International. The model is based on the finite difference scheme, employed on an orthogonal curvilinear grid, and is widely used for modelling shallow water conditions in reservoirs and estuaries (Hamrick 1992). The code was first adapted for the simulation of TRS in a study by Zhou et al. (2014c), including the numerical implementation of hydraulic structures to represent turbines and sluice gates, the use of hill chart to calculate turbine flow rate and implementation of operational sequence algorithm for different operating modes. The barrage properties were based on the characteristics presented in a study by Falconer et al. (2009). An ebb-only generation scheme was used to investigate the impact of the barrage on hydrodynamics and salinity distribution in the estuary.

The model was used in a study that investigated the effects of the barrage on the open boundary (Zhou et al. 2014c). The seaward boundary of the Severn Estuary model was extended (i) to include the Irish Sea and (ii) reaching the continental shelf. Noticeable differences along the open boundary were observed when including the barrage in the simulation. The study demonstrated the need to consider a large computational domain when investigating large scale structures in the estuary, as the effects on the maximum sea level were observed far beyond the initial boundary condition.

Next study by Zhou et al. (2014b) focused on the optimisation of the Severn barrage, as it considered different configurations of the turbines and sluice gates. With advances in technology, a new type of tidal turbines that were designed for high efficiency at very-low heads was investigated (Atkins and Rolls-Royce 2010). In addition to the conventional proposal with 216 turbines and 166 sluices, two new designs with no sluices and 382 and 764 turbines respectively were included. The study concluded that new technology offers the best mitigating effects for the flood risks and significantly reduces the environmental impact of the barrage. The resulting

flow patterns around the barrage were closest to the existing natural conditions because the barrage could operate at much lower heads.

EFDC was again used in a study by Bray et al. (2016), where the continental shelf model was used to perform sensitivity analysis of the sluice gate discharge coefficient, which showed that performance of the barrage is not sensitive to the changes of the coefficient value and that any power losses due to uncertainty of its value can be easily mitigated by increasing the sluice gate capacity.

The long list of the collected literature above indicates the gradual progression from a simple conceptual model to a flexible and stable numerical model, that can be used for tidal energy analysis in the Severn estuary and investigation of hydrodynamic processes related to the operation of tidal range structures. The Severn barrage project proved to be an ideal case for the development and innovation of numerical modelling techniques related to TRSs. The combined outcome of the selected literature is a robust framework that has been so far implemented into several different hydrodynamic software suites, including DIVAST, EFDC and Delft3D. It has been so far used for:

- hydrodynamic analysis,
- energy output estimation,
- optimisation of the barrage operation,
- sediment transport and water quality analysis,
- flood risk analysis,
- far-field impacts on water levels beyond the open boundary,
- mitigation of flood risk due to climate change induced sea level rise, and
- informing on the design characteristics of the proposed projects (i.e. number of turbines and sluice gates, type of turbines, operation mode, etc.).

The majority of the studies above were based on a 2D depth-averaged model of the estuary. While 2D models are generally accurate for predicting water elevation, they are unreliable for simulating more complex flow patterns due to the depth-averaging of the vertical velocity profile. Such flow properties are commonly present during the operation of TRSs, especially in the vicinity of the turbines where submerged high-velocity jets radically change the shape of the vertical velocity profile. An expansion to 3D modelling of TRSs has been scarcely reported to date; 3D models would greatly contribute to the appreciation of the complex flow conditions generated by the hydraulic structure-induced water jets (Neill et al. 2018). This was the main motivation for the implementation of the TRS methodologies into the Delft3D software.

2.3.7. Evolution of numerical modelling of the Swansea Bay lagoon

Swansea Bay lagoon is the most recent TRS project that is currently being considered in the UK (Waters and Aggidis 2016a). It is considerably smaller than the proposed Severn barrage and is viewed as a pilot project for TRS deployment in the Severn Estuary and Bristol Channel region. A number of studies have emerged in recent years, that focused mainly on predicting and optimising the power output of the scheme.

The initial estimation came from a study by Petley and Aggidis (2016), which employed a zero-dimensional (0D) computational model. 0D model is a simplified method for estimating the performance of a TRS (Aggidis and Benzon 2013). It works by accounting the changes of the water level inside the lagoon, assuming they are equivalent to the volume transferred in/out of the lagoon, divided by the surface area of the impoundment at that specific time. Because it is fast, simple to compose and computationally inexpensive, it can be particularly useful for the preliminary studies of the TRS performance in the design stage of a project. Utilizing a hill chart for tidal-range specific turbines (Andritz Hydro 2016), the study tested lagoon's efficiency under different operational modes, i.e. two-way generation, ebb-only generation, and ebb generation with pumping. The study predicted an annual power generation of 596.04 GWh for the ebb-only scheme, significantly more than a 479.8 GWh prediction for a two-way scheme. These predictions assumed a constant starting head difference throughout the simulation; the starting head has been carefully selected with an aim to achieve the most efficient power generation on average over a spring-neap tidal cycle.

However, the generation could be further optimised by regulating the operational parameters in order to account for the variability of the tidal range. A methodology for such optimisation was presented in a study by Angeloudis et al. (2018), which considered a simultaneous operation of Swansea Bay and Cardiff lagoons. The optimisation method resulted in a significant increase in annual power production. For the Swansea Bay lagoon with a two-way generation mode, it resulted in 463 GWh annually, rising to 569 GWh when including pumping. A similar study was performed by Xue et al. (2019), where a 10 per cent increase in efficiency was reported for the Swansea Bay lagoon with a two-way generation. These studies have illustrated the usefulness of the 0D method for the preliminary assessment and its contribution towards a more informed design process.

However, there is a downside to the 0D modelling. For computational efficiency, the method sacrifices the information on local hydrodynamics. While this trade-off is acceptable for the needs of preliminary assessments, it falls short when performing more advanced studies, such as analysis of environmental impacts, which require a more complex and accurate hydrodynamic model.

A 2D hydrodynamic simulation of Swansea Bay lagoon was first presented in a study by Angeloudis et al. (2016b). The study employed a 2D finite-volume model with an unstructured grid and included an additional refinement to the internal boundary condition to conserve the momentum on the incoming and outgoing flow through the structure. The results showed that the deviation on power predictions between the 0D and 2D methodologies depends on the manner the impoundment interferes with the existing flow and may vary on a case by case basis. For Swansea Bay lagoon the deviation was shown to be small enough to still consider 0D valid; 2D model predicted 490 GWh annually compared to 530 GWh annually predicted by the 0D model. A model with an optimised operational sequence in a later study (Angeloudis and Falconer 2017) increased the predicted power output to 586 GWh annually. The predicted annual power output estimates across the mentioned studies are collated in Table 4

Table 4: Estimated annual energy output in GWh/yr. for Swansea Bay tidal lagoon as predicted across different studies.

Study	**0D [GWh/yr.]**	**2D [GWh/yr.]**
(Petley and Aggidis 2016)		
Two-way	479	-
Ebb-only	596	-
Ebb-only (optimised)	727	-
Ebb-only (w/ pumping, optimised)	732	-
(Angeloudis et al. 2016b)		
Two-way	530	490
(Angeloudis and Falconer 2017)		
Ebb-only	315	292
Two-way (conservative)	507	474
Two-way (optimised)	615	586
(Angeloudis et al. 2018)		
Two-way	-	417
Two-way (optimised)	-	463
Two-way (w/ pumping)	-	515
Two-way (w/ pumping, optimised)	-	569

So far, the studies involving numerical modelling of the Swansea Bay lagoon were mostly interested in the energy efficiency of the scheme. Little attention was given to the assessment of the environmental impacts. Angeloudis et al. (2016b) did investigate the effects of the refined momentum treatment on the local flow patterns, however, the main motivation behind this was to determine the extent of the 2D hydrodynamic effect on the energy extraction. A more detailed analysis of the environmental impacts is required to provide a more informed view of the appropriateness of the scheme.

2.3.8. 3D models

As already mentioned before, regional scale 3D models of TRSs have been scarcely reported in the literature. This is mainly due to the expensive computational costs of the 3D models; due to the present limitations of computational resources, they are currently constrained to smaller scale hydraulic engineering applications, such as laboratory-scale flows (Jeffcoate et al. 2017; Jeffcoate et al. 2013; Oh et al. 2016) and turbomachinery simulations (Wilhelm et al. 2016b; Wilhelm et al. 2016a).

The regional scale 3D models are usually based on a 2D grid that was extended in a vertical direction by the addition of several vertical layers. They are derived from the large-scale oceanic models and can employ hydrostatic or non-hydrostatic forms of Navier-Stokes equations (Marshall et al. 1997). At the time of writing, the use of a 3D hydrostatic model on a regional scale has been limited to the modelling of tidal stream extraction (Lin et al. 2015; Rahman and Venugopal 2015). Both studies employed a Delft3D model, where tidal stream turbines were modelled as an actuator disk – a methodology commonly used with wind turbines. In both studies, the 3D modelling resulted in increased accuracy of the results. However, even though the authors have not reported the required computational time, a concern was raised about the number of vertical layers. A full set of the PDEs has to be solved for each layer, meaning that the total computational time increases by the factor equivalent to the number of layers.

A study by Stansby et al. (2016) employed a 3D Telemac model to investigate the oscillatory flow around a headland. This study is not directly connected to the tidal range modelling, however, the recirculating flow conditions resulting from flow around a headland closely resemble the large eddies induced by the high-velocity jets from a TRS. The results showed marked differences between the 2D and 3D models, with the depth-averaged model considerably over predicting the velocity magnitude. For TRS modelling this could have a notable impact on the local

hydrodynamic conditions, directly affecting the water surface levels in the vicinity of the turbines, and indirectly affecting the estimation of generated energy that is governed by the head difference across the structure. In addition, a 2D depth-averaged model has been proved inadequate for predicting local scour and deposition (Jeffcoate et al. 2017). A 3D model will result in more accurate predictions of the bed shear stress downstream of the turbines, which is important from an environmental point of view - bed shear stress is instrumental for the sediment transport processes.

Therefore, the main reason for 3D modelling of TRS structures are:

- appreciation of the 3D conditions generated by the TRS-induced water jets,
- increased accuracy of the hydrodynamic conditions in the vicinity of the hydraulic structures, and
- accurate prediction of the bed shear stress downstream of the hydraulic structures.

2.3.9. Momentum conservation

The flow through hydraulic structures, that represent turbines and sluice gates in a TRS hydrodynamic model, is calculated off the numerical grid and added to the simulation as a source/sink term or an internal boundary condition. A study by Angeloudis et al. (2016b) highlighted the importance of the correct momentum transfer through hydraulic structures of a TRS. The study showed that the velocity of the jet exiting a turbine could easily exceed 10 m/s. Such a magnitude would have a significant influence on the simulated velocity field, water quality, sediment transport, morphological and ecological processes due to the corresponding momentum of the jet. The paper tested certain formulations for their effect on the momentum flow through the depth-averaged model. The momentum conservation was applied to a finite-volume model by the way of a special internal boundary; the water depth across the boundary was artificially fixed to the value that forced the cell interface area to match the flow-through area of the turbine. The study found that the treatment of momentum can play a significant role in the prediction of the velocity field. Tests on TRSs of different sizes showed that the effect is particularly pronounced for the smaller schemes, such as lagoons, and less so for larger schemes; for the Severn Barrage, the results were largely independent of the momentum treatment.

The value of 10 m/s in (Angeloudis et al. 2016b) was obtained by dividing the discharge of a turbine with the minimum flow area at a turbine section (i.e. cross-

sectional area at the location of the runner blade, the diameter of which also signifies the size of the turbine; denoted as D_M in Figure 13). This value is questionable, as it would mean that the flow through a turbine completely ignores any hydraulic losses due to the flow through the diffuser-shaped draft tube. The main role of a draft tube is to increase the pressure of the exiting fluid at the expense of its velocity (Gubin 1973), which would imply that the draft tubes were either not designed properly or that their effect was ignored in the case above.

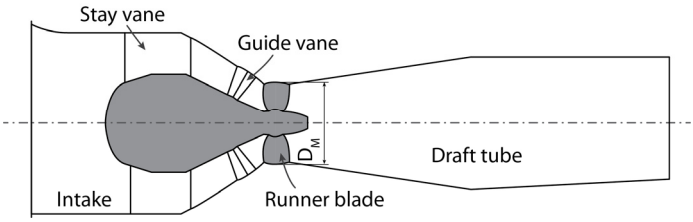

Figure 13: Bulb turbine cross-section. Adapted from Wilhelm et al. (2016a).

The difference in the velocity profile at the turbine runner and at the draft tube exit was demonstrated in a study by Wilhelm et al. (2016b). The magnitude of the axial velocity at the draft tube exit was between 40 and 60 per cent of the magnitude at the runner and was relatively evenly distributed across the draft tube cross-section. Such a velocity distribution would have a significantly lesser impact on the hydrodynamic velocity field compared to the velocity profile assumed in the study by Angeloudis et al. (2016b).

To further investigate the impact of the momentum, transfer through the hydraulic structures, a new methodology was developed and applied to the case studies presented in this book. The method is compatible with the Delft3D's finite-difference numerical scheme and can be applied to both 2D depth-averaged and 3D hydrostatic models. A detailed description and formulation of the method are given in Section 3.3.3.

2.4. Conclusions

Tidal range technology has great potential for expanding UK's renewable energy portfolio, due to the enormous amounts of available capacity on the West Coast, particularly in the Severn Estuary and Bristol Channel. The technology has been proven successful by several projects worldwide, some of them operational for more than half of century. The scientific knowledge is rapidly advancing, making the

technology more efficient and resilient. Significant investigations into the impacts of tidal power are required to reduce the uncertainties connected with TRS operation and make the technology worthwhile. This includes hydrodynamic modelling of the TRS structures, which requires a robust and flexible numerical model that can provide accurate and reliable predictions.

The overview of the existing numerical models has shown that a multi-scale approach has to be undertaken when simulating TRS operation. The models usually employ a relatively large domain, to assure that TRS operation does not interfere with the open boundary conditions. At the same time, special attention has to be given to local hydrodynamic effects deriving from the TRS operation, i.e. high-velocity jet exiting the turbines. Certain studies have identified the importance of the correct application of momentum transfer in regard to the turbine discharge, however, the implications of the method have not been thoroughly assessed, with a limited explanation of the theoretical background for the used methodology. To address these shortcomings, a novel method for momentum conservation is presented in this study, that was applied to the Delft3D model and tested on the Swansea Bay lagoon model. The study provides an assessment of how the novel method affects the hydrodynamic predictions, as well as its impacts on bed erosion and sediment transport.

The review has also identified a lack of 3D simulations in TRS studies. Because of the shallow water aspect, 3D models are often considered unnecessary for modelling estuarine hydrodynamics. However, due to the complexity of the high-velocity jets in the vicinity of the structures, 3D simulations could provide a more informed understanding of the flow patterns forming downstream of the turbines, which are essential for correct estimations of power output as well as for accurate predictions of the bed shear stress. Using the Delft3D software, this study also provides the comparison between the 2D and 3D simulations of the same case study, with an aim to evaluate the differences between the two and to assess the role of 3D simulations in TRS models.

3
THEORETICAL BACKGROUND

This chapter presents the theoretical background of methods that were applied to the case studies presented in this book. This includes description of fundamental hydrodynamic equations, on which the numerical model is based; description of numerical methods commonly associated with hydrodynamic modelling; overview of the Delft3D software suite; and methodology for implementing a TRS module into the model. The methodologies include routines for simulating the operation of TRSs, numerical representations of hydraulic objects, and method for momentum conservation of flow through turbines and sluices.

3.1. Governing equations

Any type of fluid flow can be simulated using a set of four Partial Differential Equations (PDE):

- continuity of mass,
- conservation of momentum,
- equation of state, and
- conservation of energy.

However, in most practical hydro-environmental engineering problems, only the continuity and momentum equations are required for accurate simulation of the fluid flow (Rajar 1997).

The continuity equation governs the conservation of mass. By definition, it demands that the net fluid mass entering a control volume equals the amount by which the mass of the control volume changes in a specific time interval (Rajar 1997). Considering the assumption of the incompressible flow, which can be applied in the

majority of hydro-environmental engineering problems, the density of the fluid will stay constant over time. The continuity equation in its incompressible form can be written as:

$$\frac{\partial u}{\partial x}+\frac{\partial v}{\partial y}+\frac{\partial w}{\partial z}=0 \tag{1}$$

here *u*, *v* and *w* are the velocity components in the main Cartesian directions *x*, *y* and *z*.

The momentum equations describe the motion of viscous fluids. The equations are derived by applying Newton's second law of motion to an infinitesimal fluid element, assuming the stress in the fluid is the sum of the viscous and pressure terms. The Momentum equations in the three cardinal directions of the Cartesian coordinate system in their general form are given as (Rajar 1997):

$$\begin{aligned}&\frac{\partial u}{\partial t}+\frac{\partial u}{\partial x}u+\frac{\partial u}{\partial y}v+\frac{\partial u}{\partial z}w\\&\qquad=f_x-\frac{1}{\rho}\frac{\partial P}{\partial x}+\nu\left(\frac{\partial^2 u}{\partial x^2}+\frac{\partial^2 u}{\partial y^2}+\frac{\partial^2 u}{\partial z^2}\right)+\frac{\nu}{3}\frac{\partial}{\partial x}\left(\frac{\partial u}{\partial x}+\frac{\partial v}{\partial y}+\frac{\partial w}{\partial z}\right)\end{aligned} \tag{2}$$

$$\begin{aligned}&\frac{\partial v}{\partial t}+\frac{\partial v}{\partial x}u+\frac{\partial v}{\partial y}v+\frac{\partial v}{\partial z}w\\&\qquad=f_y-\frac{1}{\rho}\frac{\partial P}{\partial y}+\nu\left(\frac{\partial^2 v}{\partial x^2}+\frac{\partial^2 v}{\partial y^2}+\frac{\partial^2 v}{\partial z^2}\right)+\frac{\nu}{3}\frac{\partial}{\partial y}\left(\frac{\partial u}{\partial x}+\frac{\partial v}{\partial y}+\frac{\partial w}{\partial z}\right)\end{aligned} \tag{3}$$

$$\begin{aligned}&\frac{\partial w}{\partial t}+\frac{\partial w}{\partial x}u+\frac{\partial w}{\partial y}v+\frac{\partial w}{\partial z}w\\&\qquad=f_z-\frac{1}{\rho}\frac{\partial P}{\partial z}+\nu\left(\frac{\partial^2 w}{\partial x^2}+\frac{\partial^2 w}{\partial y^2}+\frac{\partial^2 w}{\partial z^2}\right)+\frac{\nu}{3}\frac{\partial}{\partial z}\left(\frac{\partial u}{\partial x}+\frac{\partial v}{\partial y}+\frac{\partial w}{\partial z}\right)\end{aligned} \tag{4}$$

where *t* is time, *P* is the pressure gradient, f_x, f_y and f_z are the external body forces and *v* is the kinematic viscosity defined as:

$$\nu=\frac{\mu}{\rho} \tag{5}$$

with μ the dynamic viscosity of the fluid.

The continuity equation (1) and momentum equations (2)–(4) together form the fundamental system of equations for simulating fluids in motion, also commonly known as Navier-Stokes equations.

3.1.1. Numerical methods

Numerical methods are mathematical tools designed to solve complex numerical problems, e.g. solving a system of PDEs over large-scale spatial and temporal dimensions. As such, numerical methods are widely used for analysis of the

underlying fluid dynamic behaviour governed by system of hydrodynamic equations (Rijkswaterstaat 2016). The numerical methods replace the complex PDEs with a set of algebraic equations, which calculate the system variables at discrete points in space and time domains (Neelz and Pender 2009). The process of obtaining these algebraic equations is called discretisation, and there are numerous methods available for the space-time discretisation of governing equations.

Spatial discretisation

There are three main strategies for spatial discretization of PDEs:

- finite difference methods (FDM);
- finite element methods (FEM); and
- finite volume methods (FVM) (Neelz and Pender 2009).

The FDM solves the differential equations by replacing the derivatives of state variables with their finite difference approximation via the Taylor series expansion, which describes the derivatives of the variables as finite differences between the values of the neighbouring points (Neelz and Pender 2009). The main advantage of the FDM is its straightforward solution and well defined implementation, however, it is limited to structured regular grids (Alcrudo 2004).

In FEM, the whole domain is divided into a number of smaller finite elements, where each element is represented by an individual set of simplified equations (Zienkiewicz and Taylor 2000). A large advantage of the method comes from a very flexible sub-division of the domain that allows for a fully unstructured mesh for more accurate representation of complex geometries (Reddy 1993). On the other hand, this does make it computationally expensive, with a large amount of computational time consumed at every time-step.

The FVM is one of the most versatile and most commonly used discretisation techniques for hydrodynamic models (Alcrudo 2004). It follows the concept of control volume formulation used in analytical fluid dynamics, where the domain is subdivided into several smaller control volumes, also referred to as cells. The PDEs are then integrated over each cell based on fluxes through the control volume boundaries (Neelz and Pender 2009). The method is highly popular in fluid dynamics due to its full conservation of mass and momentum, its applicability to all types of meshes and the simplicity of its formulation (Alcrudo 2004).

Temporal discretisation

Strategies for time-discretisation of hydrodynamic equations can be divided into three main categories:

- explicit schemes,
- implicit scheme, and
- semi-implicit schemes.

In explicit or forward-looking schemes, the state of the system at the current time-step is calculated directly from the known values of the state variables from the previous time-step. Because explicit schemes are easy to implement, they are used in the vast majority of the newly developed models and research codes (Hunter et al. 2007). However, they are prone to numerical instability in the shape of unphysical numerical oscillations in the numerical solution (Neelz and Pender 2009).

In implicit or backward-looking schemes, the calculation of the dependant variables involves both the state of the system at the current time-step and previous time-step. All the computational cells are coupled together to form a single matrix that is solved using an iterative technique. This enables the transmission of the hydraulic effects across the entire computational domain, but also increases the computational cost due to the increased complexity of the model (Hunter et al. 2007).

Semi-implicit schemes, also used by Delft3D, combine the advantages of both by treating some of the derivatives explicitly and some implicitly. Conceptually, the schemes split up the terms in such a way that the largest stable time-step for the semi-implicit discretisation is significantly larger than for a corresponding explicit discretisation, significantly reducing the computational time required to solve the equations (Fulton 2004). Therefore, the semi-implicit schemes are computationally efficient, while at the same time producing numerically stable solutions with no loss in accuracy (Rosatti et al. 2011).

3.2. Short description of Delft3D

Delft3D is a 3D modelling software suite that integrates flow and transport modelling systems for aquatic environments. It was developed by Deltares in the Netherlands and is available in open source. The software package consists of several integrated modules, with Delft3D-FLOW module being the main engine for hydrodynamic simulations. All simulations presented within this research were performed with the

Delft3D-FLOW numerical model. For brevity we will refer to Delft3D-FLOW as just Delft3D from here on.

Delft3D provides a numerical algorithm for the solution of Navier-Stokes equations in shallow-water conditions and for incompressible fluids. It is capable of solving both 2D depth-averaged and 3D unsteady flow problems. The system of PDEs, in combination with an appropriate set of initial and boundary conditions, is solved on a staggered finite difference grid, illustrated in Figure 14. This particular arrangement of the variables is called the Arakawa C-grid in which all scalar variables, for example density and water level, are located at the cell centre, whereas the velocity component in a given direction is stored at the cell side orthogonal to that direction. Using the staggered grid, the number of computational values is decreased by a factor of four, significantly increasing the computational efficiency, while the same level of accuracy is preserved as with a collocated grid (Rijkswaterstaat 2016).

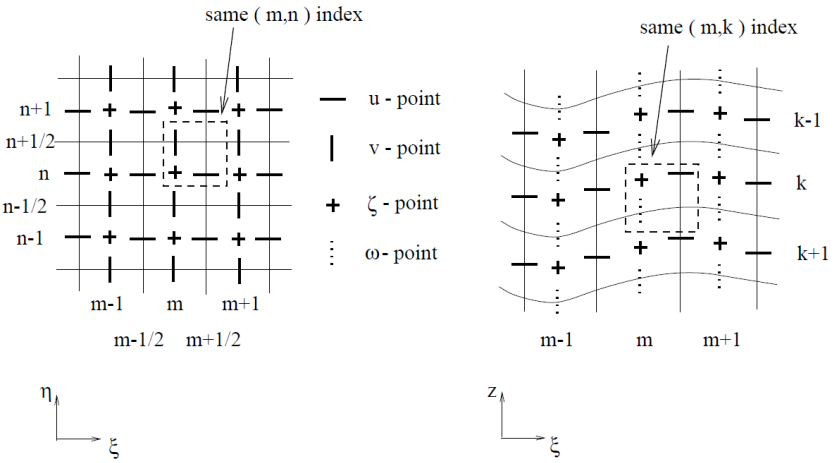

Figure 14: Arrangement of the unknowns for staggered grid (Rijkswaterstaat 2016).

The computational domain is represented with an orthogonal curvilinear grid, that can be defined in Cartesian or spherical coordinates. Its advantage over regular rectangular grids is its ability to smoothly follow the irregular land features, such as rivers, estuaries and coastlines. In Cartesian space, the coordinates of the grid nodes are assigned as easting and northing in meters. Alternatively, they can be defined with the spherical coordinates, which are especially useful for large-scale numerical models, where it makes more sense to define the grid in degrees of longitude and latitude (Deltares 2014).

The curvilinear grid is numerically transformed from the physical space (Ω) to the computational space (G_H), by the way of transformation coefficients $\sqrt{G_{\xi\xi}}$ and $\sqrt{G_{\eta\eta}}$ (Deltares 2014). The coefficients can be computed from the coordinates of the cell vertices, as illustrated in Figure 15.

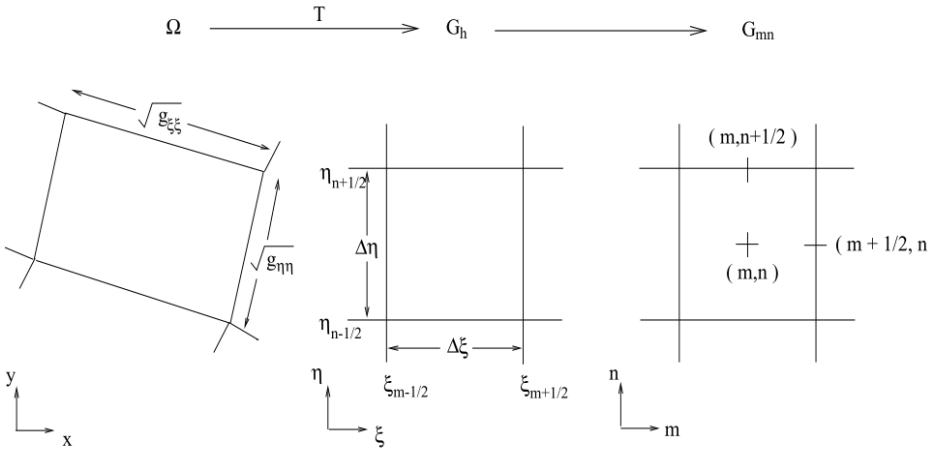

Figure 15: Mapping of physical space Ω to computational space G_H. G_{mn} represents the locations of the unknown variables (Rijkswaterstaat 2016).

Delft3D offers two different grid systems in the vertical direction: i) the σ vertical coordinate system also known as σ-grid for short, and ii) Z vertical coordinate system (also Z-grid). The equations for both systems are similar, as both grids split the model into several layers in the vertical direction (Deltares 2014). The fundamental difference between the two is how these layers are illustrated in Figure 16.

All simulations in this study employed the σ-grid (Figure 16a) which is defined by a σ coordinate system (Figure 17). The layers of the σ-grid are not strictly horizontal, but instead, follow the shape of the free surface at the top and the shape of the closed boundary at the bottom. The relative thickness of the layers is predetermined at the input by the user and is uniform over the entire horizontal domain. In a 3D shallow-water model each layer is solved with a set of coupled conservation equations, representing the vertical interaction between the layers. The sole exceptions are the topmost and bottommost layers where horizontal boundaries have to be taken into account (Deltares 2014).

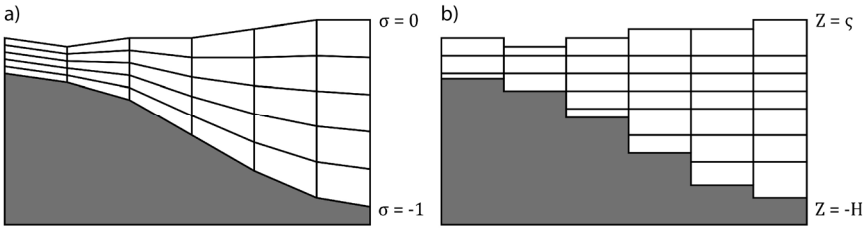

Figure 16: Illustration of the fundamental differences between the σ-grid (a) and Z-grid (b) vertical coordinate systems available in Delft3D.

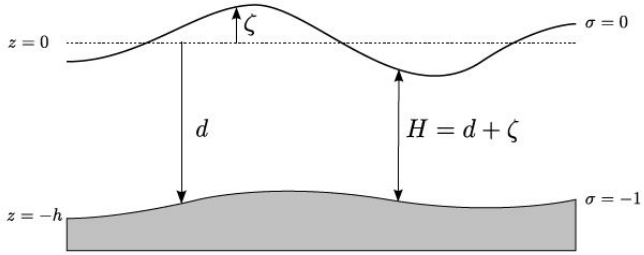

Figure 17: Definition of the σ coordinate system and characteristic parameters describing depth (d), water level (ς) and total depth (H) (Deltares 2014).

The depth-averaged form of the continuity equation (6) is derived from the general form for incompressible fluids by integrating it over the total depth (Deltares 2014):

$$\frac{\partial \zeta}{\partial t} + \frac{1}{\sqrt{G_{\xi\xi}}\sqrt{G_{\eta\eta}}}\frac{\partial HU\sqrt{G_{\eta\eta}}}{\partial \xi} + \frac{1}{\sqrt{G_{\xi\xi}}\sqrt{G_{\eta\eta}}}\frac{\partial HV\sqrt{G_{\xi\xi}}}{\partial \eta} = \mathrm{H}Q \qquad (6)$$

where t is time (s), ξ and η are the horizontal, curvilinear coordinates [m], and $\sqrt{G_{\xi\xi}}$ and $\sqrt{G_{\eta\eta}}$ are the transformation coefficients [m] between the curvilinear grid and rectangular coordinate system, and Q a global source or sink per unit area (ms^{-1}). U and V are the depth averaged velocities (ms^{-1}) in ξ and η directions which can both be, considering Figure 17, expressed in the Cartesian and σ-grid forms:

$$U = \frac{1}{H}\int_d^{\zeta} u\, dz = \int_{-1}^{0} u\, d\sigma \qquad (7)$$

$$V = \frac{1}{H}\int_d^{\zeta} v\, dz = \int_{-1}^{0} v\, d\sigma \qquad (8)$$

with u and v representing flow velocities (ms^{-1}) in ξ and η directions. Finally, Q represents the contribution of the external water discharge or water withdrawal per unit area, including the precipitation and evaporation:

$$Q = \int_{-1}^{0} (q_{in} - q_{out})\, d\sigma + P - E \tag{9}$$

where q_{in} and q_{out} represent the local source and sink terms per unit volume (s^{-1}), while P and E characterise respectively the source term of precipitation and sink term of evaporation (ms^{-1}).

The momentum equations (2) and (3) in the horizontal direction are accordingly adapted for the curvilinear grid ξ and η (Deltares 2014). The equations are formulated per layer (layer-averaged), and are given as Equations (10) and (11):

$$\begin{aligned}&\frac{\partial u}{\partial t} + \frac{u}{\sqrt{G_{\xi\xi}}}\frac{\partial u}{\partial \xi} + \frac{v}{\sqrt{G_{\eta\eta}}}\frac{\partial u}{\partial \eta} + \frac{\omega}{d+\varsigma}\frac{\partial u}{\partial \sigma} - \frac{v^2}{\sqrt{G_{\xi\xi}}\sqrt{G_{\eta\eta}}}\frac{\partial \sqrt{G_{\eta\eta}}}{\partial \xi} \\ &\quad + \frac{uv}{\sqrt{G_{\xi\xi}}\sqrt{G_{\eta\eta}}}\frac{\partial \sqrt{G_{\xi\xi}}}{\partial \eta} - f_v = -\frac{1}{\rho_0\sqrt{G_{\xi\xi}}}P_\xi + F_\xi + \frac{1}{(d+\zeta)^2}\frac{\partial}{\partial \sigma}\left(\nu_V \frac{\partial u}{\partial \sigma}\right) + M_\xi\end{aligned} \tag{10}$$

$$\begin{aligned}&\frac{\partial u}{\partial t} + \frac{u}{\sqrt{G_{\xi\xi}}}\frac{\partial u}{\partial \xi} + \frac{v}{\sqrt{G_{\eta\eta}}}\frac{\partial u}{\partial \eta} + \frac{\omega}{d+\varsigma}\frac{\partial u}{\partial \sigma} - \frac{v^2}{\sqrt{G_{\xi\xi}}\sqrt{G_{\eta\eta}}}\frac{\partial \sqrt{G_{\eta\eta}}}{\partial \xi} \\ &\quad + \frac{uv}{\sqrt{G_{\xi\xi}}\sqrt{G_{\eta\eta}}}\frac{\partial \sqrt{G_{\xi\xi}}}{\partial \eta} - f_v = -\frac{1}{\rho_0\sqrt{G_{\xi\xi}}}P_\xi + F_\xi + \frac{1}{(d+\zeta)^2}\frac{\partial}{\partial \sigma}\left(\nu_V \frac{\partial u}{\partial \sigma}\right) + M_\xi\end{aligned} \tag{11}$$

where u and v are the flow velocities (ms^{-1}) in the ξ and η directions for a horizontal curvilinear coordinate system respectively, ζ is the water level above a reference datum [m], while d is the depth below the reference datum and together they form the total depth H. ω is the vertical velocity related to the moving σ plane (ms^{-1}), f_u and f_v are the Coriolis parameters (s^{-1}), ρ_0 is the density of water (kg/m^3), ν_V is the vertical eddy viscosity (m^2s^{-1}), P_ξ and P_η are the pressure gradients ($kg/(m^2s^2)$), forces F_ξ and F_η represent the imbalance of the horizontal Reynold's stresses (ms^{-2}), M_ξ and M_η represent the contributions due to external body forces (ms^{-2}), such as sources or sinks of momentum resulting from hydraulic structures, and $\sqrt{G_{\xi\xi}}$ and $\sqrt{G_{\eta\eta}}$ are the transformation coefficients between the curvilinear grid and rectangular coordinate system [m].

Delft3D employs the so-called three-dimensional hydrostatic model. In contrast to fully 3D RANS models, where the system of hydrodynamic equations is solved in all three dimensions, the 3D hydrostatic model instead solves the system under the shallow-water approximation neglecting the variation of velocity across the depth. The vertical momentum equation is thereby reduced to a hydrostatic pressure equation (Casulli and Stelling 1998). To account for the fundamental loss of information in the vertical direction, the model is divided into a fixed number of horizontal layers (Stelling and Van Kester 1994). The loss of information in the vertical direction is reduced by integrating the shallow-water equations over all the layers.

The 3D hydrostatic models are therefore not fully 3D, nevertheless, they have proved useful for providing additional information about the vertical structure of the flow quantities in shallow-water conditions, while not requiring computational resources for solving full 3D RANS models (Lesser et al. 2004).

Vertical velocities are consequently not involved in the process of solving the PDEs. If required, Delft3D calculates the "physical" vertical velocity (w) in the post-processing part of the simulation:

$$w = \omega + \frac{1}{\sqrt{G_{\xi\xi}}\sqrt{G_{\eta\eta}}}\left[u\sqrt{G_{\eta\eta}}\left(\sigma\frac{\partial H}{\partial \xi}+\frac{\partial \zeta}{\partial \xi}\right)+v\sqrt{G_{\xi\xi}}\left(\sigma\frac{\partial H}{\partial \eta}+\frac{\partial \zeta}{\partial \eta}\right)\right]+\left(\sigma\frac{\partial H}{\partial t}+\frac{\partial \zeta}{\partial t}\right) \qquad (12)$$

where ω is the relative vertical velocity of the moving σ-layer interfaces, which can be calculated from the continuity equation (6).

Delft3D allows the implementation of hydraulic structures in the numerical model. They are used to model the local effects of sub-grid scale disturbances of the flow, emanating from inclusion of structures such as gates, sluices, porous plates, bridges, weirs, culverts, etc. In the case of culverts, the flow through the object is simulated by a virtual transfer of the flow between the inflow at the intake and the discharge at the outfall. Culverts were used as foundation for the development of the subroutines for TRS operation. This was achieved by modifying the existing culvert subroutine to simulate the turbines and sluice gates of a tidal range power plant.

3.3. Modelling tidal range structures

TRSs are commonly modelled by splitting the domain into two physically separated subdomains by an impermeable structure. One subdomain covers the seaward side, spanning between the open boundary and the impoundment walls, and the other covers the retention basin on the inside of the impoundment walls. The transfer of the water between the two domains is achieved via hydraulic structures that represent the turbines and sluice gates of a TRS. There are two conceptually different ways for implementing the hydraulic structures, either as a special type of an internal boundary condition (Falconer et al. 2009), or as an external sink and source terms in the hydrodynamic equations (Brammer et al. 2014). This study employed the latter approach, implementing the hydraulic structures into the Delft3D model through the term Q in the continuity Equation (6), and terms M_ξ and M_η in the momentum Equations (10) and (11). It is worth emphasising that the flow through a hydraulic structure is not resolved on the grid. It is instead calculated off-grid through a sub-

grid scale model of the flow through the hydraulic structure and included in the solutions through sink and source terms in the hydrodynamic equations.

In order to simulate TRSs, a new subroutine (Figure 18) was added to the Delft3D source code. The subroutine requires user to set additional input parameters for TRS operation. They include:

- Locations of water level points (for head calculation)
- Locations of grid cells with turbines and sluices (intake/outfall)
- Turbine Q-H and P-H relationships
- Turbine and sluice loss coefficient
- Selected operational sequence

The subroutine is executed at every time step of the simulation, just before the programme proceeds to the routine for solving the system of hydrodynamic equations. Its main task is to determine the instantaneous flow rate and velocity through the implemented hydraulic structures and pass them on to the solution algorithm where they are included in the sink and source terms of the hydrodynamic equations.

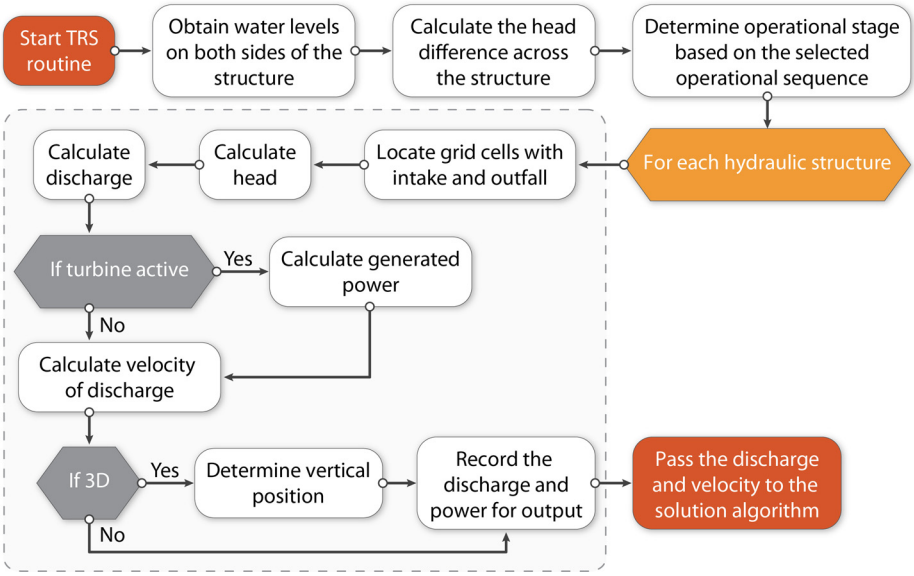

Figure 18: General algorithm for simulation of TRSs that was implemented in Delft3D

3.3.1. Operational sequence

TRSs take advantage of the difference in water level between the high and low tide by impounding the water within a basin (Roberts et al. 2016). When a sufficient hydraulic head difference is created, the water is released through the turbines installed in the impoundment walls to generate the electricity. The potential power of a TRS (P) is fundamentally proportional to the wetted surface area of the impoundment (A) and the square of the head difference (h^2) between the two sides of the structure, as given by the Equation (13) (Angeloudis et al. 2016b):

$$P \propto Ah^2 \tag{13}$$

Both factors are foremostly determined by the geographical location of the structure, however, the head difference can be artificially altered and hence optimised by adjusting the operational sequence of the scheme.

The operational sequence of a TRS is a pre-programmed list of commands that govern the power generation by manipulating the discharge through the turbines and sluice gates. TRSs can be operated under various operational sequences, such as ebb generation, flood generation (both one-way), and two-way generation (Xia et al. 2010a). The selection of an appropriate scheme is constrained by the location of the impoundment, the design of the installed turbines and sluice gates, the requirements of the National Grid, and other considerations such as environmental constraints or maintaining the required depth for navigation (Angeloudis and Falconer 2017).

In a one-way generation operational sequence, the power can be generated during either ebb or flood tide, but not during both. If, for example, an ebb tide is used for power generation, then the flood tide will be used for filling of the retention basin. This scheme is commonly known as ebb generation and is illustrated in Figure 19. The stage-by-stage description is given from the point of the low tide, just as the water starts rising at the beginning of the flood cycle. At this point, the TRS is at the filling stage, the sluice gates are wide opened and turbines are closed, allowing the water to flow into the impoundment. When the difference in water levels between the two sides falls to zero, the sluice gates are closed and the holding stage is instigated. The role of the holding stage is to achieve a sufficient head difference for power generation between the water levels inside and outside. While the closed sluice gates hold the inside water level at the high point, the water level on the outside is falling due to the ebb tide. The generation stage begins once a sufficient head difference, shown as H_{st} in Figure 19, is established. The turbines start operating, allowing the water to flow out of the basin while generating power. The

generation stage is terminated as soon as the head difference falls below the minimum required head difference for efficient power generation, denoted by H_{min}. This triggers a second holding stage, preventing the inside water level to fall even further. The sluice gates are reopened when the water surface again starts rising and the whole process is repeated for the next tidal cycle.

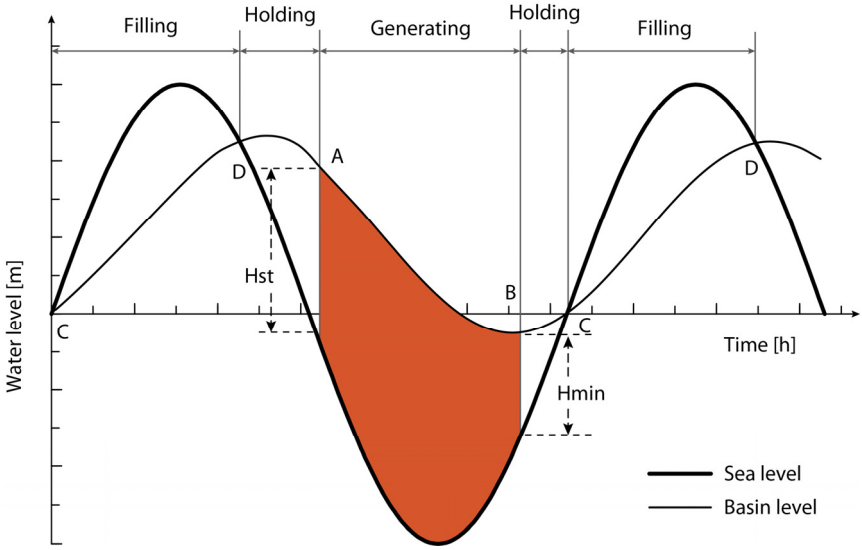

Figure 19: Diagram of a one-way operating sequence with generation during ebb tide (i.e. ebb-generation). Adapted from Xia et al. (2010b).

Flood generation operational scheme works in a reverse fashion compared to the ebb generation. Here, power is generated during the flood tide and the releasing stage occurs during the ebb tide instead. The aim of the releasing stage here is to empty the basin as much as possible to maximise the head difference of the next generation stage. The sequence is generally much less efficient as the available head difference reduces more quickly than it would for an ebb generation. This is because the volume in the upper half of the basin, where ebb generation operates, is normally much greater than the volume of the lower half, where flood generation operates (Xia et al. 2010a).

Two-way generation operational sequence generates power on both ebb and flood tides, as shown in Figure 20. The scheme is more complicated and involves more stages compared to the one-way schemes. It also requires a more complex type of turbines that can generate power in both directions (Waters and Aggidis 2016b).

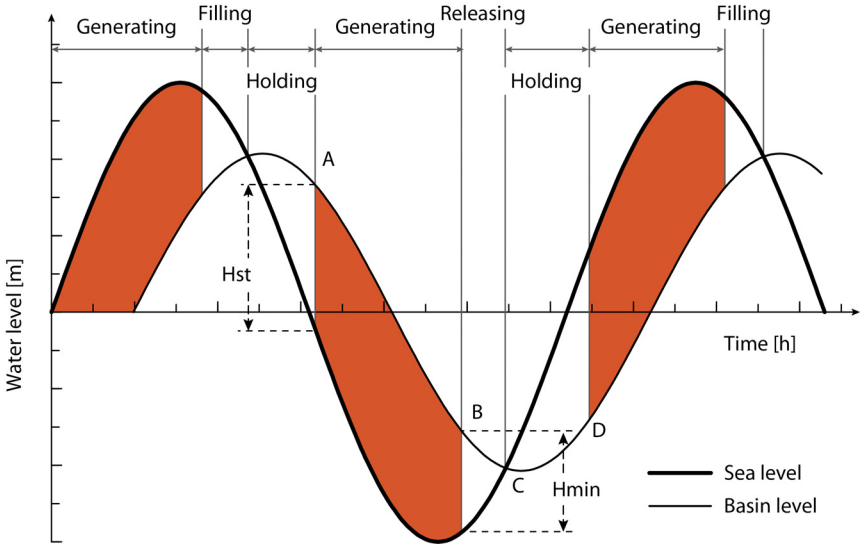

Figure 20: Diagram of a two-way operating sequence with generation during both ebb and flood tides. Adapted from Xia et al. (2010b).

Starting at high water, the first generation stage begins during an ebb tide after a sufficient head difference is established, same as in the ebb-only mode. However, when the head difference falls under the minimum value for efficient generation, a releasing (or sluicing) stage is initiated instead of the holding stage. During the releasing stage the turbines are not operating but opened and sluice gates are opened in order to draw down the water level inside the basin as much as possible. Only when the water levels on the inside and outside are equal and no water can flow out of the basin, the holding stage can begin. During the holding stage, the water on the inside is retained at the lowest possible level while the water level outside rises due to the flood tide. The second generation stage (on a flood tide) begins as soon as a sufficient head difference is established. It is followed by a second sluicing stage, with an aim to achieve highest possible water level inside the basin. A second holding stage is then required until a sufficient head difference is reached for the second cycle of operation to begin.

This scheme results in a tidal range inside the basin that is much closer to the natural conditions (Xia et al. 2010a) and is therefore viewed as more acceptable in terms of environmental impacts. Due to four power generation cycles per day instead of just two, it offers a more evenly distributed power output over time, which makes it easier to be absorbed into the local grid (Baker 1991).

3.3.2. Turbines and sluice gates

Turbines and sluice gates are the principal components of every TRS. Their main role, from a hydrodynamic point of view, is transferring water between the two subdomains of the TRS. The numerical grids of regional-scale numerical models are typically too coarse to resolve the flow through turbines and sluice gates on the grid. The technique used to reconcile this limitation is to employ a sub-grid scale model of the flow, that calculates it separately from the system of hydrodynamic equations. Once resolved, the flow through the hydraulic structures is included in the solution algorithm through sink and source pairings.

The calculation of the discharge through the hydraulic structures is performed at every time step of the computation, right after the current operational stage is determined, as illustrated in Figure 18. The programme proceeds with the calculation of turbine discharge only when a generation stage is active, during any other stage it assigns a zero value to the variable. Same goes for the calculation of discharge through sluices, however, this time only the sluicing stages (releasing or filling) are considered active.

Turbines

Turbines used in this study are based on the Andritz Hydro model of a bulb turbine, using scaled turbine characteristics that were first presented in a study by Aggidis and Feather (2012). This type of turbine has already been successfully deployed in existing tidal range projects, such as Annapolis and Sihwa tidal range plants in Canada and South Korea respectively, and was also chosen for the on-going design of the units for the Swansea Bay Lagoon tidal plant in the UK (Andritz Hydro 2016).

The use of a Q-H relationship from Equation (14), based on the so-called turbine hill chart, has now already been established as the preferred method for determining the flow rate through the turbine (Q_T), in contrast to a more crude orifice equation that was used in the early TRS numerical models (Bray et al. 2016; Xia et al. 2010a; Angeloudis et al. 2016b; Falconer et al. 2009). A hill chart is unique for every type of turbine and is generally obtained experimentally by the manufacturing company.

$$Q_T = f(H) \tag{14}$$

This study included two turbines of 7.2 and 9.0 m diameter size, that were proposed in the design stages of the Swansea Bay lagoon and Severn barrage projects respectively. The resulting Q-H relationships, with respective Power-Head (P-H) relationships, are shown in Figure 21.

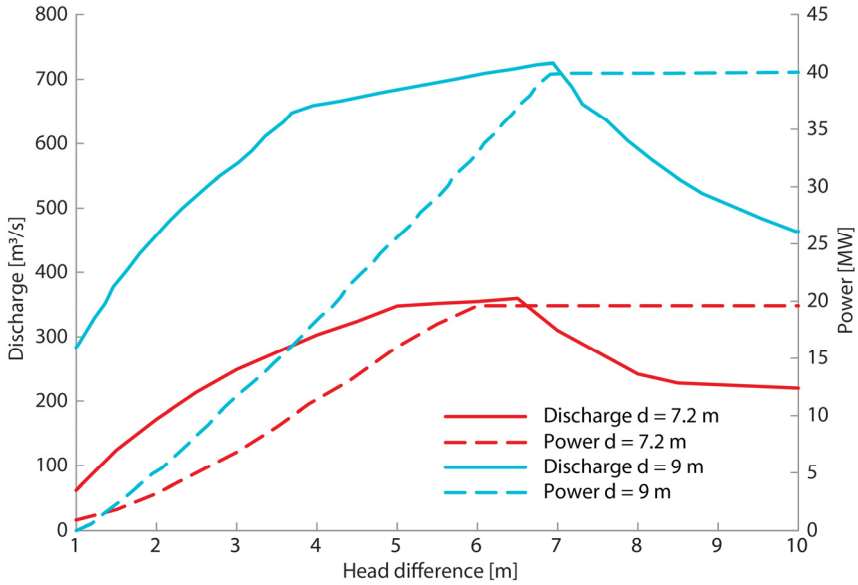

Figure 21: Discharge (Q-H) and power curve (P-H) relationships for bi-directional turbines used in this study.

Sluice gates

Sluice gates are hydraulic structures that can regulate the water flow through an impermeable structure, such as an impoundment wall. In their most simple form, they consist of a channel or a pipe with an installed movable gate that can control the flow rates through the structure. The term sluice gate technically refers to the gate structure only, however, in the context of this study the term is used to describe the entire sluice caisson, including the water passageway and the mechanical sliding gate.

The sluice gates in TRSs are designed to maximize the water discharge capability in order to increase the efficiency in tidal power generation (D. S. Lee et al. 2010). The gates are lowered (closed) during the generation and holding stages of the operation and raised (opened) during the releasing and filling stages of the operation in order to equalise the water levels on both sides of the structure.

The instantaneous discharge through sluice gates is described by the orifice equation (15), establishing a simple relationship between the flow rate (Q_S) and the corresponding head difference (H) across the structure (Xia et al. 2010a):

$$Q_S = C_d A_S \sqrt{2gH} \tag{15}$$

where C_d is the discharge coefficient, A_S the flow area through the sluice structure in m^2, and g is gravitational acceleration.

3.3.3. Momentum conservation

There are different conceptual approaches to model the correct transfer of momentum through tidal range turbines. The most accurate method would be a full 3D computational fluid dynamics (CFD) model, where the flow through a turbine itself would be included in the computations (Adcock et al. 2015). However, such simulations are computationally very demanding and too expensive to be used at the regional scale. A more conventional method, also used in the study herein, is to resolve the flow through the hydraulic structures with a sub-grid model. After it is calculated, the information relating to the time varying flow through the structure is added to the appropriate computational cells. This information does not contain only the volume of the water transferred, but more importantly it also includes the velocity of the discharged flow, which is directly linked to the transfer of momentum. The treatment of momentum is therefore paramount to the accuracy of the flow conditions in the area at the turbine exit.

The momentum flux was treated as an induced external force on the body of water. The momentum was conserved by adding an extra term into the momentum equations. The term represents an external force that is acting on the body of water due to the high-velocity jet entering the domain. An equivalent concept is used in simulations of tidal stream power extraction, where the stream turbine acts as a momentum sink (rather than a source) as it takes the energy out of the passing water flow (Ahmadian et al. 2012). While the approach of momentum sink within the computational domain is already commonly used in tidal stream studies, the momentum source represents a novel method of modelling the TRSs and other hydraulic structures.

In Delft3D, this momentum source term is denoted as M_ξ and M_η in equations (10) and (11). The force of a jet entering a body of water can be characterised as the rate of change of momentum of the fluid and is commonly defined by Equation (16):

$$\overrightarrow{F_T} = \rho_0 Q(\overrightarrow{v_1} - \overrightarrow{v_2}) \tag{16}$$

where ρ_0 is water density, Q is the flow rate entering/leaving the control volume, v_1 and v_2 are velocities of the flow entering and exiting the control volume respectively. For the sake of simplicity, the equation (16) can be rewritten into a scalar form for each direction. This is shown for ξ direction through Equation (17) below:

$$F_{T\xi} = \rho_0 Q(\hat{u} - u) \tag{17}$$

where $u\hat{}$ is the velocity of the incoming jet and u the background velocity in the target cell. From here on, the derivation will be shown only for a component in ξ direction, however, the same is applied to the component in η direction.

Assuming the force is acting on the whole volume of the computational cell and taking into account Newton's law of motion, a body force is divided by m_{cell} (the mass of water in the computational cell). The momentum source terms M_ξ and M_η are now defined as:

$$M_\xi = \frac{F_{T\xi}}{m_{cell}} = \frac{F_{T\xi}}{\rho_0 V_{cell}} \tag{18}$$

where V_{cell} is the volume of the targeted computational cell in m^3. Substituting the equation (17) into the equation (18) gives:

$$M_\xi = \frac{\rho_0 Q(\hat{u} - u)}{\rho_0 V_{cell}} = \frac{Q}{V_{cell}}(\hat{u} - u) \tag{19}$$

and can be easily simplified to:

$$M_\xi = q_{in}(\hat{u} - u) \tag{20}$$

where u is obtained from the existing velocity field, while $\hat{u}$ and q_{in} are calculated from the turbine (Q_T) or sluice gate (Q_S) discharge (Equations (14) and (15)) during the power generation and sluicing stages of the lagoon's operation:

$$\hat{u} = \begin{cases} \frac{Q_T}{A_T}, & \dots for\ turbines \\ \frac{Q_S}{A_S}, & \dots for\ sluice\ gates \end{cases} \tag{21}$$

$$q_{in} = \begin{cases} \frac{Q_T}{V_{cell}}, & \dots for\ turbines \\ \frac{Q_S}{V_{cell}}, & \dots for\ sluice\ gates \end{cases} \tag{22}$$

where A_T and A_S represent the flow-through area of the turbine and sluice gate respectively.

4
CASE STUDY 1: SEVERN BARRAGE

The case study presented in this chapter was used to develop, implement and test a new module for simulation of TRS in Delft3D. The module was based on the methodology used in previous TRS simulations found in literature. It was developed to be specifically used for tidal energy analysis in the Severn Estuary and Bristol Channel, however, the flexibility of the Delft3D code means that it can be easily modified and calibrated for assessment of any tidal energy projects worldwide. To date, much of the hydrodynamic analysis of TRSs in the UK has focused on the STPG Severn Barrage proposal, as was systematically portrayed in Section 2.3.6. The same tidal barrage scheme was chosen to be used in this study for comparison and validation of the newly developed routines for TRS simulation in Delft3D. This study acts as a sort of "development model" that will be used for future hydraulic simulations of other tidal power projects proposed in the region.

4.1. Methodology

Hydrodynamic model of the studied domain, without a barrage in place, was first used for validation of the hydrodynamics. After the validation was completed, the barrage was introduced into the domain of the Continental Shelf (CS) model. The CS domain is considerably larger than a typical estuary-scale domain and is required when tidal range schemes induce far-field changes to the hydrodynamic conditions. It was used to compare the changes in the hydrodynamic regime, particularly to assess the far-field impacts, pre- and post-construction of the barrage, shown as CS0 and CS1 respectively. The main downside of the CS model is that it is computationally expensive and therefore unpractical for analysis of local hydrodynamic phenomena generated by the barrage operation. The model also employs a coarser

computational grid, sacrificing the level of detail for computational efficiency. In practice, the larger scale models are mainly used to obtain boundary conditions for models with smaller domains and high-resolution grids, which are then used for more detailed analysis (Zhou et al. 2014c). Such a model with a smaller and more refined domain was also employed in this study. Its extents were limited to the Severn Estuary and Bristol Channel (for brevity denoted by SE), providing a more detailed understanding of the local impacts of the barrage on the flow conditions. Boundary conditions for the SE model were exported and converted from the water level results of the CS model. Same as with the CS model, two simulation runs were performed with the SE; first without the barrage (SE0) and second after the inclusion of the barrage (SE1).

4.1.1. Severn Barrage scheme description

The barrage layout used in this study is based on the STPG scheme as described in Section 2.1.3. This layout has been the most studied of the barrage proposals and is therefore ideal for benchmarking the performance of the developed model. The proposed barrage would be 16 km long, impounding a 573 km^2 area by spanning the estuary between Barry on the north and Weston-Super-Mare on the south bank. The scheme would incorporate 216 bulb turbines, 166 sluice gates, ship locks and other hydraulic structures such as smaller locks and fish passage (Xia et al. 2010c). Of those, only turbines and sluice gates were included in the numerical model (Figure 22). Other hydraulic structures could be ignored without affecting the results of the simulation. The turbines were located in the central span of the barrage. They were surrounded by two sections of sluice gates on the north part and one section on the south part of the barrage wall. All the turbines were of equal size, measuring 9 m in diameter, with a combined area of the sluice gates amounting to 35 000 m^2.

Table 5: Specifications of the Severn Barrage scheme used in this study.

Starting head [m]	4.0
Minimum head [m]	1.5
Wall length [km]	16
Impounded area [km^2]	573
Turbine number	216
Turbine diameter [m]	9
Turbine capacity [MW]	40
Total capacity [MW]	8 640
Number of sluice gates	166
Combined sluice gate area [m^2]	35 000

The scheme was designed for the ebb-only power generation, as described in Section 3.3.1. The turbines were designed for a driving head of 4 m with a minimum head of 1.5 m and were represented by a Q-H relationship (Figure 21) that was described in Section 3.3.2. The sluice gates were represented by an orifice equation (Equation (15)). A summary of the scheme's specifications is outlined in Table 5.

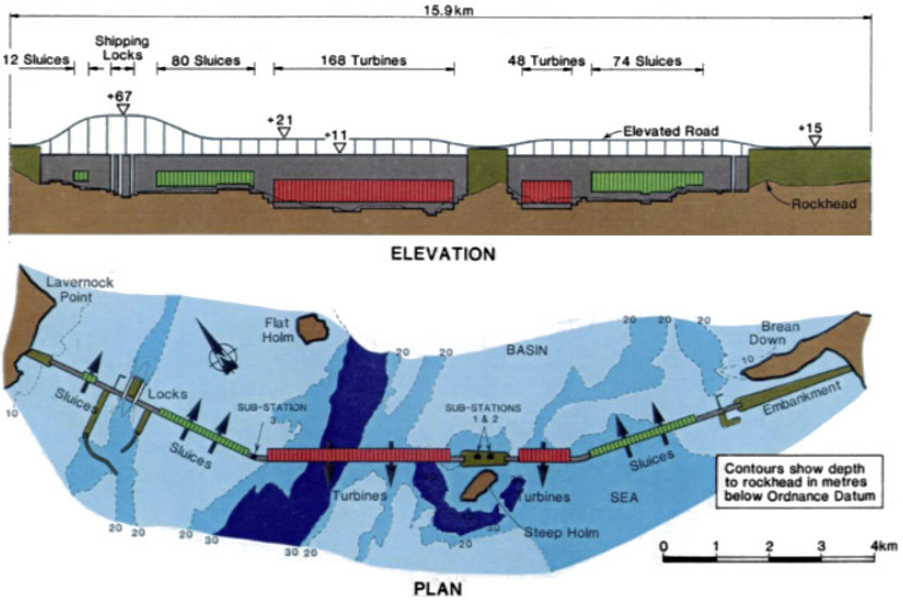

Figure 22: Layout of the barrage wall and locations of turbines and sluice gates. Image courtesy of Severn Tidal Power Group (STPG 1989).

4.1.2. Domain extent

The study area (Figure 24) was situated off the west coast of the UK, with a particular interest in the Severn Estuary.

The Severn Estuary has the second largest tidal range in the world, which can reach more than 14 m during the spring tides. It is around 200 km long and relatively shallow. At its widest point it measures approximately 14 km across, which is between Cardiff and Weston-super-Mare. This is also the presumed location of the Severn Barrage. Continuing westward, the estuary opens up into the Bristol Channel, a major British inlet that separates South Wales from England, extending westward all the way to the Celtic Sea. Its western-most boundary is often denoted by an

imaginary line between Hartland Point in England and St. Govan's Head in Wales; the same line was also selected as the open boundary of the SE domain. The CS domain covered a significantly larger region, encompassing the area between the island of Great Britain and the edge of the continental shelf, including the Irish Sea, entire island of Ireland, and part of the Scotland's west coast in the north, as well as a part of the French Atlantic coast in the south. The extent of the domain and the locations of the SE and CS boundaries are illustrated in Figure 24.

The CS domain was represented by a grid with a relatively coarse resolution, covering approximately 850 000 km^2 surface area at mean tidal level. The grid consisted of nearly 260 000 cells of variable sizes. In the areas of specific interest, i.e. around the barrage, the computational cells measured around 250 x 250 m^2, with the cell size gradually increasing towards the open boundary, measuring as much as 5 000 x 5 000 m^2. The area covered a diverse topography (Figure 23), with bottom elevations ranging from 5000 m below Ordnance Datum in the deep ocean to 5 m above Ordnance Datum along the narrower reaches of the Severn Estuary.

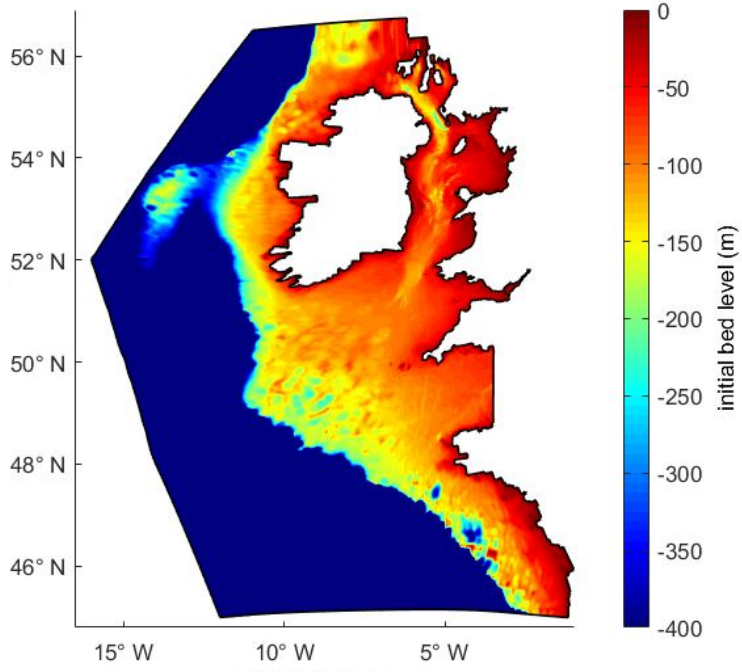

Figure 23: Computational domain of the CS model, showing the bathymetry data in Delft3D.

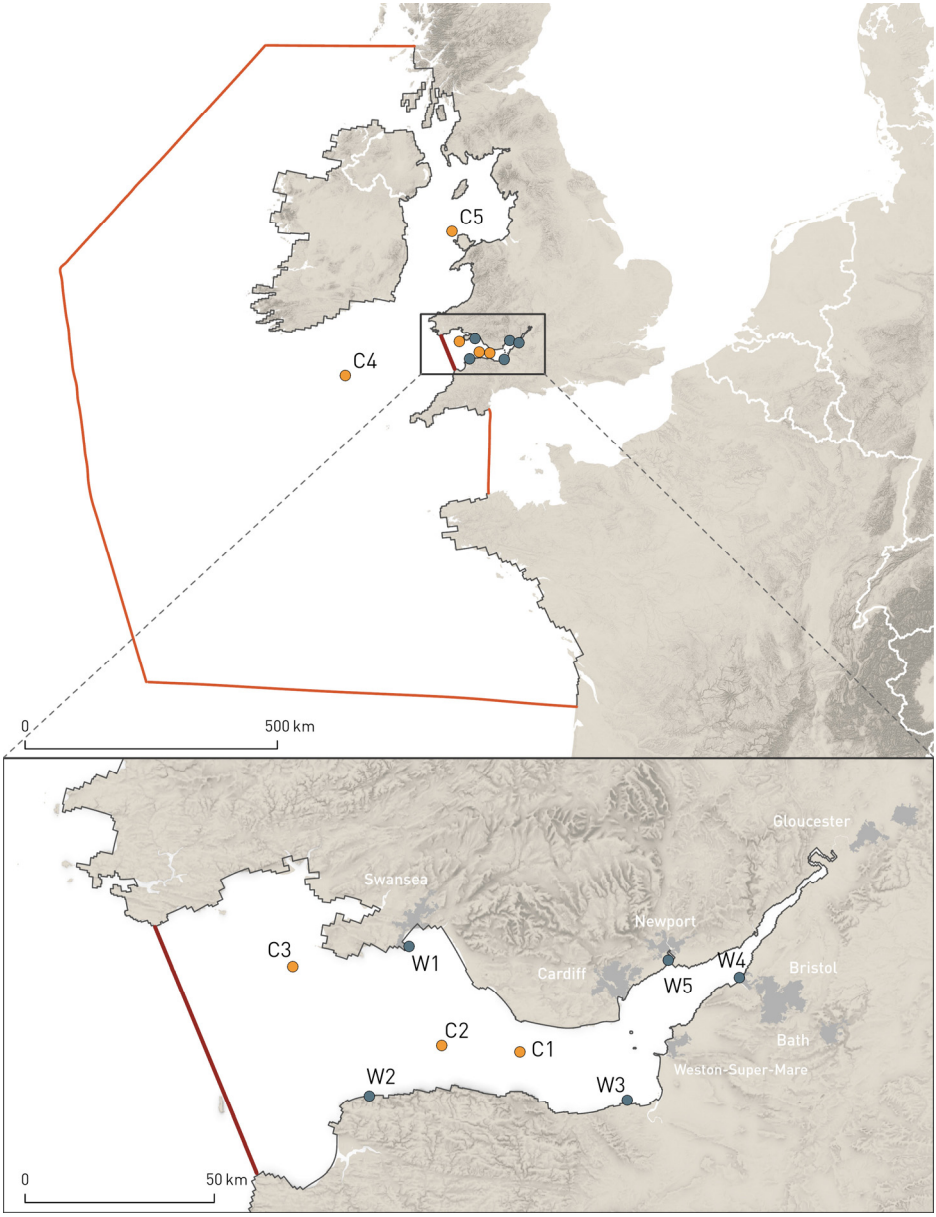

*Figure 24. Study area showing open boundaries of the Continental Shelf domain (orange) and Severn Estuary model (red). Closed boundaries were characterized by the coastline (grey)**.** Locations of the observation sites used for validation of the tidal flow are shown in yellow (C) and the observation sites of water levels in blue (W).*

The SE domain covered a considerably smaller region, with a surface area measuring approximately 5 800 km^2 at the mean tidal level. Its computational grid was obtained by cutting the CS grid at the location of the open boundary (i.e. at the entrance into the Bristol Channel at Heartland Point) and refining it to a higher resolution. For a higher resolution and better accuracy, cells in the area around the barrage were reduced from 250 x 250 m^2 to around 100 x 100 m^2. The refined mesh introduced additional grid nodes, for which the bottom elevation values were interpolated from the CS grid (Figure 25). The water elevation time series for the open boundary condition was extracted from the CS model results, which meant that both CS and SE models used the same time interval for the simulation.

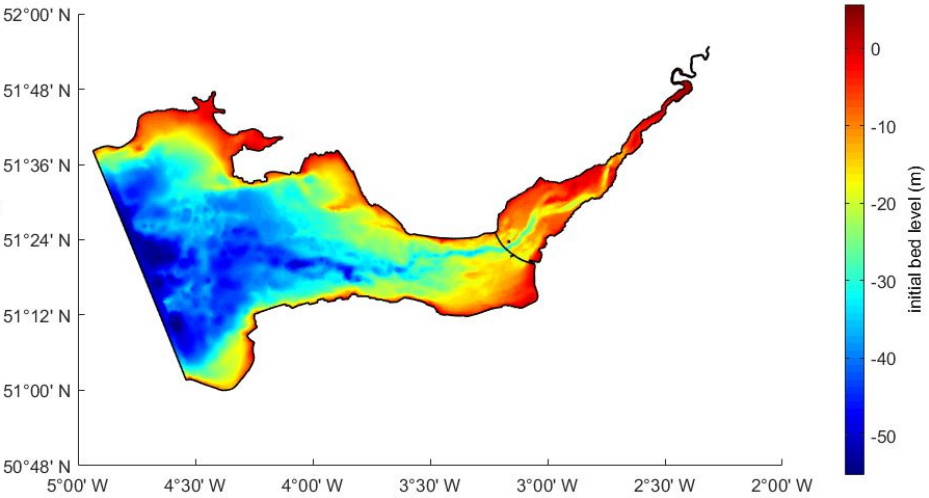

Figure 25: Computational domain of the SE model, showing the bathymetry data in Delft3D.

4.1.3. Model set-up

In order to obtain a holistic view of the tidal barrage operation, the simulation time spanned over a 14-day period that covered both neap and spring tidal regimes. Selected was a representative period between 1st and 14th March 2005, that could be used for estimation of the annual power production by extrapolating the results over the entire year. The tidal elevation time series used as the model boundaries were obtained from the MIKE21 global model (Warren and Bach 1992).

All simulations used the same time step of 3 seconds, which was selected to satisfy the CFL condition. On a standard desktop PC, with 3.60 GHz Intel® Core™ i7

series CPU, the total elapsed time for the full simulation of the SE model was 18 hours, while the CS model required almost 90 hours to complete the computation. To increase the efficiency of the CS model, it was subsequently adapted to run on the Cardiff University's High-Performance Computing (HPC) cluster, cutting the computational time to around 36 hours using 6 CPU threads.

4.2. Model Validation

Initially, the CS model was run without the barrage. It was validated against observed tidal elevations and velocity data across the whole domain. The domain was split into four regions and a uniform value of the bottom roughness, represented by the Manning's roughness coefficient, was selected for each region. A value of 0.035 was selected for the region of the Severn Estuary, 0.030 and 0.025 in the upper and lower reaches of the Bristol Channel respectively and 0.020 everywhere else. This distribution of roughness coefficient was selected based on an already calibrated model from Bray et al. (2016), which used identical input data as the model presented herein. Figure 24 shows the locations of the selected observation points that were representative for the entire domain. The data for the direction and magnitude of the flow velocity was collected from the Admiralty Charts (No. 1123, 1165 and 1826). The velocity was additionally compared to results produced by the EFDC model Bray et al. (2016). The time series for the tidal elevations were obtained from the British Oceanic Data Centre (BODC 2017).

Several different performance indicators were used to quantify the performance of the hydrodynamic model. First, the correlation coefficient r was calculated to measure the strength of the linear relationship between predictions and observations, where an r value closer to 1 indicates a strong relationship between the two variables. Correlation was calculated using Equation (23):

$$r = \frac{\sum(S_i - \bar{S})(O_i - \bar{O})}{\sqrt{\sum(S_i - \bar{S})^2 \sum(O_i - \bar{O})^2}} \tag{23}$$

Where O_i are the observed data points, S_i are the simulation results, and $\bar{O}$ is the mean of the observed data, and $\bar{S}$ mean of the simulation results.

To evaluate the error of the simulation results the Root Mean Squared Error (RMSE) was used, which has the same units as the quantity being estimated. A smaller RMSE value indicates good model performance. RMSE was calculated using Equation (24):

$$RMSE = \sqrt{\frac{\sum(O_i - S_i)^2}{n}} \quad (24)$$

Where *n* is the total number of data points in the time series.

The Nash-Sutcliffe model efficiency (NSE) was initially developed to assess the forecasting performance of hydrological models. However, it can be used for evaluation of any predictive model when comparing it to observed data (Nash and Sutcliffe 1970). The NSE is based on the Equation (25):

$$NSE = 1 - \frac{\sum_{i=1}^{n}(O_i - S_i)^2}{\sum_{i=1}^{n}(O_i - \bar{O})^2} \quad (25)$$

An efficiency value of 1 corresponds to an exact match between predictions and observations, while a value of 0 indicates that the model predictions are as accurate as the mean of the observed data and becoming less accurate if the value falls below zero.

In addition to this, scatter index (SI) was also used in the analysis. It is calculated using the Equation (26) and presents the proportion of RMSE difference with respect to mean observation:

$$SI = \frac{RMSE}{\bar{O}} \quad (26)$$

Figures 026 to 030 show the validation of the velocity results at three different locations along the centreline of the Bristol Channel (C1–C3) and two additional points further away from the estuary, one in the middle of the Celtic Sea (C4) and the other in the middle of the Irish Sea (C5). At each site, the predicted tidal currents were compared against the tidal data for a 12-hour interval, showing flow direction of a typical tidal cycle, as well as velocity magnitude of mean spring and neap tides. In addition, four statistical parameters (Equations (23) to (26)) were calculated for each site to quantify the performance of the hydrodynamic model. The performance indicators for current direction, spring current speed and neap current speed are collected in Table 6, Table 7 and Table 8 respectively.

In general, there was a good agreement between the predicted and observed data at all five locations. Both correlation factor and NSE were very high, above 0.9 for all three variables at all five locations. The only exception was site C5 in the Irish Sea with a slightly worse performance in predicting the current direction (NSE of 0.794). However, because the correlation factor was good (0.933) and since point C5 located far away from the estuary, this result was still considered acceptable. Delft3D has on general produced better predictions than the EFDC model. At the three sites in the Bristol Channel (C1–C3), Delft3D was especially accurate at predicting the

incoming tide, showing much closer fit to observations than EFDC (Figures 26bc, 27bc, 28bc). In the Celtic Sea (C4), where larger depths result in a significantly lower velocity, both models predicted the correct amplitude for both spring and neap tides (Figure 29bc), however, Delft3D managed to better capture the timing of the slack water, while EFDC was slightly out of phase. The difference between the two models was the least apparent at the location in the Irish Sea (C5), where both models predicted similar velocities, showing a good match with the observed data (Figure 30bc). Both models also produced similar predictions for the flow direction at locations C2, C3 and C5, as shown in Figures 27a, 28a, 30a. However, Delft3D again managed to better capture the timing of the slack water at locations C1 and C4, where the EFDC model was approximately 1 hour out of phase (Figures 26a, 29a).

Table 6: Validation results for current speed at five observation locations C1 to C5.

Location	r [-]	RMSE [°]	NSE [-]	SI [-]
C1	0.999	8	0.991	0.045
C2	0.959	25	0.902	0.136
C3	0.983	19	0.948	0.099
C4	0.994	10	0.988	0.066
C5	0.933	36	0.794	0.237

Table 7: Validation results for spring tide speed at five observation locations C1 to C5.

Location	r [-]	RMSE [m/s]	NSE [-]	SI [-]
C1	0.999	0.334	0.999	0.238
C2	0.999	0.236	0.999	0.226
C3	0.999	0.094	0.999	0.140
C4	0.999	0.048	0.999	0.205
C5	0.999	0.187	0.999	0.173

Table 8: Validation results for neap tide speed at five observation locations C1 to C5.

Location	r [-]	RMSE [m/s]	NSE [-]	SI [-]
C1	0.999	0.081	0.999	0.106
C2	0.999	0.098	0.999	0.193
C3	0.999	0.075	0.999	0.210
C4	0.999	0.016	0.999	0.126
C5	0.999	0.194	0.999	0.356

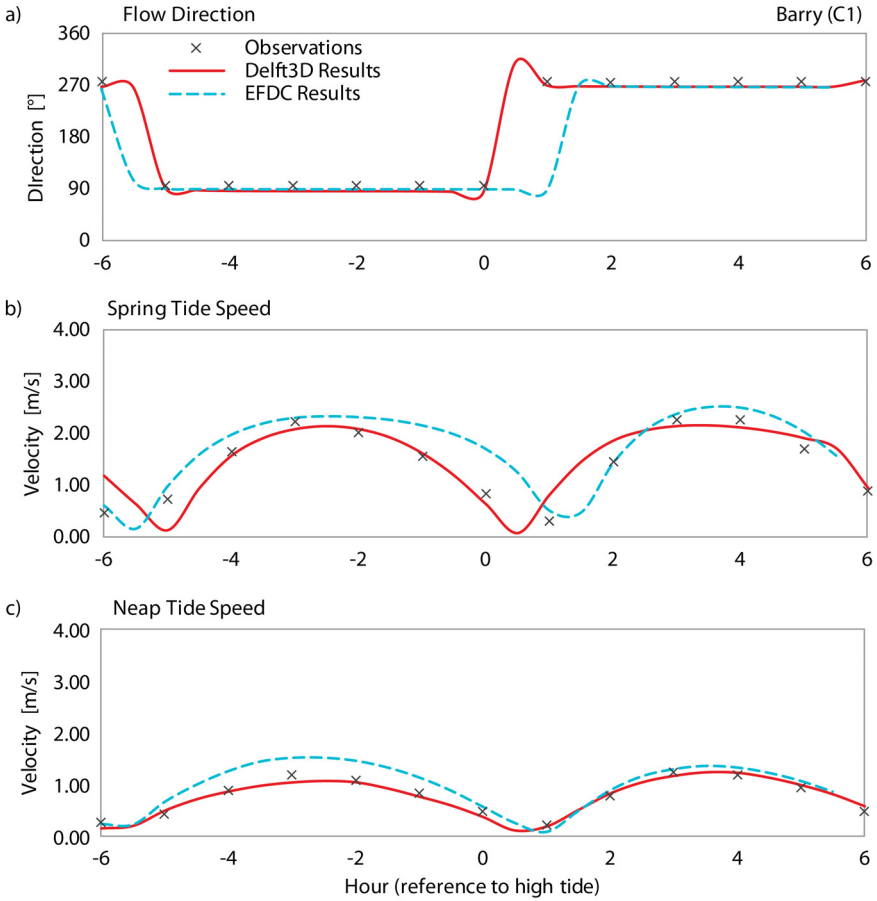

Figure 26: Comparisons between Delft3D results, EFDC results and observed data for the validation site C1, located in the upper reaches of the Bristol Channel, near Barry.

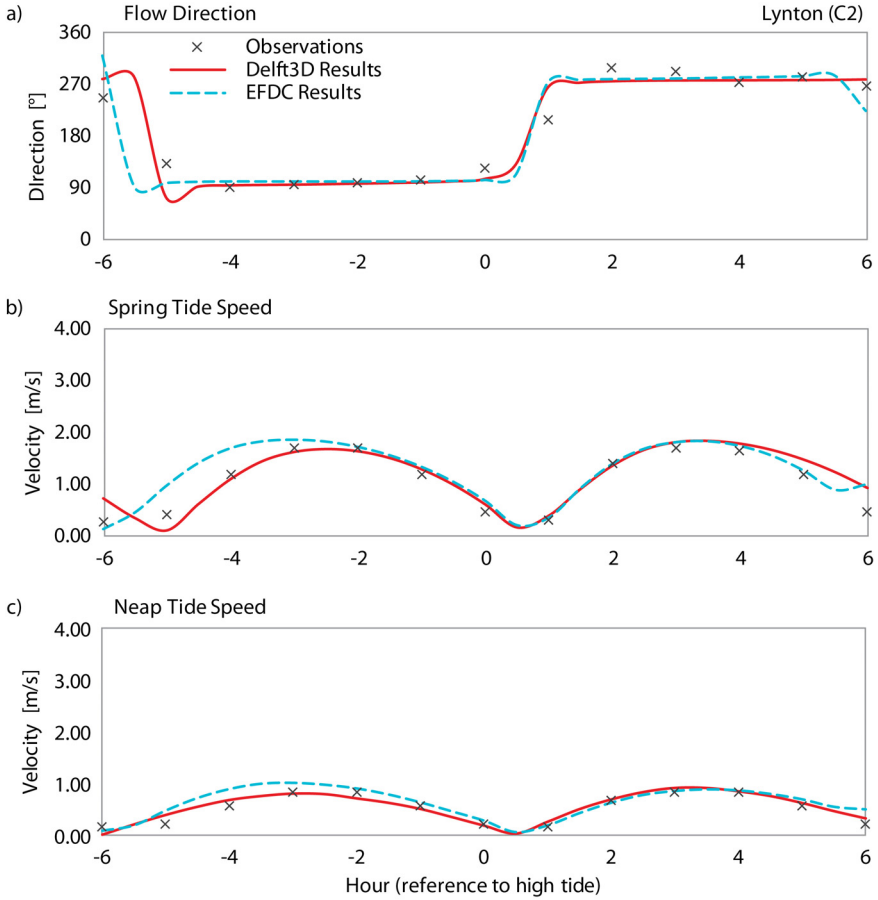

Figure 27: Comparisons between Delft3D results, EFDC results and observed data for the validation site C2, located in the middle reaches of the Bristol Channel, near Lynton.

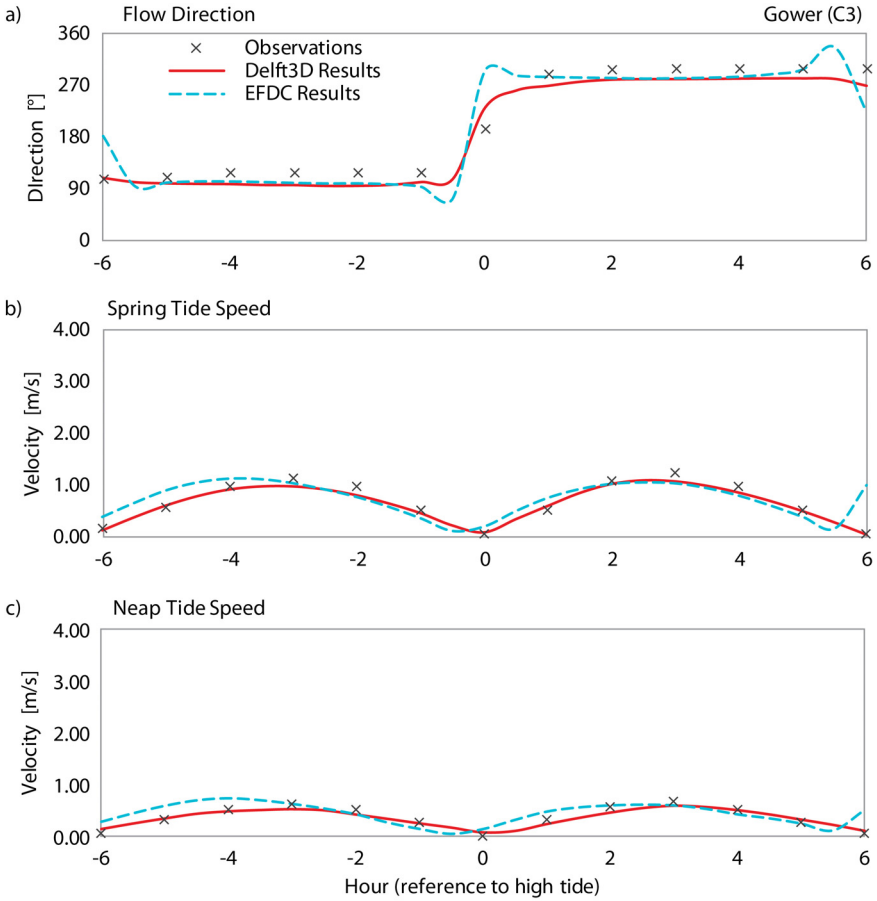

Figure 28: Comparisons between Delft3D results, EFDC results and observed data for the validation site C3, located in the middle reaches of the Bristol Channel, near Gower.

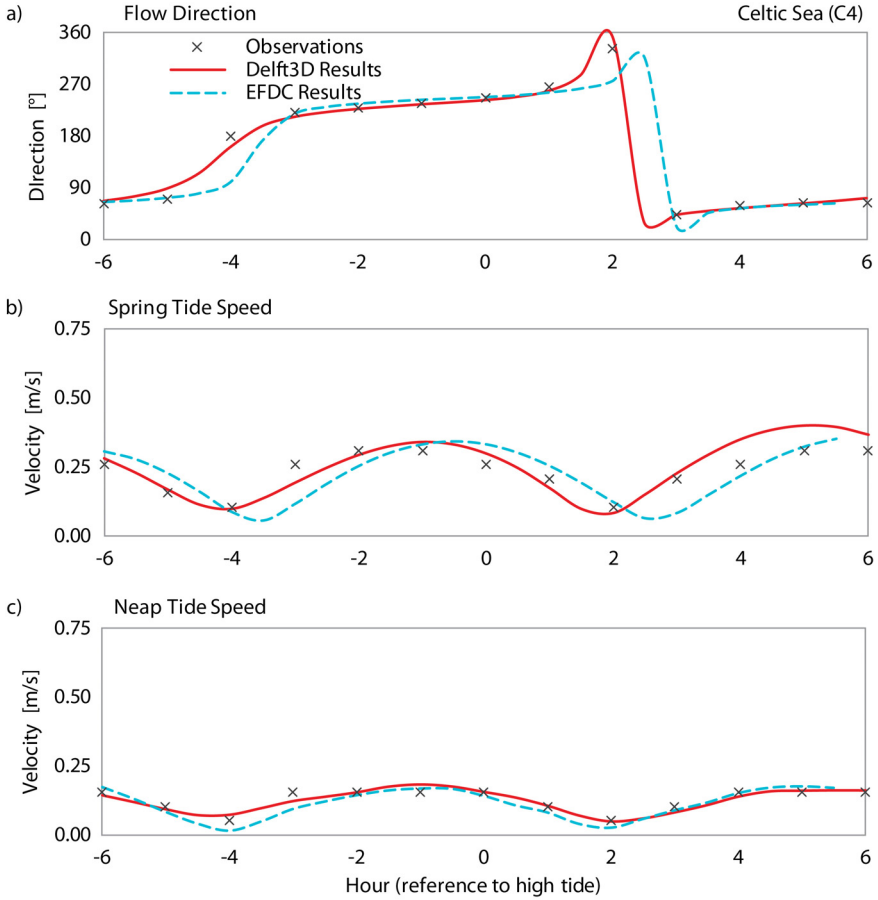

Figure 29: Comparisons between Delft3D results, EFDC results and observed data for the validation site C4, located in the Celtic Sea.

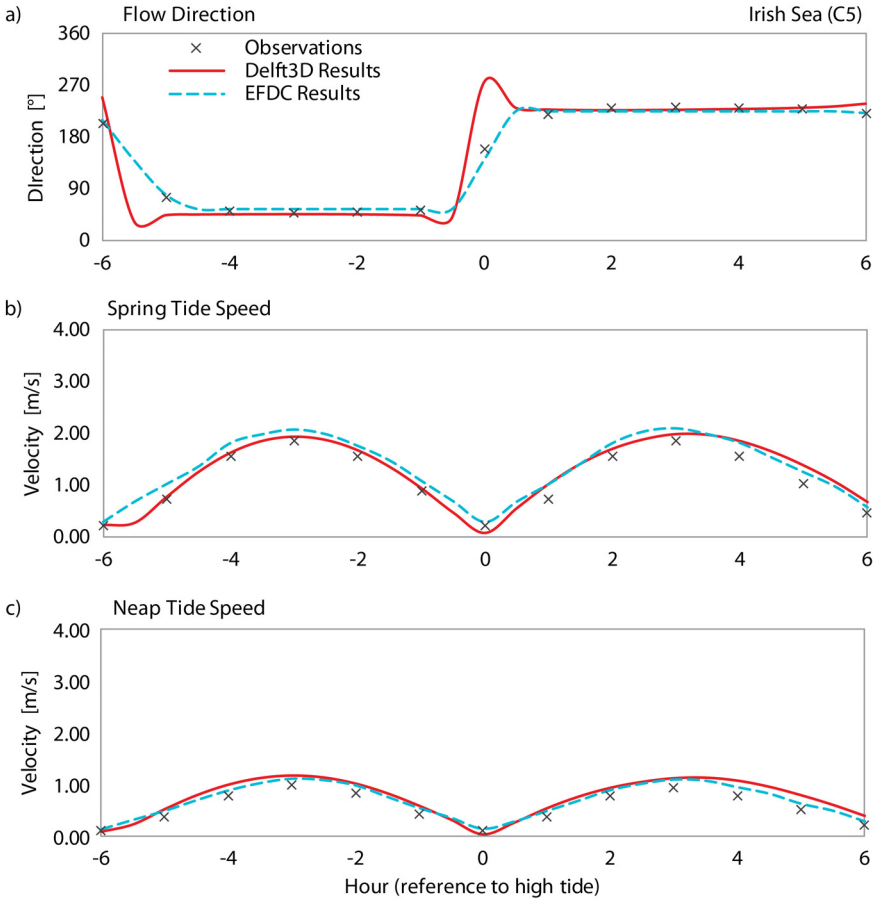

Figure 30: Comparisons between Delft3D results, EFDC results and observed data for the validation site C5, located in the Irish Sea.

The predicted water levels were validated against the observed tidal amplitude at five locations across the Severn Estuary and Bristol Channel (Figure 24), at Mumbles (W1), Ilfracombe (W2), Hinkley Point (W3), Avonmouth (W4) and Newport (W5). At each site, the comparisons were made over the entire duration of the simulation, including neap and spring tides (Figure 31). In addition, four statistical parameters (Equations (23) to (26)) were calculated at each site to quantify the performance of the hydrodynamic model on water elevations, shown in Table 9.

The simulation results showed good agreement with the observation data, especially during the spring tides, matching well in terms of both magnitude and tidal phase. Correlation and NSE were again high at all five locations. Delft3D slightly underpredicted the magnitude of neap tides, which was also reflected in a slightly higher RMSE and SI, however, such discrepancies were consistent with findings from literature (Zhou et al. 2014c; Xia et al. 2010c). In previous studies, this degree of accuracy has been regarded as acceptable, especially when taking into consideration the complexity of the tidal hydrodynamics in such a large domain and for such extreme conditions.

Table 9: Validation results for water levels at five observation locations W1 to W5.

Location	r [-]	RMSE [m]	NSE [-]	SI [-]
W1	0.987	0.500	0.963	2.357
W2	0.987	0.497	0.962	1.311
W3	0.992	0.437	0.982	0.416
W4	0.937	0.521	0.877	0.578
W5	0.975	0.570	0.951	0.438

The comparisons between predicted results and field data have shown that Delft3D was able to adequately reproduce the tidal conditions in the studied region, establishing the model as a reliable numerical tool for the assessment of impacts caused by tidal energy projects proposed in the Severn Estuary and Bristol Channel.

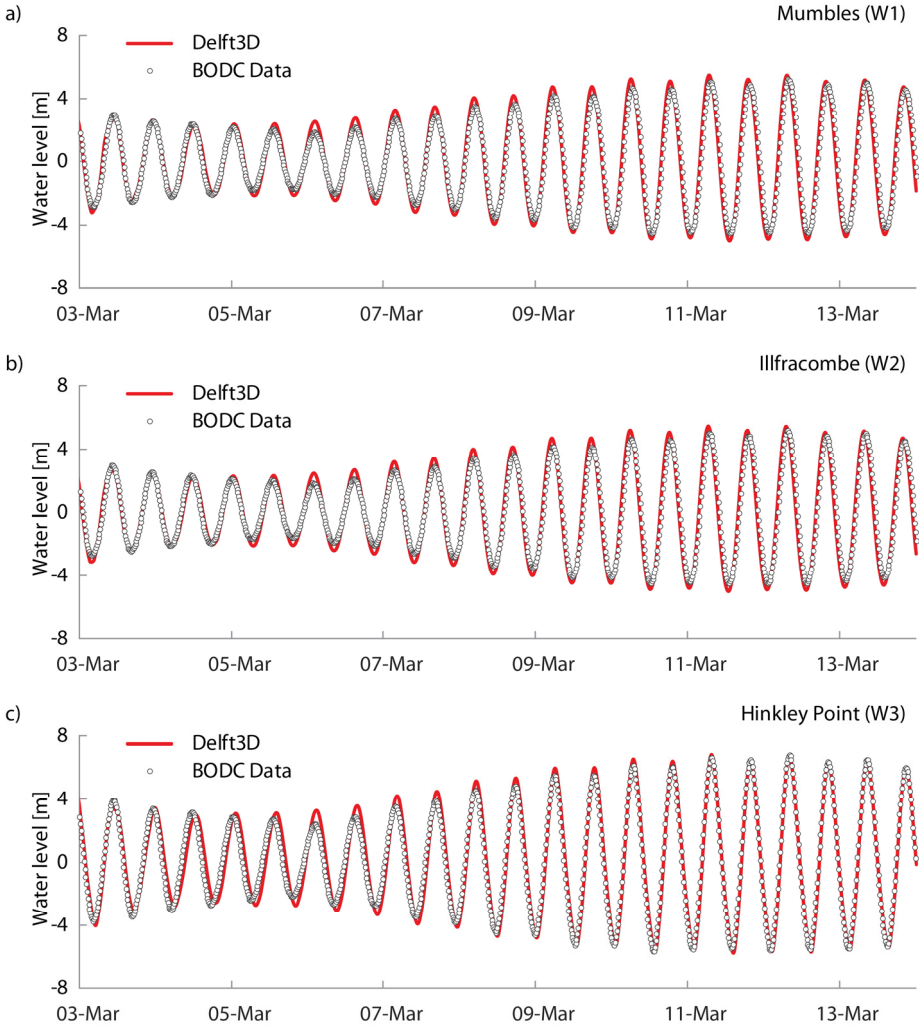

Figure 31: Water level results from Delft3D compared with the observed data from BODC at Mumbles (a), Illfracombe (b), and Hinkley Point (c).

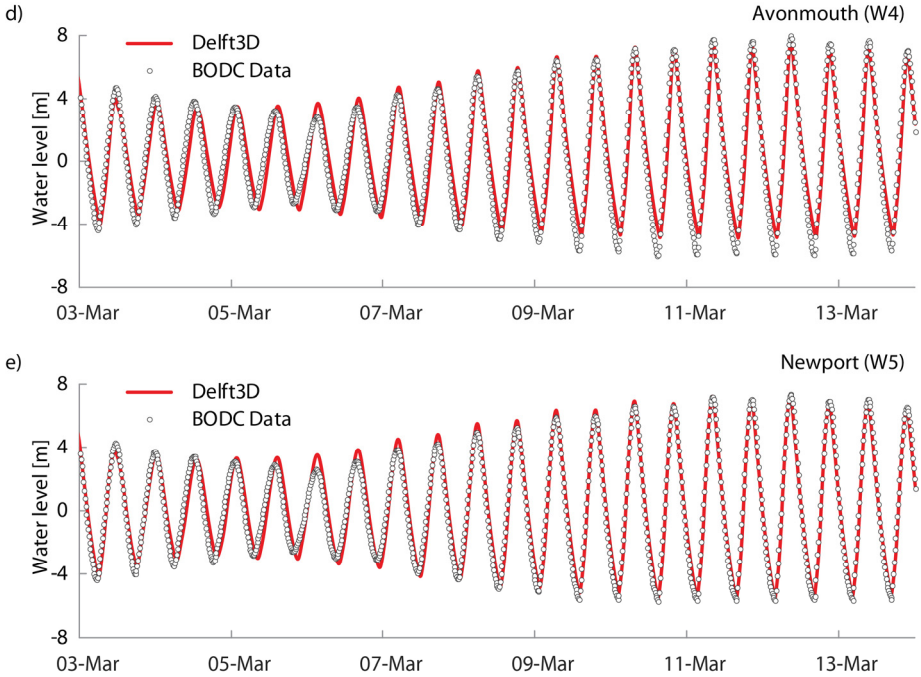

Figure 31: Continued - Water level results from Delft3D compared with the observed data from BODC at Avenmouth (d) and Newport (e).

4.3. Results

4.3.1. Barrage operation

After the validation of the hydrodynamic conditions, the model was modified to include the tidal barrage and was used to simulate the hydrodynamic processes with the barrage in operation. The operation of the barrage is best illustrated by a time series of water levels either side of the barrage. The head difference across the barrage governs the quantity of water passing through the turbines and production of power. To calculate the head difference, the water surface elevations were obtained from 10 evenly distributed points at the distance of approximately 1 km either side of the barrage, as illustrated in Figure 32. The final value of the water elevation on each side was calculated as a mean value of the 10 points. This approach guaranteed a more smooth operation of the barrage, avoiding any local disturbances to the water level records that could occur if the measurements were taken from a single point only.

During the 14-day period of the simulation the tidal range across the barrage varied significantly from 5 m during neap tides to 11 m during spring tides. This can be observed in Figure 33, with the light blue line representing the tidal amplitude outside the barrage impoundment. A distinct period of smaller tidal amplitudes was observed between 3rd and 7th March, representing the neap tides. During the spring tides, between 9th and 13th March, the tidal amplitudes were noticeably larger and had practically doubled in size. During the spring cycle, the water elevation in the Estuary reached 6 m above Mean Sea Level (MSL) during the high tide and fell to 5 m below MSL at low tides, bringing the tidal range to 11 m. During the neap tides, the tidal range was reduced to only 5 m, with the maximum elevation just short of 3 m above MSL and minimum elevation slightly below 2 m below MSL.

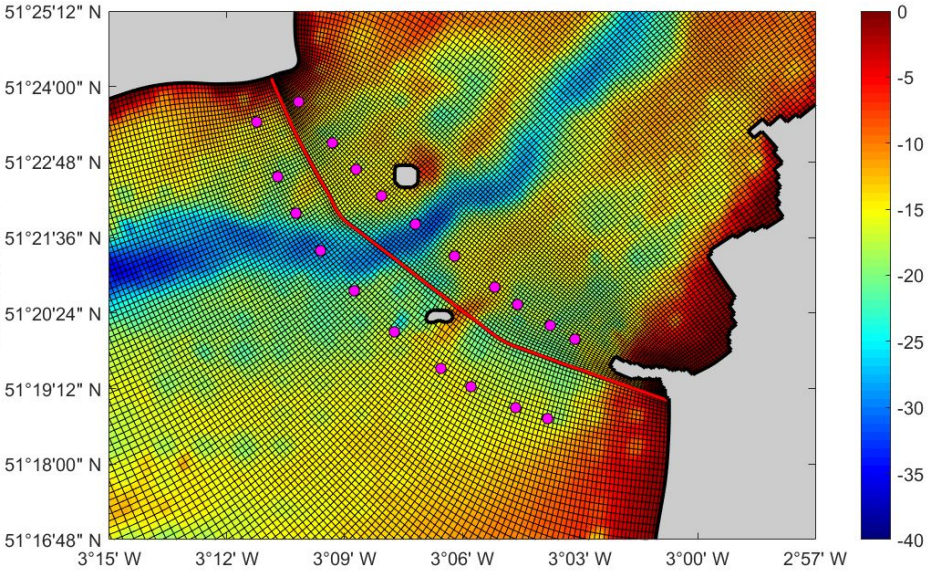

Figure 32: Location of the points used to calculate the mean head difference on the SE computational grid, showing the bathymetry and location of the barrage.

The barrage has had a clear impact on the tidal regime inside the impoundment, rising low tides and significantly reducing the tidal range. The change in amplitude was mostly affected by the substantial rise of the minimum water levels. It rose by approximately 2 m during neap and by 4 during spring tides. The maximum water levels have not been affected as much, however, there was a more noticeable reduction of the high water by approximately 1 m during spring tides, while it was almost negligible during neap tides. Such changes to the inside water levels are

characteristic of the ebb-only operation sequence. A flood-only generation would result in a reverse situation, where maximum water levels would be reduced and minimum water levels stayed the same, while a two-way generation generally produces a more symmetrical change between the two extremes (Xia et al. 2010a).

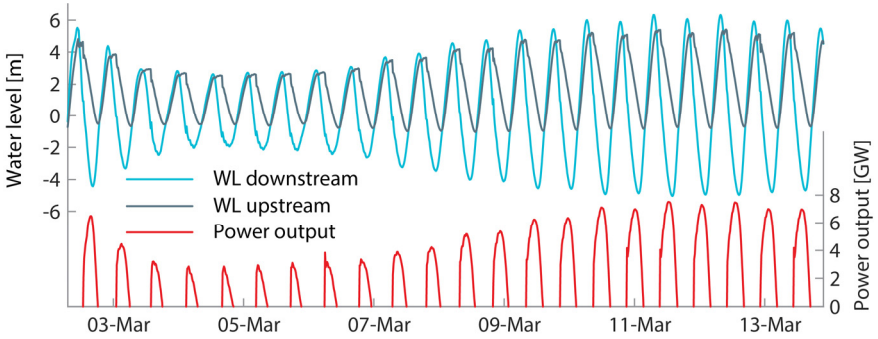

Figure 33: Predicted water levels on either side of the Severn Barrage and the corresponding power output over a typical neap-spring tidal cycle.

Figures 34 and 35 provide a more detailed view of the barrage operation during spring and neap tides respectively, showing a close-up of the predicted water levels either side of the barrage during a 24-hour period. The direct comparison between the two figures illustrates how the operation of the barrage has been affected by the variation of the tidal amplitude. The four distinct operational stages have been marked and numbered on both figures – (1) holding at high water stage, (2) generating stage, (3) holding at low water stage, and (4) filling stage.

The duration of both holding stages was evidently longer during the neap tides. It took longer for the Stage (1) to establish the required starting head difference because the water surface was falling at a lower rate compared to spring tides. Similarly, the lower rate of water level change during neap tides also meant that Stage (3) was triggered earlier than during spring tides. This discrepancy between spring and neap tides occur because the operational characteristics (starting and minimum head) are constant throughout the entire cycle. This can be mitigated by the use of variable operational characteristics as was demonstrated in a recent study by Xue et al. (2019). The study used a variable starting head, that was carefully tailored to each individual tidal cycle, thereby maximising the efficiency of power generation even during the neap tides.

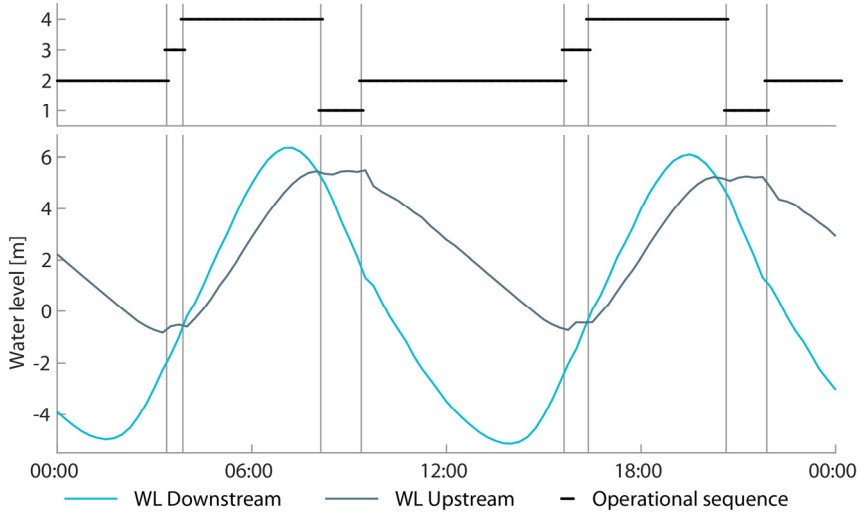

Figure 34: Predicted water levels either side of the barrage and operation stages showing the operation of the Severn Barrage during a typical spring tidal cycle. Operational sequences: (1) holding stage - high water, (2) generating stage, (3) holding stage - low water, (4) filling stage.

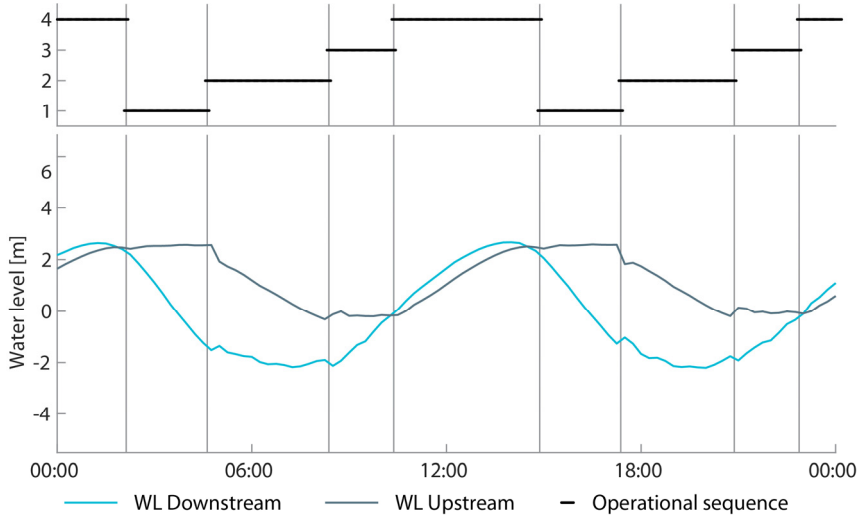

Figure 35: Predicted water levels either side of the barrage and operation stages showing the operation of the Severn Barrage during a typical neap tidal cycle. Operational sequences: (1) holding stage - high water, (2) generating stage, (3) holding stage - low water, (4) filling stage.

In both cases, the power could be generated only during the ebb tide, which is twice per day because of the semidiurnal nature of the tides in the Severn Estuary. The longer holding stages during neap tides resulted in a considerably shorter duration of power generation. The generating stage in the case of the neap tide (Figure 35, Stage (2)) lasted for only 3.6 hours, significantly shorter compared to 6.3 hours during spring tides (Figure 34, Stage (2)). Shorter generating stage, combined with a lower tidal amplitude, meant a significant reduction of the predicted power output during the neap tides. This is also illustrated in Figure 33, where power output was plotted below the corresponding tidal amplitude.

The maximum head difference during neap tides never exceeded 4 m, a value which was also used as the starting head for triggering the generation stage. Integrating power output over the generating period resulted in 7.3 GWh of produced power for a typical neap tidal cycle. The maximum head difference during the spring tides was recorded to be around 6.3 m, corresponding to an instantaneous power output of 7.6 GW.

Power production during the maximum spring tidal cycle amounted to 35.3 GWh, almost 5 times more compared to the neap cycle. The total power output over the entire neap-spring tidal cycle was predicted to be 0.63 TWh. Extrapolating this value over the entire year gave a neap-spring-averaged estimation of 15.3 TWh output annually and a capacity factor of 20.2 per cent. These values were consistent with findings from literature (Xia et al. 2012; Bray et al. 2016), confirming the successful development of the modifications for simulating TRSs in Delft3D software.

4.3.2. Continental Shelf model results

To assess the impacts on the extreme water levels, maximum water elevations across the whole CS domain were calculated for cases both with (CS1) and without (CS0) the barrage. Figure 36 shows a comparison between the two, obtained by subtracting the maximum water elevations of CS0 from CS1 simulation results. The changes were consistent with the findings of Bray et al. (2016), indicating a correct implementation of the hydraulic structure in the model. The rise of the maximum water levels could be observed throughout the Bristol Channel and beyond. In the Irish Sea and Cardigan Bay the extent of increased maximum elevation was slightly smaller but of the same order of magnitude (5 cm – 15 cm) as predicted by Bray et al. (2016). Water levels at the entrance into the Bristol Channel have increased for the same order of magnitude, confirming that the open boundary conditions of the SE domain would be affected by the construction of the barrage. The largest increase occurred in the

mid-section of the Bristol Channel (between Swansea Bay and Lynton) and was of order magnitude between 15 cm and 25 cm. The maximum water elevations in the estuary have been drastically reduced, decreasing by more than 1 m inside the impoundment and between 5 cm and 25 cm on the seaward side of the barrage.

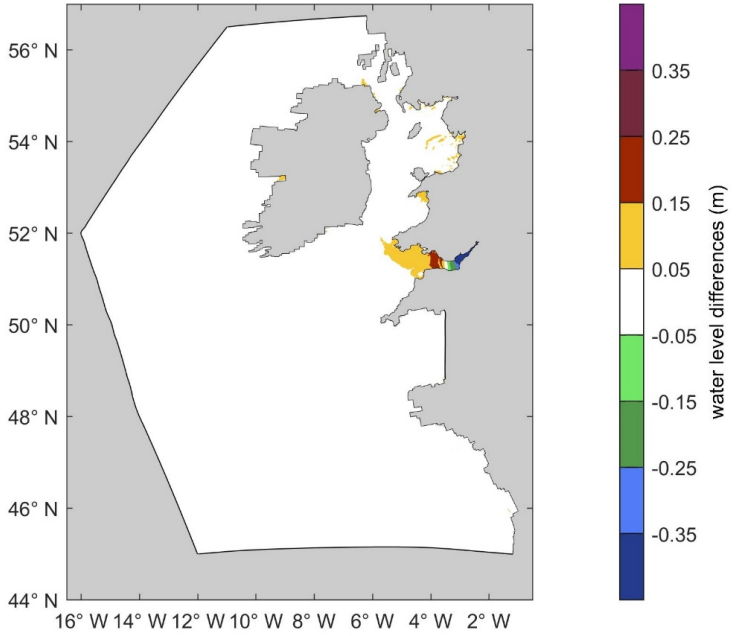

Figure 36: Maximum water elevation changes due to the barrage operation. Positive differences denote an increase and negative a decrease in water elevations after including the barrage in the simulation.

Six observation sites were selected to provide a more detailed analysis of impacts resulting from the operation of the tidal barrage. The locations of the sites are shown in Figure 37. They were selected in the areas where notable changes in the maximum water levels were observed, as can be seen in Figure 36. First two sites (P1 and P2) were located beyond the boundary of the SE domain, near Liverpool in the Irish Sea and in Cardigan Bay respectively. To observe the impacts of the barrage on the open boundary the third site (P3) was located directly on the boundary of the SE domain. The rest of the points were located inside the SE domain. Two of them were located in the middle of the Bristol Channel, where the largest increase of maximum water elevations was observed, namely in the Swansea Bay (P4) and just offshore from Lynton (P5). Lastly, a site just offshore from Newport (P6) was selected to illustrate the changes in water elevation inside the barrage basin. These locations provided

good coverage of the entire computational domain, providing a thorough insight into both far-field (P1, P2 and P3) and near-field (P4, P5 and P6) impacts of the barrage on the hydrodynamic processes in the domain.

Figure 37: Locations of observation points for the analysis of water elevation changes due to the barrage operation. SE model computational domain boundary is shown in dark red, the barrage in light red.

For each of the observation sites, a water level time series has been extracted from the results to compare the changes in the water elevations due to the operation of the barrage, shown in Figures 38 to 43. The interval of the time series was taken during the spring tides, during which the largest tidal amplitude and therefore the highest maximum water elevations were to be expected. Because the magnitude of water elevation change was small compared to the tidal amplitude, another time series, representing the difference between the two, was added to the. The difference was calculated by subtracting CS0 results from CS1 results, by which positive values denoted a higher water elevation in the post-barrage case compared to pre-barrage construction and vice versa for negative values.

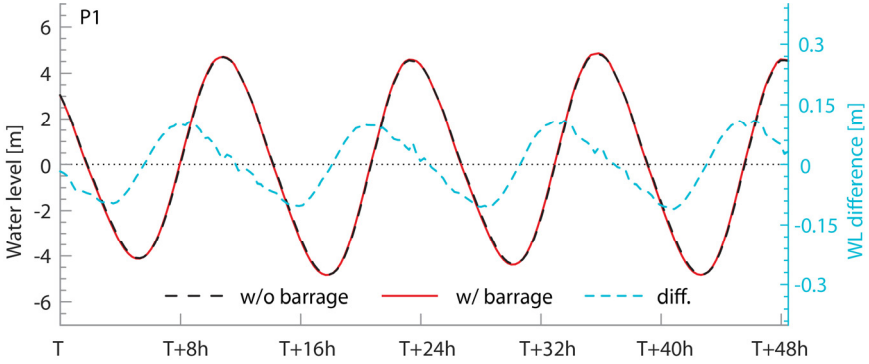

Figure 38: Time series of water level change between CS0 (without barrage) and CS1 (with barrage) over two typical neap tidal cycles at the observation site P1 in the Irish Sea.

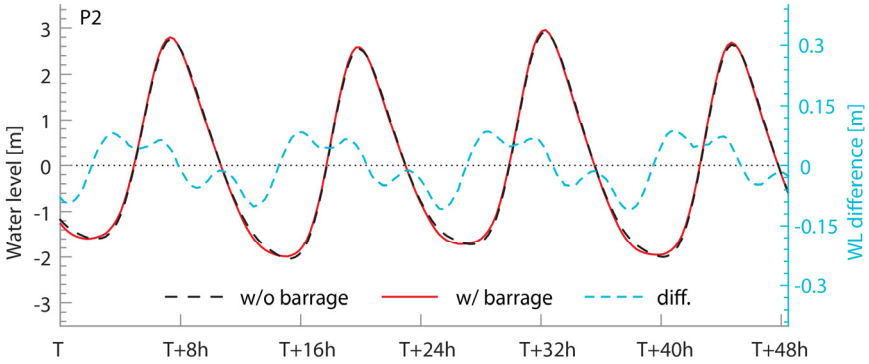

Figure 39: Time series of water level change between CS0 (without barrage) and CS1 (with barrage) over two typical neap tidal cycles at the observation site P2 in the Celtic Sea.

Locations P1, P2 and P3 were specifically chosen to investigate the far-field impacts of the tidal barrage. The tidal range in the Irish Sea (P1) was 9.6 m, while Cardigan Bay (P2) had a much smaller range of 4.8 m. The maximum increase in both locations was around 10 cm which occurred during flood tide. During the ebb tide, the water levels decreased by roughly the same amount. During the high tides the difference still showed an increase, however, it was considerably smaller, contributing only around 5 cm to an overall maximum elevation increase. Tidal amplitude in the Irish Sea (P1) was practically symmetric, unlike in Cardigan Bay where tidal wave formed steep crests but flatter troughs. The same phenomenon was previously observed in a study by Zhou et al. (2014a), where it was attributed to the nonlinearity of the tidal wave, caused by extremely shallow depths of 10-15 m in the bay.

Figure 40 shows results at site P3, located directly on the open boundary of the SE domain. The tidal range at this location was 8.7 m. The maximum increase of surface elevation was 15 cm, occurring during low tide, flood tide and high tide. Because both high and low tides increased by roughly 7 cm, the tidal range remained the same, only the overall surface elevation was shifted upwards. A decrease occurred only during the ebb tides; it lasted for a much shorter period but by a considerably larger magnitude of 27 cm.

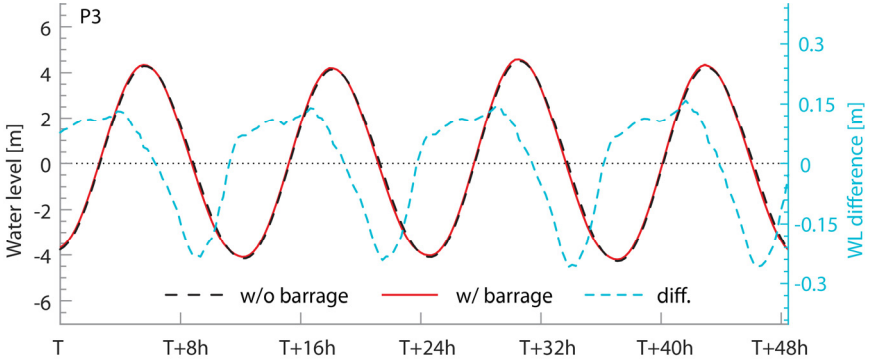

Figure 40: Time series of water level change between CS0 (without barrage) and CS1 (with barrage) over two typical neap tidal cycles at the observation site P3 at the location of the SE open boundary.

These results indicate that the impacts from the barrage operation propagate over large distances and can affect areas beyond the entrance to the Bristol Channel. Results at the location of the SE boundary showed a significant change in tidal amplitude. In order to account for these impacts, the SE boundary conditions have to be modified accordingly when barrage is included in the simulations.

Sites laying inside the SE domain were used for assessment of near-field effects caused by the barrage operation. Figures 41 and 42 show the differences in water elevations for points P4 and P5 respectively. Both sites were located in the part of the Bristol Channel that experienced the largest increase in maximum water elevations (Figure 36) after the inclusion of the barrage.

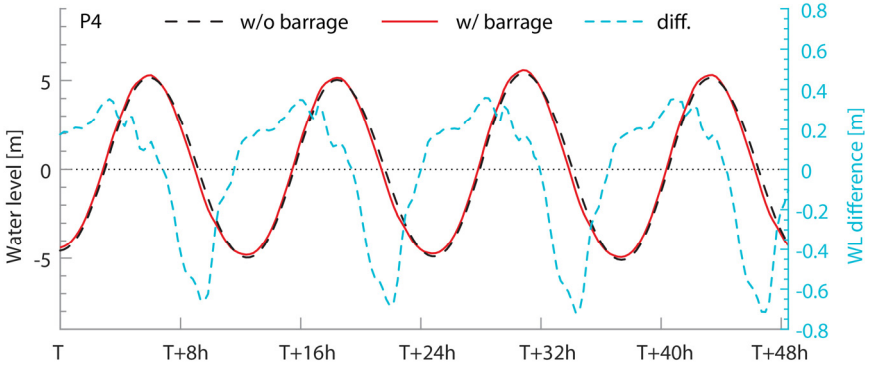

Figure 41: Time series of water level change between CS0 (without barrage) and CS1 (with barrage) over two typical neap tidal cycles at the observation site P4 in the Swansea Bay.

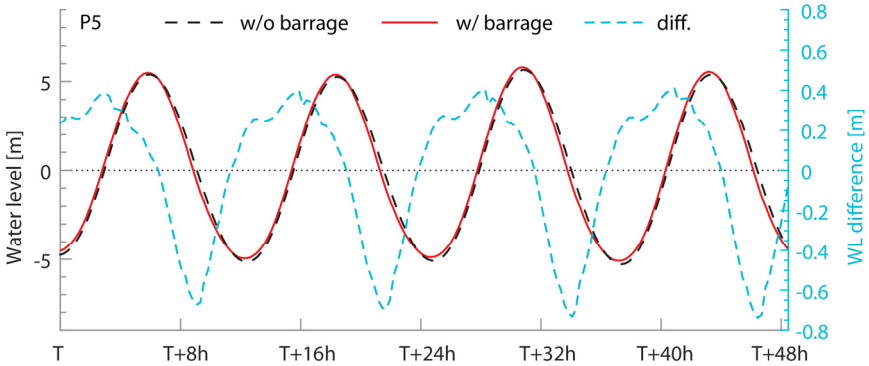

Figure 42: Time series of water level change between CS0 (without barrage) and CS1 (with barrage) over two typical neap tidal cycles at the observation site P5 in the middle of Bristol Channel, downstream of the barrage.

The tidal amplitudes at both locations were similar. The value recorded at locations P4 and P5 was 10.4 and 10.8 m respectively. A similar pattern of differences occurred at both locations. Water elevation started increasing right before the slack water of low tide and continued increasing throughout the period of the flood tide when it also reached its maximum increase at approximately 0.4 m at both locations.

It stayed above the CS0 elevation during the high tide, before becoming equal at the start of the ebb part of the cycle.

During the ebb flow, water elevation experienced a decreased from the CS0 value by as much as 0.75 m at both locations. Even though the maximum increase was more than 0.4 m, it did not occur during the peak of the high tide. The increase of maximum water elevation during the high peak was instead only around 0.2 m for both locations P4 and P5. A similar increase was also observed during the peak of the low tide, meaning that tidal range remained practically unchanged, only the values of both extremes were shifted upwards.

Finally, Figure 43 shows the time series of water level differences inside the impoundment. The construction of the barrage had radically changed the water level regime on the upstream side of the estuary. The tidal range had decreased from 12.7 m in CS0 to only 6.9 m in CS1. The maximum increase occurred during low tides, with minimum water levels rising by more than 4.5 m. However, the barrage actually helped to lower the maximum water levels during high tides, decreasing by 1.2 m.

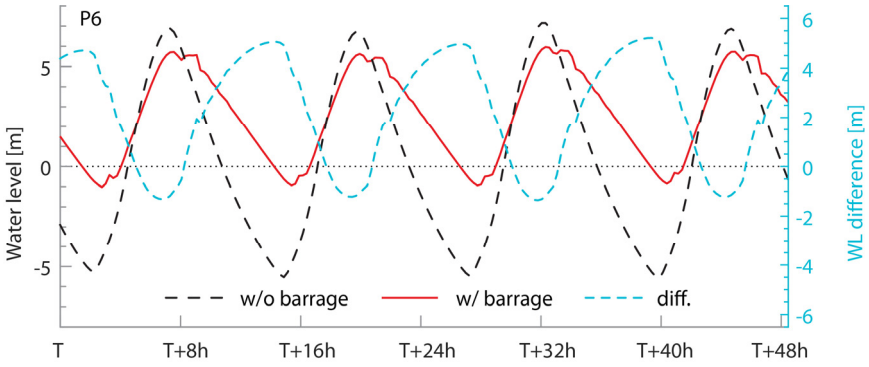

Figure 43: Time series of water level change between CS0 (without barrage) and CS1 (with barrage) over two typical neap tidal cycles at the observation site P6 upstream of the barrage, close to Newport.

4.3.3. Severn Estuary model results

The boundary condition for the SE1 model was extracted from the CS1 results. The SE model was used to obtain a high-resolution image of the near-field hydrodynamic impacts due to the barrage operation. To provide a benchmark, the SE model was first run without the barrage and using the initial boundary conditions (SE0). The barrage was included for the second scenario (SE1), using the boundary conditions extracted from CS1 results.

The CS results have already shown that the construction of the barrage caused changes to the maximum water levels throughout the domain. Figure 44 focuses on the comparison of the predicted maximum water levels inside the SE domain. The maximum water elevation has occurred during the largest spring tidal cycle when the estuary also experienced the largest tidal range. The barrage has had a lesser influence on the maximum water levels downstream of the barrage, increasing by up to 0.3 m. The increase was more prominent near the barrage and was gradually diminishing towards the open boundary. The change was much more pronounced upstream of the barrage, with maximum water levels decreasing by more than 1 m. Only the uppermost reaches of the Severn Estuary were left unaffected by the inclusion of the barrage.

Figure 45 shows the comparison of the minimum depths between the SE0 and SE1 cases. Similar to the changes in maximum elevations, the changes to the minimum depths were much more prominent inside the tidal impoundment. The depths were predicted to increase by more than 5 m, permanently submerging a large portion of intertidal mudflats located upstream of the barrage.

Figure 46 shows the impact of the barrage on tidal currents in the Severn Estuary and Bristol Channel, recorded during a typical spring tidal cycle. The results showed a considerable reduction in maximum tidal currents throughout the SE domain. The decrease in the magnitude of the velocity field came primarily from the decrease in the water volume entering the estuary due to the construction of the barrage. The reduction was therefore especially prominent in the main channel of the Severn Estuary (upstream of the barrage) and in the upper reaches of the Bristol Channel (downstream of the barrage), while the coastal areas remained largely unaffected throughout the domain. Figure 46c shows the difference in maximum velocity magnitude in a close-up view around the barrage. The differences illustrate an impact on the near-field velocity profiles due to the barrage operation. Even though the majority of the domain experienced a decrease in velocity magnitude, certain places in the vicinity of the barrage experienced a notable increase. Such was the case just behind the sluice gates, on the upstream side of the barrage, where a large increase in velocity magnitude in a form of jets was recorded. The jets formed during the filing stage of the barrage operation, when the sluice gates were opened and turbines closed, with an aim to fill the impoundment as quick as possible. The velocity of the jets behind sluice gates largely exceeded 2 m/s, while in contrast, the currents behind the turbines fell almost to a standstill. The patterns on the downstream side were just reversed, with a high-velocity jet forming at the exit from the turbines, while the sluice gates remain closed during the generation stage of the barrage

operation. This contrast between high and low velocity is not important only from the hydrodynamic point of view, but can also play a significant role in erosion and deposition, as well as on transport processes of suspended sediments and solutes.

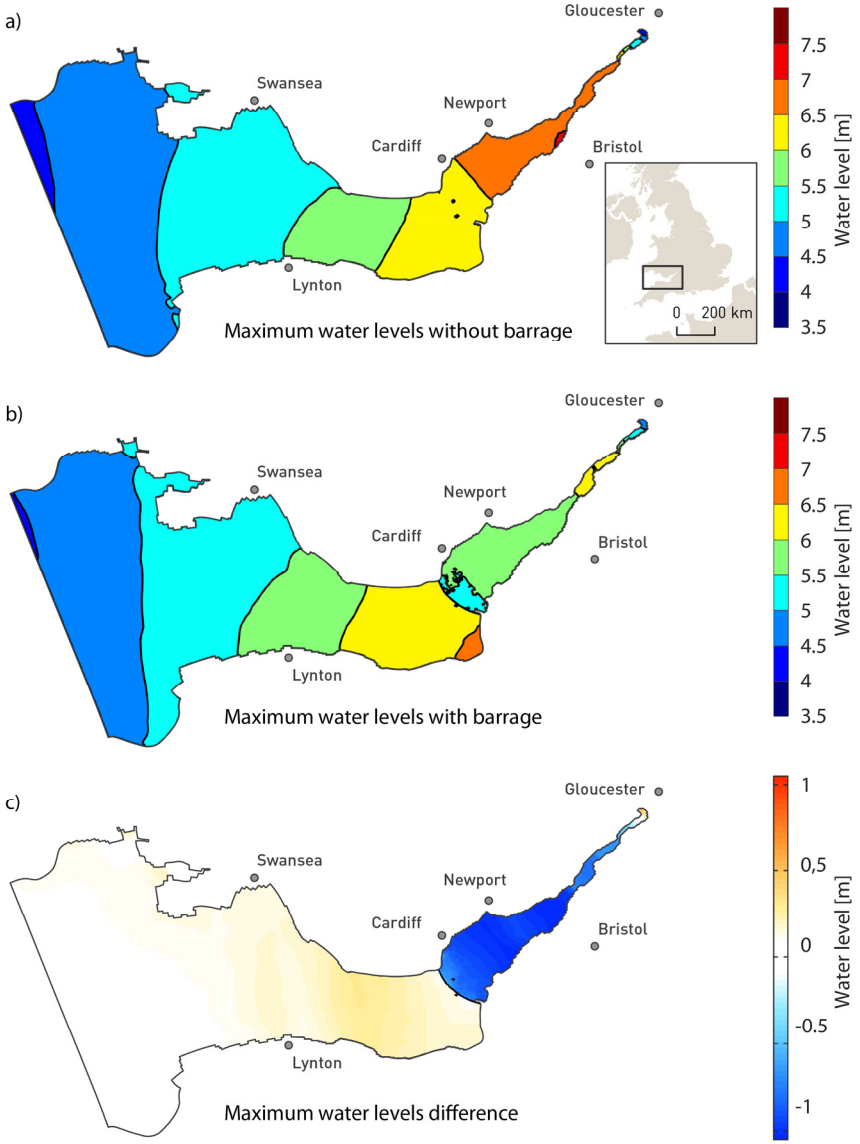

Figure 44: Maximum water levels (a) without and (b) with the barrage and (c) the differences between the two.

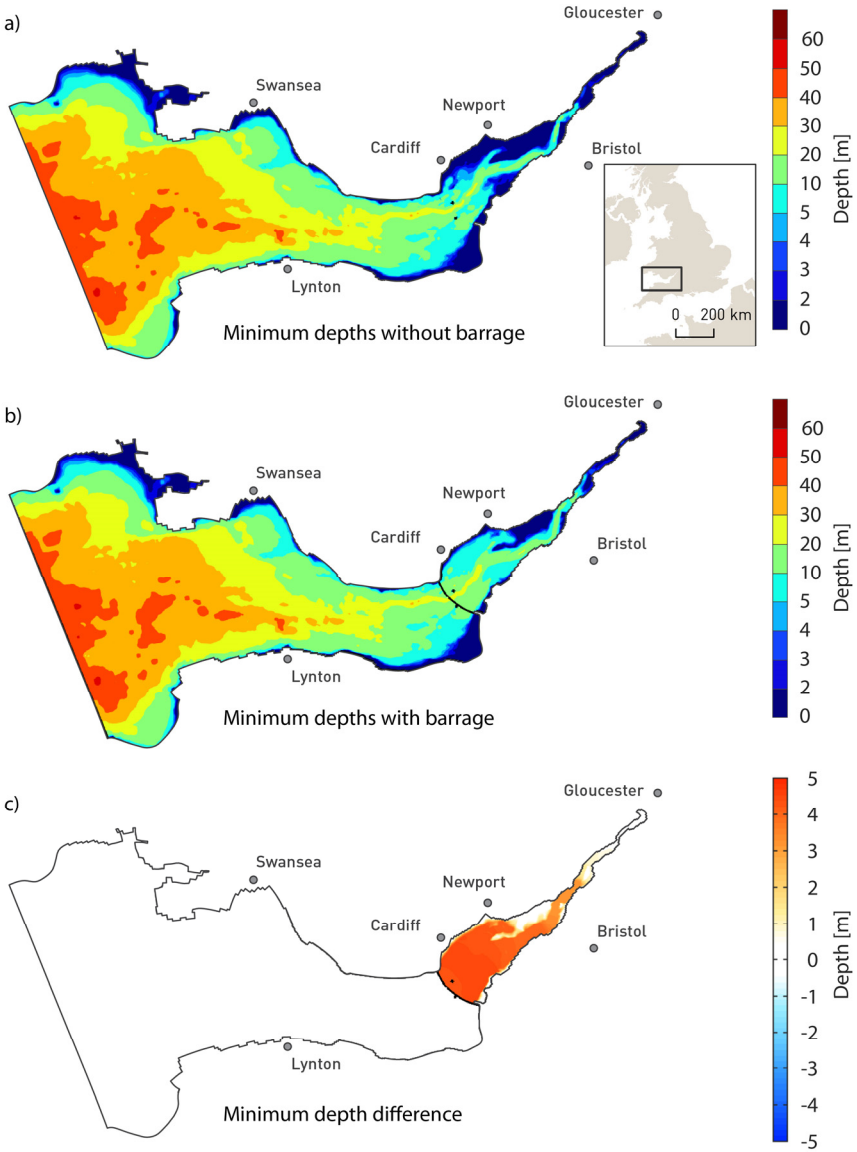

Figure 45: Minimum water depths (a) without and (b) with the barrage and (c) the differences between the two.

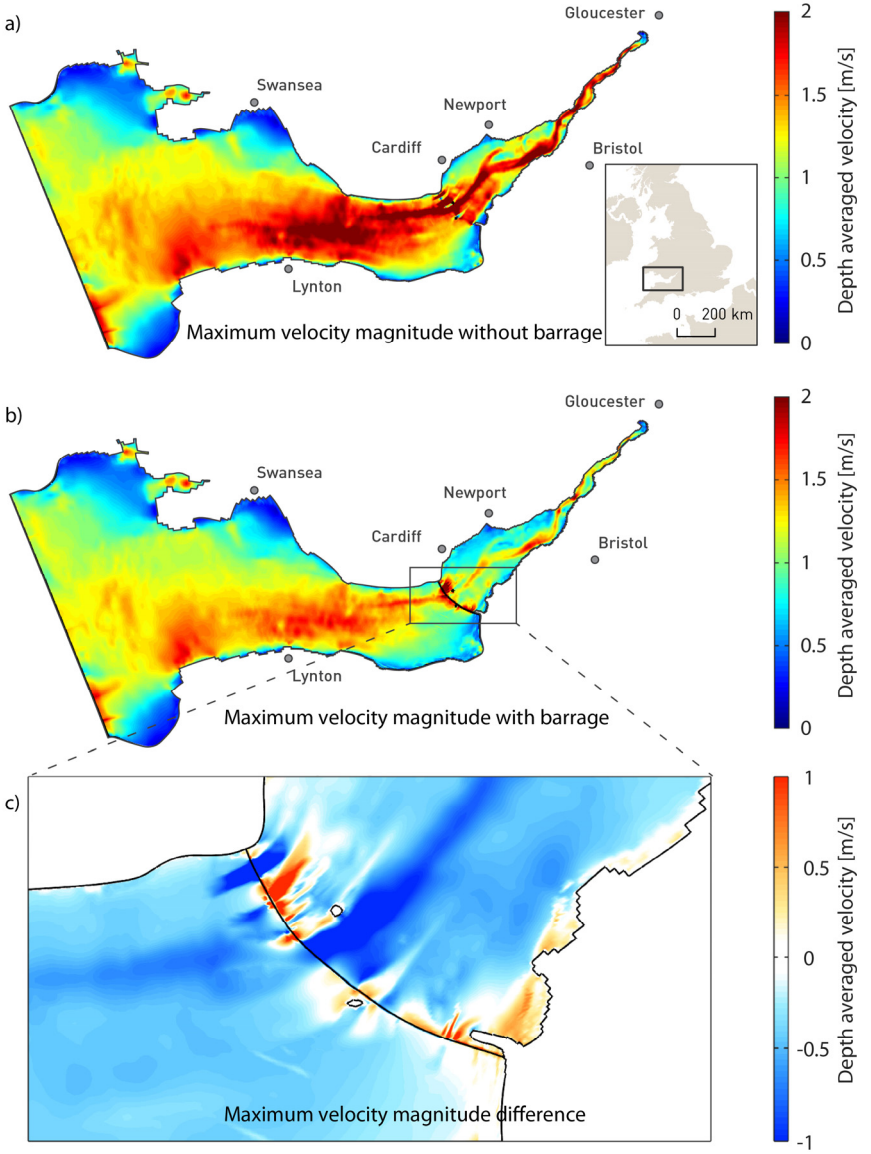

Figure 46: Maximum tidal currents (a) without and (b) with the barrage and (c) a close-up of the differences between the two around in the vicinity of the barrage.

4.4. Summary

The TRS module for Delft3D model was developed by implementing new subroutines into the source code, required for simulating the operation of a tidal power plant. The modifications were based on the existing numerical techniques for TRS simulation, that were judiciously adopted from the literature. The model was tested on the Severn Barrage to demonstrate the effectiveness of the developed procedure. Special attention was given to the assessment of the barrage operation regarding the predicted energy output and its impact on local and far-field hydrodynamics. This being the case, the simulations were performed with and without barrage in place. By calculating the difference between the two sets of results, the impacts of the barrage operation could be observed and compared with the results from the literature.

Validation showed that Delft3D was able to adequately reproduce the hydrodynamic conditions of the initial model before the construction of the barrage. Results also showed a good agreement with the results from the literature. A direct comparison between Delft3D and EFDC (Bray et al. 2016) showed that the former actually outperformed the latter in the prediction of flow velocity and direction. Following the successful validation, the results from the simulation with the barrage were analysed. The water levels time series on both sides of the barrage provided an insight into the barrage operation. The ebb-only generation operational sequence showed comparable predictions to similar schemes found in the literature (Xia et al. 2010c; Zhou et al. 2014a; Bray et al. 2016). The estimated annual energy production was predicted to be 15.3 TWh, similar to 14.7 TWh predicted by Angeloudis et al. (2016b), slightly less but still of the same order of magnitude as 17 TWh predicted by Xia et al. (2010c) and 17.1 TWh by Bray et al. (2016). These results were satisfactory within the scope of this study; however, it should be acknowledged that energy output is highly sensitive to the characteristics of turbines, which are not publicly available, thereby raising the uncertainty of the estimated power production.

The impacts on the far-field water elevations were also consistent with the findings in the literature (Bray et al. 2016; Zhou et al. 2014c), confirming the requirement for extending the domain to the continental shelf to avoid impacts on the boundary conditions. Local impacts were investigated using a smaller domain with a higher resolution for which the boundary conditions were extracted from the continental shelf model. Local impacts were also consistent with findings from the literature, including:

- The increase of maximum water surface elevations downstream of the barrage resulting in an increased risk of coastal flooding in the area.
- The decrease of maximum water surface elevations upstream of the barrage resulting in a decreased flood risk of coastal flooding in the area.
- A significant increase of minimum water surface elevations upstream of the barrage, permanently flooding intertidal mudflats, raising concerns from the ecological point of view.
- A significant reduction in maximum current velocities domain-wide and increase in maximum flow velocity at the exit from turbines and sluice gates, substantially altering the sediment transport processes in the estuary.

Overall, the results presented in this chapter indicate that the modifications made to Delft3D are appropriate for modelling the impacts of tidal range energy structures in the Severn Estuary and Bristol Channel. The model includes all the necessary procedures to reliably simulate the operation of any tidal range structure and can be easily modified to include other tidal range projects proposed in the region. The extended domain also allows for the analysis of any large projects that would have the power to disrupt the boundary conditions of the smaller domain.

5
CASE STUDY 2: SWANSEA BAY TIDAL LAGOON

The case study of the proposed Swansea Bay tidal lagoon was used to assess the impacts of the developed methods on the performance of a hydrodynamic model on a regional scale. This chapter focuses particularly on the treatment of momentum associated with the jets exiting the lagoon and investigates its impacts on the hydrodynamic predictions. Adding to the developed numerical techniques that were already introduced in the Severn Barrage model, the study also adopted the novel approach to conserving the momentum through hydraulic structures, as described in Section 3.3.3.

5.1. Methodology

A high-resolution 2D modelling approach is commonly considered suitable for a regional scale study of tidal energy projects in estuaries (Angeloudis et al. 2016b). Due to the modifications to the momentum treatment of the turbine discharge, an increase in the flow complexity was expected in the vicinity of the lagoon that would be unlikely to be captured using conventional depth-averaged models. Therefore, an additional 3D model with five horizontal layers was also implement in this study. The vertical dimension was modelled by splitting the domain proportionally into five layers, where each layer was still considered depth-averaged. The horizontal velocities of adjacent layers were coupled by the vertical advection and the vertical viscosity term (Deltares 2014).

For the calculation of the vertical turbulent velocity and eddy diffusivity, a k-ε turbulence model was used, which included a second-order turbulence closure model (Launder and Spalding 1974). The new 3D model retained the same resolution of the horizontal grid from the original 2D model as well as all other attributes, such

as boundary conditions, bathymetry, bottom roughness etc. Five different model revisions, including different representations of the turbine, were implemented for this study, as explained below and summarised in Table 10.

Firstly, a 2D model simulation with no modifications to the momentum treatment (SBL1) was set up to act as a baseline for the subsequent model set-ups. The other four scenarios included the implementation of two different velocity distributions for the exiting jet, for 2D and 3D models. These velocity distribution scenarios are summarised below and are shown in Figure 48.

5.1.1. Realistic velocity distribution

As illustrated in Figure 47, horizontal bulb turbines are designed with a draft tube in the shape of a diffuser behind the turbine runner. The role of the draft tube is to minimise head losses and increase the efficiency of the turbine, by increasing the static pressure while simultaneously decreasing the velocity of the exiting flow (Gubin 1973). The shape of the velocity profile was acquired from the experimental work by Wilhelm et al. (2016b) and was distributed over the square-shaped area of the diffuser. For the case of the 5-layer model, this velocity was equally divided amongst the middle three layers as shown in Figure 48. The velocity for momentum conservation in Equation (21) was therefore calculated using the square-shaped area at the diffuser exit (A_{T1}) as shown in Figure 47. This velocity distribution has been applied to scenarios SBL 2 and SBL 4 (Table 10).

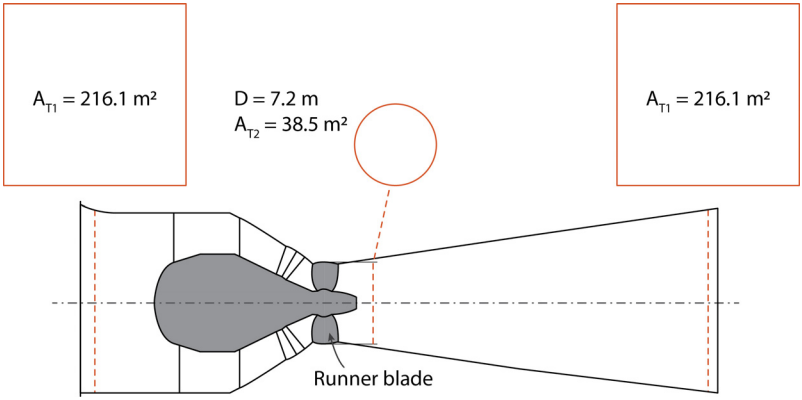

Figure 47: Turbine cross-section – the flow-through area at the duct entrance and exit is rectangular and it transitions to a smaller circular shape in the middle at the location of the turbine runner.

5.1.2. Simplified velocity distribution

In this case, the velocity stays concentrated in a narrow jet assuming the shape of a bell curve as illustrated in Figure 48. The discharge was applied to a single horizontal layer that was located at the same location as the vertical position of the turbine's centreline and the energy loss due to the expansion of the flow through the diffusor was ignored. The velocity for momentum conservation in Equation (21) was calculated using the turbine flow-through area at the runner (A_{T2}) as shown in Figure 47. This velocity distribution has been applied to scenarios SBL 3 and SBL 5 (Table 10).

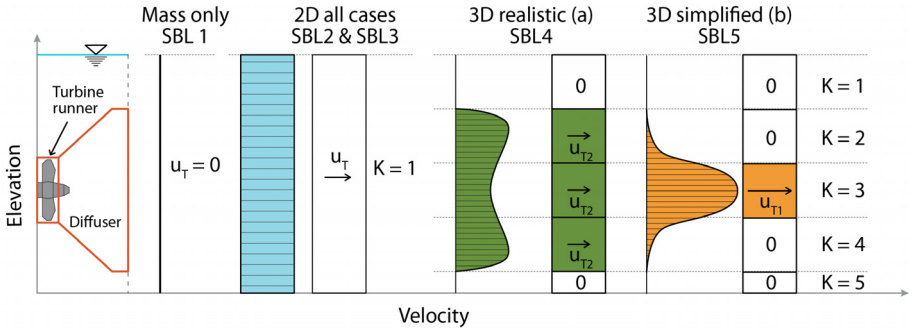

Figure 48: Representation of velocity distribution in the numerical model for a 2D and 3D configuration.

Table 10: Summary of the five different scenarios investigated in this study.

Dimension	2D	2D	2D	3D	3D
Simulation Run	SBL1	SBL2	SBL3	SBL4	SBL5
Momentum conservation	No	Yes	Yes	Yes	Yes
Velocity distribution	-	Diffuser	Simplified	Diffuser	Simplified
A_T [m^2]	-	A_{T1} 216.1	A_{T2} 38.5	A_{T1} 216.1	A_{T2} 38.5

5.1.3. Tidal lagoon scheme description

Tidal lagoons are conceptually a novel adaptation of an existing and proven technology of tidal barrages (Waters and Aggidis 2016a). Instead of spanning the entire width of an estuary, the lagoon is created by constructing an embankment in a horseshoe shape attached to the coastline. In the same way as a barrage, the lagoon takes advantage of the large tidal amplitude to create a head difference across the structure that drives flow through the turbines. Swansea Bay is potentially a suitable

site for deployment of such a scheme due to its location on the north bank of the Bristol Chanel which, together with the Severn Estuary, represents one of the largest tidal range resources in Europe (DECC 2010).

A tidal lagoon in Swansea Bay was first proposed more than a decade ago (Petley and Aggidis 2016). In 2015, the project received a development consent order (DCO) from the UK government (The Planning Inspectorate 2015) and in 2016 a backing from an independent review, namely the Hendry Review of Tidal Lagoons, commissioned by the UK government (Hendry 2016). However, the UK government has recently withdrawn its support for the project and put the project indefinitely on hold, with the main concern being the cost of electricity compared to alternatives, such as wind farms and nuclear power (Guardian Media Group 2018).

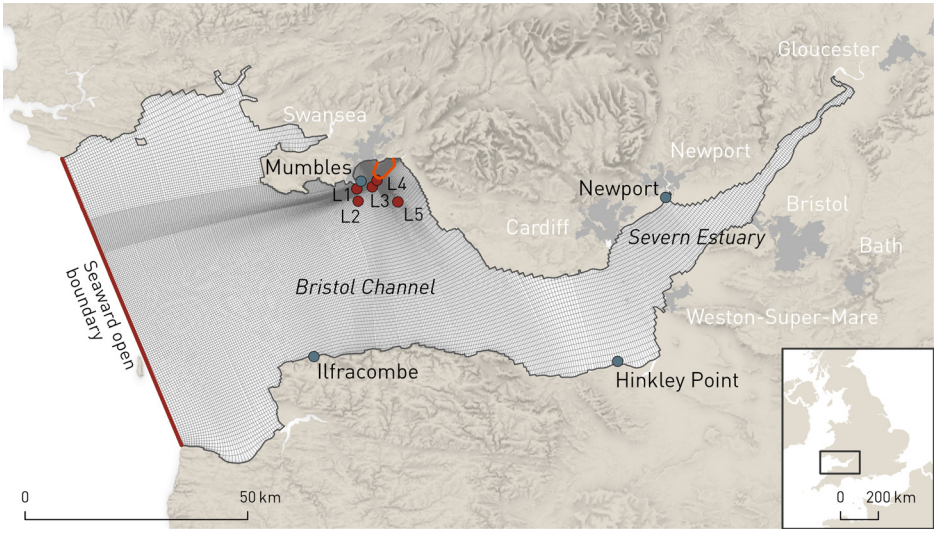

Figure 49: The distinctive horseshoe shape of the current lagoon proposal (orange) and its location in the Swansea Bay.

Since the initiation of the project, several alternative proposals with different lagoon layouts and turbine capacities were considered. The shape and layout of the structure used in this study were taken from the latest proposal put forward by Tidal Lagoon Plc (Tidal Lagoon Plc 2018) and is shown in Figure 49.

If built, Swansea Bay tidal lagoon would become the largest TRS to-date and the first of its kind in the world. The scheme proposes a 9.5 km long embankment that would form an impoundment, with a surface area of 11.5 km^2 (Tidal Lagoon Plc 2016). The proposed power plant would have an installed capacity of 320 MW, providing

power to over 155,000 homes (Hendry 2016). This would be achieved through a set of sixteen bulb turbines, each with a diameter of 7.2 m and an output power of 20 MW, with an additional 800 m^2 of sluice gates to aid with the maximisation of the head difference. This design allows for a two-way operation, where power is produced during both ebb and flood tides. The starting head for generating was designed to be 2.5 m and a minimum head was designed to be 1.5 m. The same characteristics were also used in other recent studies (Angeloudis and Falconer 2017; Angeloudis et al. 2016b; Petley and Aggidis 2016). A summary of the scheme's specifications is outlined in Table 11.

Table 11: Specifications of the Swansea Bay lagoon scheme used in this study.

Starting head [m]	2.5
Minimum head [m]	1.5
Wall length [km]	9.5
Impounded area [km^2]	11.5
Turbine number	16
Turbine diameter [m]	7.2
Turbine capacity [MW]	20
Total capacity [MW]	320
Combined sluice gate area [m^2]	800

5.1.4. Numerical model set-up

The tidal flows in Swansea Bay have been extensively studied (Xia et al. 2010c; Ahmadian et al. 2010a; Angeloudis et al. 2016b; Falconer et al. 2009; Uncles 1984). The hydrodynamics in the region have been shown to be highly complex due to the exceptional tidal range, the complex land boundary and the highly variable gradients of the seabed elevations (Xia et al. 2010c). However, the estuary was found to be well-mixed with no evidence of stratification, suggesting that natural flow conditions are primarily two-dimensional (Uncles 1984). Usually, a high-resolution 2D model would be considered suitable for such a study. A regional scale model covering the Severn Estuary and Bristol Channel was constructed in order to fully model the lagoon. This extent of the model was selected to ensure an appropriate location for the boundaries, enabling the hydrodynamic processes within the area of interest to be captured.

A rectangular, curvilinear grid with a variable mesh resolution was employed to increase the efficiency by reducing the mesh size only in the areas of interest (Figure

49). The grid resolution in and around the lagoon was therefore relatively large at 30 m x 30 m while retaining a coarser mesh size of 500 m x 500 m at the edge of the domain. An extended domain model (continental shelf model) was also used during the validation process to determine whether boundary conditions could be affected by the lagoon operation.

The seaward boundary was located at the entrance to the Bristol Chanel (Figure 49), which stretched from Heartland Point in south-west England, to the south-west tip of Pembrokeshire in Wales. The open boundary condition was set up as a water elevation time series obtained from the National Oceanography Centre (NOC) Continental Shelf Model (CS3) (The National Oceanography Centre 2018). The predictions from the CS3 model are based on up to 50 tidal harmonic constituents (M2, S2, N2, etc.) and the resulting water levels are separated into (i) tidal only results and (ii) residual surge results. Only the tidal component was used for the construction of the boundary condition time series, which covered a full neap-spring tidal cycle between 19 January and 2 February 2012 in 1 hour intervals, as illustrated in Figure 50.

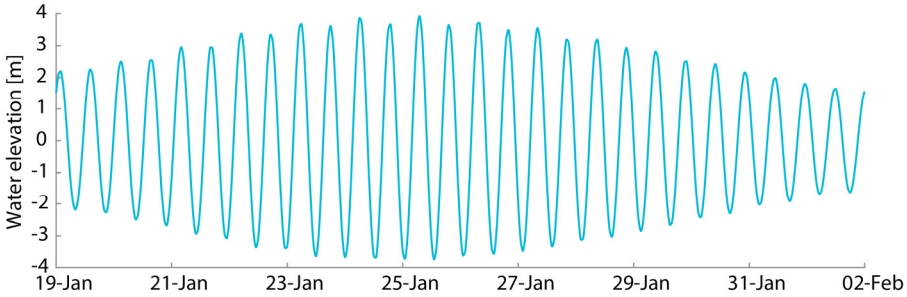

Figure 50: Water elevation time-series at the open boundary for a full neap-spring tidal cycle.

The bathymetry for the model was obtained from EDINA Digimap service. The original data was relative to Lowest Astronomic Tide (LAT)/Chart Datum (CD) on a 1 arc-second by 1 arc-second grid (Seazone 2013). The data was converted to the Mean Sea Level (MSL) by subtracting the differences between CD and MSL obtained from the Severn Estuary, Cornwall and Devon coastal charts, which were interpolated to the EDINA grid. Finally, the bathymetry relative to MSL was interpolated onto the Severn Estuary grid used in this model. The bathymetry of the model is shown in Figure 51.

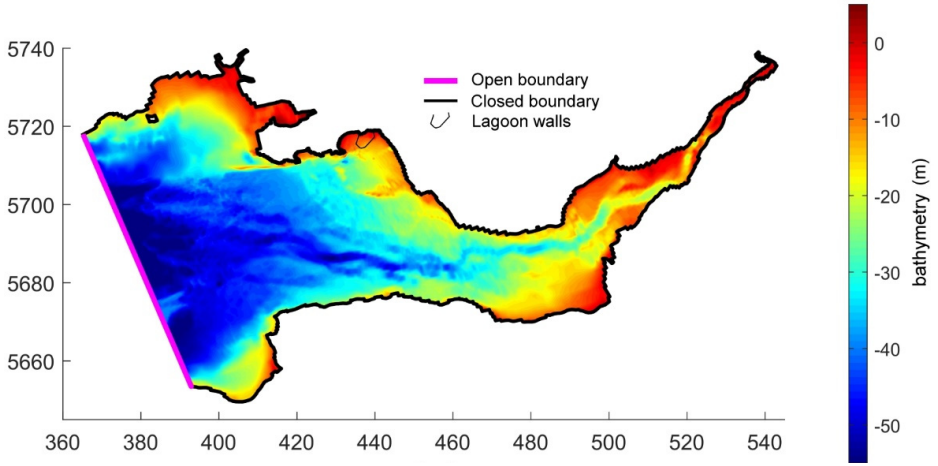

Figure 51: Bathymetry of the numerical model, showing the lagoon and domain boundaries.

For simplicity, the Manning's n was set to a constant value across the entire domain. The model could be further improved by using more complex formulations of the roughness coefficient related to the spatial distribution of bed characteristics. However, this was considered beyond the immediate scope of this study given that the focus has been on demonstrating the relative impacts of the momentum conservation method on the jets and wakes exiting the turbines and with the general bed characteristics across the computational domain being fairly uniform and constituting sand and generally smooth bed slope and morphological changes. It was therefore assumed that spatial changes in the Manning's roughness coefficient (without appropriate data) would have little impact on the main thrust of this study, which was to assess the impact of including improved momentum conservation characteristics as potential energy is converted to kinetic energy through the turbines and sluice gates.

All simulations used the same time step of 3 seconds, which was selected to satisfy the CFL condition. The total CPU time for simulating the entire 14-day neap-spring tidal cycle was 7 hrs for the 2D model and 48 hrs for the 3D model, running on a desktop PC with 3.60 GHz Intel® Core™ i7 series CPU.

5.1.5. Far-field impacts

Prior to the validation of the hydrodynamic conditions, the continental shelf (CS) model was used to determine whether the operation of the lagoon would affect the

boundary conditions of a smaller model in a similar way as the Severn barrage did in Figure 36. The CS model was run for the baseline scenario (SBL1) and compared to the CS run without the lagoon. Figure 52 shows a comparison between the maximum water levels predicted by the two models. It can be clearly seen that the impacts of the lagoon alone are negligible comparing to the impacts caused by the barrage. This was to be expected as Swansea Bay lagoon displaces significantly less water with its impoundment surface area of 11.5 km^2, compared to 573 km^2 impounded by the Severn Barrage. The only changes to the water level regime were recorded in the Swansea Bay and inside the lagoon itself, confirming that the CS model is unnecessary for the simulations of this scheme. All the consequent simulation runs were performed only using the Severn Estuary and Bristol Channel model.

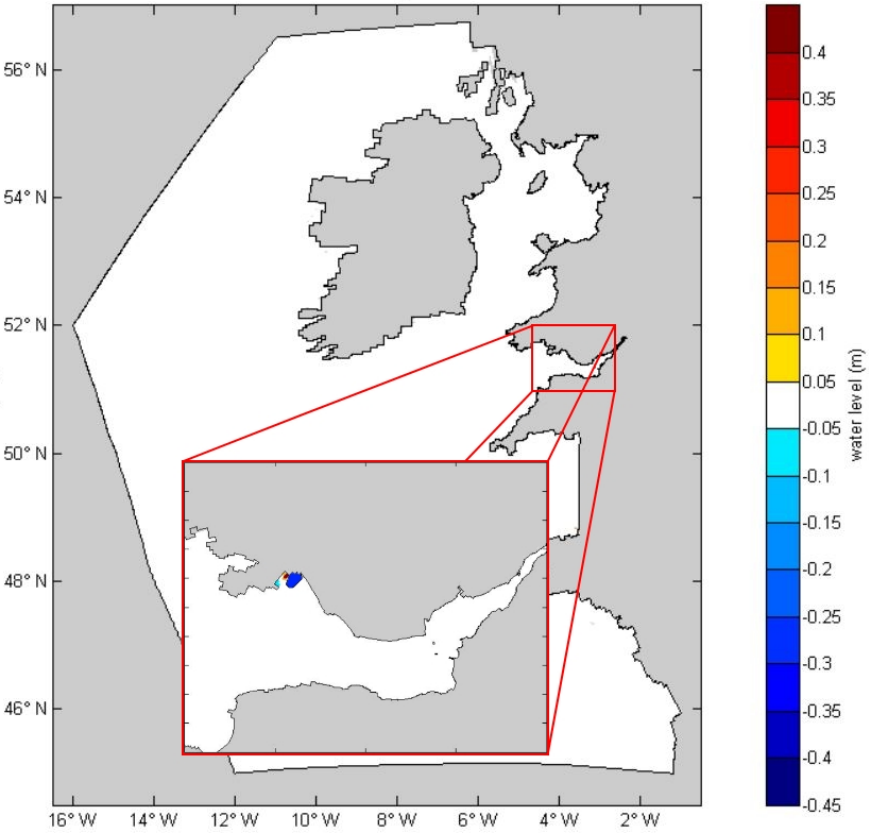

Figure 52: Impact of the lagoon on maximum water levels under a two-way operation.

5.2. Calibration and validation

The goal of calibration was to determine what value of Manning's n would provide the best fit between predicted and observed water levels across the estuary. The calibration was carried out by comparing the simulation results with tide gauge records provided by the British Oceanographic Data Centre (BODC), at four sites throughout the Severn Estuary and Bristol Channel, namely Hinkley Point, Ilfracombe, Mumbles and Newport (BODC 2017). Locations of the four sites are presented in Figure 49.

Following the calibration at BODC sites, the model was validated against data from a field survey of Swansea Bay. Acoustic Doppler profiler (ADP) measurements were taken at five locations (L1 to L5) throughout the Swansea Bay, where the tidal lagoon is proposed to be built and therefore is expected to have the most impact. The validation was performed over a 14-day period between 25 July and 7 August 2012 to capture the typical neap-spring tidal variation. The locations of the observation sites are presented in Figure 49.

The ADP data was provided through the Smart Coasts project, an EU-funded research study on water quality of bathing waters in Wales (EMU Limited 2012). The deployments consisted of seabed frame mounted ADP located at five different sites in the bay (Figure 49). The deployed instruments were Nortek's Aquapro 1 MHz (used on sites L1, L3 and L4) and Aquapro 600 kHz (sites L2 and L5) ADPs, capable of recording current profiles and pressure. They were carried out between July and October 2012 by EMU Limited. All equipment was configured to record in GMT (UT+0000) and all locations were recorded in WGS84. The ADPs were configured to acquire a water level record and current profile every 10 minutes over an averaging period of 60 seconds. To provide data security and quality assurance, each frame was equipped with a lightweight release transponder tilt sensor to make sure that the frame was deployed upright. Raw pressure data were converted to height above the sensor using density values that were pre-set for the conditions in the Swansea Bay. The calculated heights were reduced to the mean of the data set for harmonic analysis, from which the lowest astronomical tide (LAT) and highest astronomical tide (HAT) values extrapolated with reference to the data set mean. The final recordings consisted of a pure tidal height component and an inconsistent residual height variation. The observed currents were considered to be a combination of a tidal stream component, a mean drift component, and an inconsistent residual drift. Because boundary conditions of the model were driven solely by tidal harmonic

forcing, only the tidal height and tidal stream components of the ADP measurements were used in the validation of the model.

5.2.1. Calibration

The sensitivity of the Manning's n was tested through a series of hydrodynamic simulations without the lagoon in place, over a complete neap-spring tidal cycle. Previous studies of Severn Estuary have used different values of roughness coefficient in range between 0.02 and 0.035. Hence, four different roughness coefficients (0.02, 0.025, 0.03 and 0.035) were selected for calibration of the Swansea Bay model.

Table 12: Sensitivity analysis of roughness coefficient (Hinkley Point).

n	r [-]	RMSE [m]	NSE [-]	SI [-]
0.020	0.986	0.644	0.961	0.560
0.025	0.997	0.297	0.992	0.259
0.030	0.998	0.208	0.996	0.181
0.035	0.991	0.472	0.979	0.410

Table 13: Sensitivity analysis of roughness coefficient (Ilfracombe).

n	r [-]	RMSE [m]	NSE [-]	SI [-]
0.020	0.998	0.238	0.991	0.098
0.025	0.999	0.224	0.992	0.093
0.030	0.999	0.229	0.992	0.095
0.035	0.999	0.229	0.992	0.095

Table 14: Sensitivity analysis of roughness coefficient (Mumbles).

n	r [-]	RMSE [m]	NSE [-]	SI [-]
0.020	0.983	0.551	0.954	0.230
0.025	0.988	0.467	0.967	0.254
0.030	0.992	0.390	0.977	0.212
0.035	0.994	0.327	0.984	0.178

Table 15: Sensitivity analysis of roughness coefficient (Newport).

n	r [-]	RMSE [m]	NSE [-]	SI [-]
0.020	0.971	0.942	0.925	2.170
0.025	0.993	0.499	0.979	1.151
0.030	0.994	0.430	0.984	0.991
0.035	0.979	0.778	0.949	1.794

The results of sensitivity analysis are presented in Tables 12 to 10573, with corresponding scatter plots in Figure 53. The model was found to have low sensitivity to bed roughness. Based on the statistical performance indicators, which were calculated using the Equations (23) to (26), a value of 0.03 was selected as the one producing the best fit.

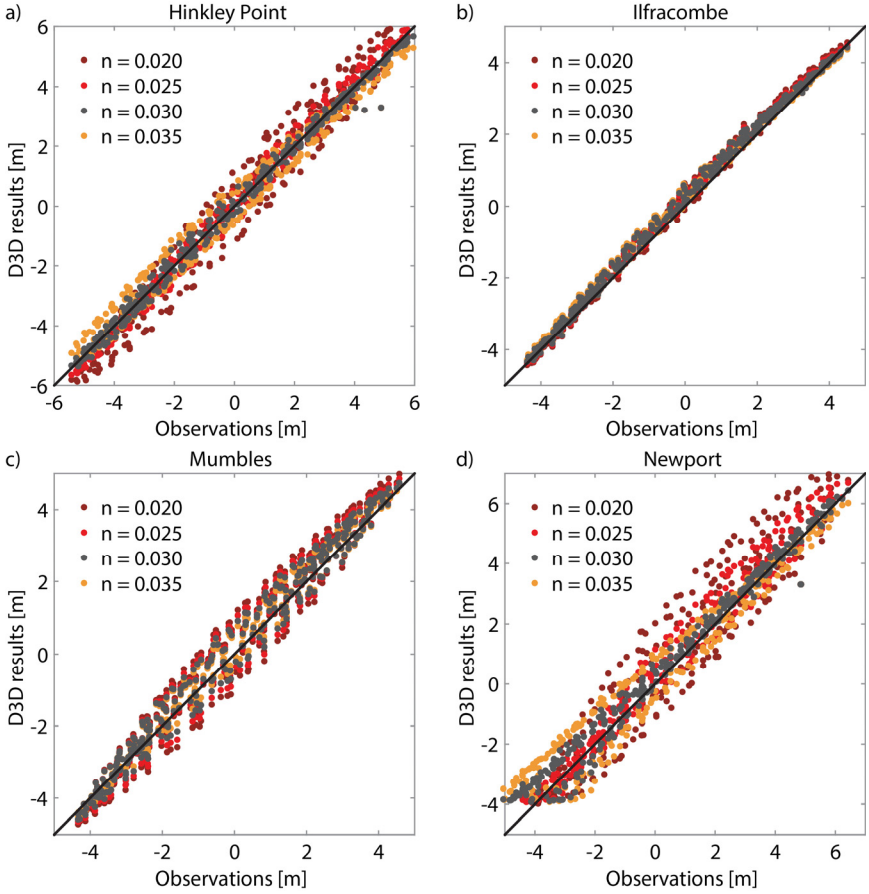

Figure 53: Sensitivity analysis of roughness coefficient at four observation sites in the Severn Estuary and Bristol Channel

5.2.2. Validation

Figure 54 shows the validation results for sites L3 and L5. The results showed good agreement with the observed data. They were also consistent with the results

reported in the literature, where different numerical models, such as DIVAST and EFDC, have been used in the past to predict the hydrodynamic conditions in the Severn Estuary and Bristol Channel (Ahmadian et al. 2010a; Bray et al. 2016; Xia et al. 2010a; Zhou et al. 2014c).

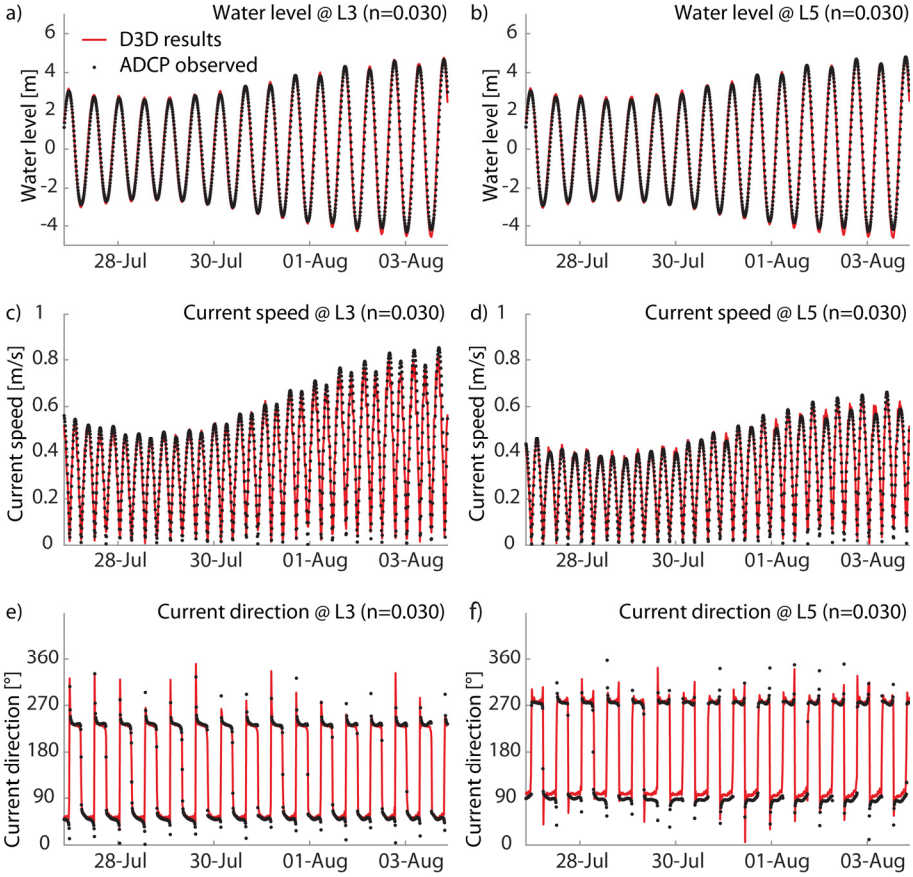

Figure 54: Validation results showing water levels and flow velocity at location L3 and L5.

To quantify the performance of the hydrodynamic model, four different performance indicators were used, i.e. correlation coefficient r, RMSE, NSE and SI, which were calculated using the Equations (23) to (26). The results for all five observation sites are presented in Tables 16 to 18, showing performance indicators for water level, current speed and current direction results respectively.

The correlation for water levels was above 0.99 at all five locations and the NSE values ranged from 0.982 to 0.988 suggesting a high level of agreement between the model results and observations. The model consistently under predicts low tide levels during spring tides, which is reflected through a slightly higher RMSE. This was believed to be due to an error in open boundary condition, however it was regarded as acceptable based on the results from previous studies of the Severn Estuary found in literature (Bray et al. 2016; Falconer et al. 2009). The SI was low in all cases and therefore of no concern.

Analysis of the current speed again showed very high correlation with values well above 0.9 for all five locations. The NSE analysis showed slightly worse performance at site L1 with a value of 0.776, however, still within an acceptable range. This discrepancy can be attributed to the location of the site close to Mumbles headland which can have an impact on velocity predictions in numerical simulations (Stansby et al. 2016). The RMSE and SI were low in all cases and therefore of no concern.

Table 16: Validation results for water levels at five observation locations.

Location	r [-]	RMSE [m]	NSE [-]	SI [-]
L1	0.992	0.350	0.982	0.189
L2	0.994	0.296	0.987	0.167
L3	0.993	0.324	0.984	0.186
L4	0.993	0.323	0.985	0.185
L5	0.994	0.292	0.988	0.164

Table 17: Validation results for current speed at five observation locations.

Location	r [-]	RMSE [m/s]	NSE [-]	SI [-]
L1	0.933	0.118	0.776	0.242
L2	0.976	0.063	0.953	0.112
L3	0.966	0.059	0.928	0.143
L4	0.952	0.056	0.898	0.166
L5	0.984	0.031	0.967	0.093

Table 18: Validation results for velocity direction at five observation locations.

Location	r [-]	RMSE [°]	NSE [-]	SI [-]
L1	0.937	32	0.840	0.198
L2	0.962	26	0.922	0.159
L3	0.936	32	0.874	0.243
L4	0.895	44	0.791	0.332
L5	0.944	33	0.878	0.191

Similarly, NSE values calculated for the current directions were between 0.791 and 0.922, with correlation generally at and above 0.9, again showing strong agreement between the two sets of results. The slightly lower NSE values were due to the sensitivity of the NSE method to data outliers. As observed in Figure 54, both the predicted and observed data for flow direction contained "spikes" which occurred during slack water and when the velocity falls close to zero. At the same time, the flow must change the direction between an incoming and outgoing tide, which appeared as outlier points in the flow direction time series. This also explains higher RMSE and SI values for current directions. However, these discrepancies have little impact on the overall performance of the model and are generally considered a good fit.

The direct comparison of the results in Figure 54, together with the quantitative statistical analysis Tables 16 to 18, indicated a robust forecasting ability of the model and justified its use for further hydrodynamic analysis with the lagoon in place.

5.3. Results

5.3.1. Lagoon operation

After the successful validation of hydrodynamics, the scenario SBL 1 was run to provide baseline results and to ensure the correct functioning of the model. The operation of the lagoon can be illustrated by a time series of water levels on both sides of the turbine housing. The water levels on each side were calculated as a mean value of four points taken at four different observation sites, that were evenly spread about 500 m away from the lagoon (Figure 55). This approach was taken to prevent any local disturbances in the water surface, that could potentially affect the head difference across the lagoon.

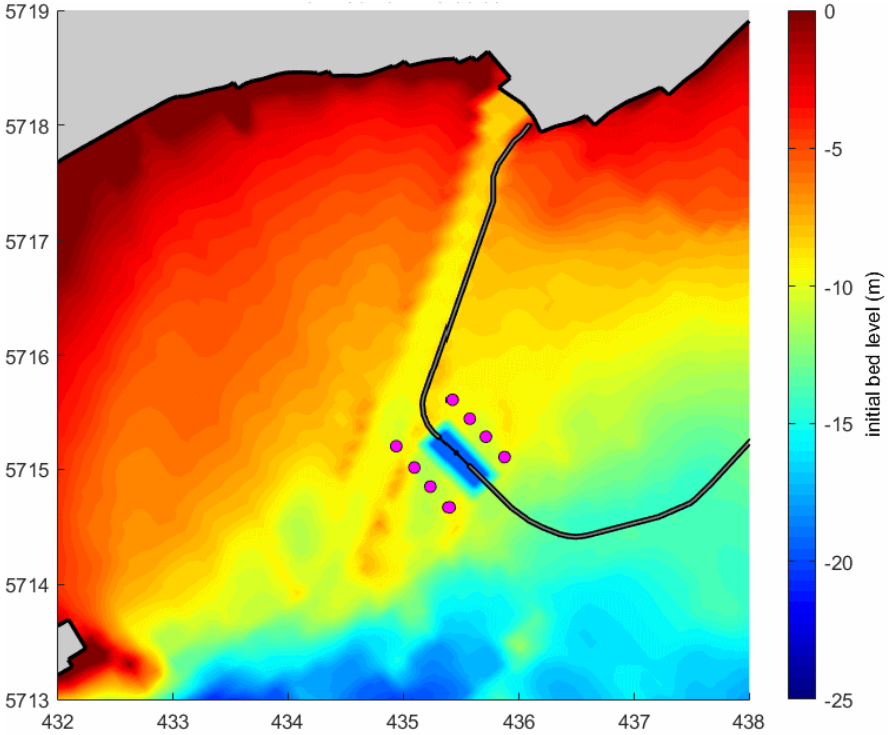

Figure 55: Location of points for determining the head difference across the lagoons.

The two-way generation sequence has resulted in four cycles of power generation per day. Generating during both flood and ebb tides means that power production is spread more evenly throughout the day compared to the one-way schemes. The water levels in Figure 56 were recorded during the maximum spring tidal cycle, during which the largest tidal range of 8.6 m was recorded in Swansea Bay. The tidal range inside the lagoon has been drastically reduced to 6.4 m. The maximum water level inside the lagoon has fallen by 0.76 m, while the minimum water level rose by 1.44 m. Water levels outside the lagoon were left unaffected by the lagoon operation.

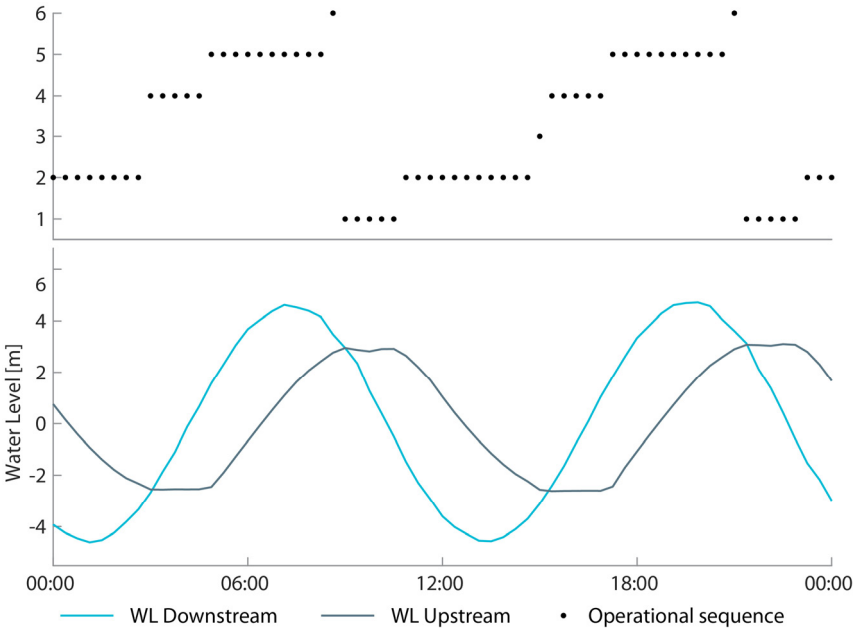

Figure 56: Two-way operation of the Swansea Bay lagoon during a typical spring tidal cycle. Showing water levels on both sides of the lagoon and the corresponding operational stages: (1) holding high water; (2) ebb generation; (3) releasing; (4) holding low water; (5) flow generation, (6) filling.

5.3.2. Velocity field

Figures 57 and 58 show the instantaneous velocity fields near the lagoon during the flood and ebb generation stages respectively. Velocities from the 3D models have been depth-averaged to allow for a direct comparison with the 2D model. Changes to the velocity pattern were limited to the vicinity of the lagoon and have never extended further than 2.5 km away. The changes were induced in the form of a high-velocity jet that has alternatingly formed on the inside and outside of the lagoon. The figures correspond to the peak flow rates during a spring tidal cycle, when the velocity magnitude of the jet was at its extreme. However, the extreme velocities are only an example that represents a general trend which was observed throughout the simulation period, regardless of the size of the tidal range. The peak velocities at the turbine exit for each scenario are collected in Table 19 for flood and in

Table 20 for ebb generation cycle.

The flow patterns in scenarios SBL2 and SBL4, with a realistic velocity distribution (Figures 57c,e and 58c,e), were very close to the baseline model SBL1 (Figures 57b and 58b), with a slight increase in the velocity at the turbine exit. For example, during the ebb generation, the velocity increased from 1.37 m/s in SBL1 to 1.48 m/s in SBL2 and 1.47 m/s in SBL4. During flood generation, the velocity increased from 1.32 m/s in SBL1 to 1.41 m/s in SBL2 and 1.40 m/s in SBL4. The average increase in velocity was under 10 per cent for both the SBL2 and SBL4 scenarios. As expected, scenarios SBL3 and SBL5, with a simplified velocity distribution, saw a more significant increase in the velocity coming out of the turbines (Figures 57d,f and 58d,f). In the 2D model (scenario SBL3), the velocities increased by almost 50 per cent. For example, the peak velocity during ebb tide increased from 1.37 m/s to 2.05 m/s and the peak velocity during flood tide increased from 1.32 m/s to 1.97 m/s. The results from the 3D model (scenario SBL5) predict a slightly lower increase in the range of around 30 per cent, with recorded peak velocities of 1.76 m/s and 1.84 m/s during the ebb and flood tide generation respectively.

Table 19: Peak flow velocity (u_T) and instantaneous discharge (Q_T) just downstream of the turbine exit for a typical spring tidal cycle during flood power generation and the corresponding head difference (H_T). Velocities for scenarios SBL4 and SBL5 are presented both with a depth-averaged value (u_T) for comparison with 2D models and with separate values for respective computational layers (u_{Tk}).

Flood-generation stage						
	Scenario	**Layer**	**u_T [m/s]**	**u_{Tk} [m/s]**	**Q_T [m^3/s]**	**H_T [m]**
2D, only mass	SBL1	-	1.32	-	4336	3.47
2D, w/ mom. transfer	SBL2	-	1.41	-	4377	3.48
	SBL3	-	1.97	-	5192	4.48
3D, w/ mom. transfer	SBL4	K=1	1.40	0.99	4348	3.44
		K=2		1.20		
		K=3		1.27		
		K=4		1.09		
		K=5		0.62		
	SBL5	K=1	1.84	1.05	4954	4.17
		K=2		1.95		
		K=3		2.77		
		K=4		2.19		
		K=5		1.90		

Table 20: Peak flow velocity (u_T) and instantaneous discharge (Q_T) just downstream of the turbine exit for a typical spring tidal cycle during ebb power generation and the corresponding head difference (H_T). Velocities for scenarios SBL4 and SBL5 are presented both with a depth-averaged value (u_T) for comparison with 2D models and with separate values for respective computational layers (u_{Tk}).

Ebb-generation stage						
	Scenario	**Layer**	**u_T [m/s]**	**u_{Tk} [m/s]**	**Q_T [m^3/s]**	**H_T [m]**
2D, only mass	SBL1	-	1.37	-	4408	3.49
2D, w/ mom. transfer	SBL2	-	1.48	-	4411	3.50
	SBL3	-	2.05	-	5364	4.60
3D, w/ mom. transfer	SBL4	K=1	1.47	1.06	4381	3.47
		K=2		1.50		
		K=3		1.40		
		K=4		1.23		
		K=5		0.93		
	SBL5	K=1	1.76	0.88	4973	4.13
		K=2		1.89		
		K=3		2.75		
		K=4		2.18		
		K=5		1.90		

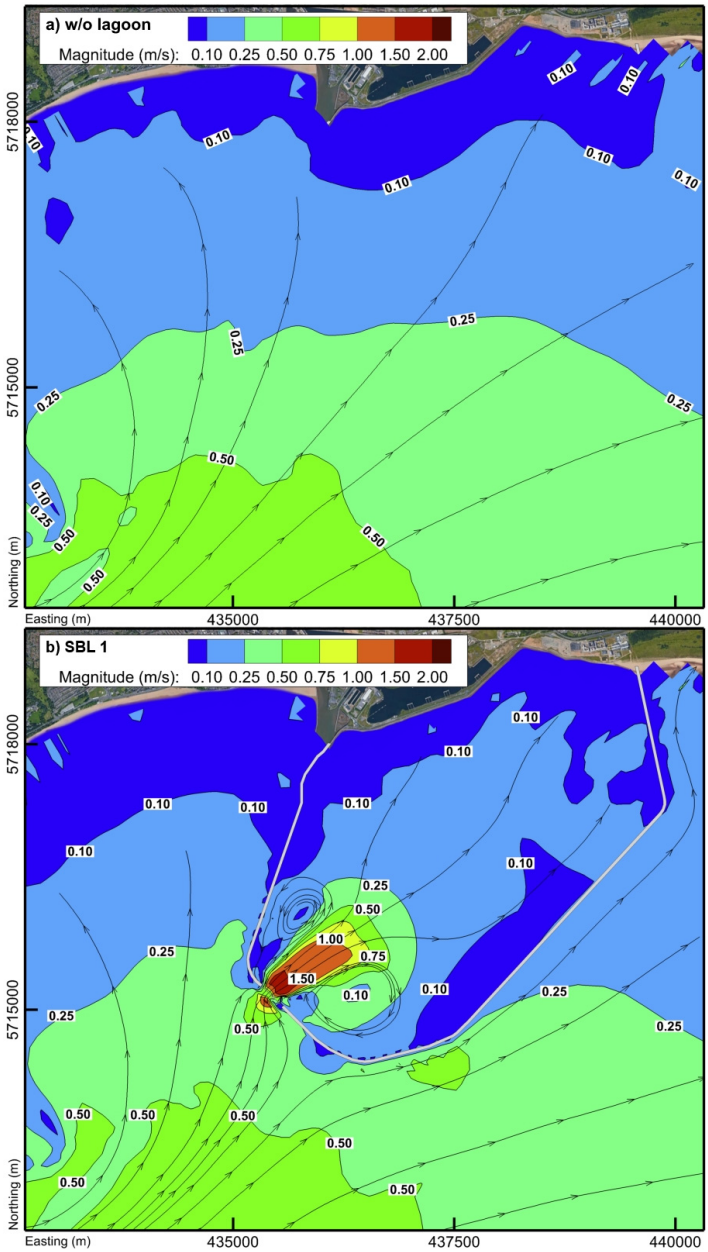

Figure 57: A comparison of velocity fields during the flood generation for a typical spring tidal cycle – (a) without lagoon, (b) SBL 1, (c) SBL 2, (d) SBL 3, (e) SBL 4, and (f) SBL 5.

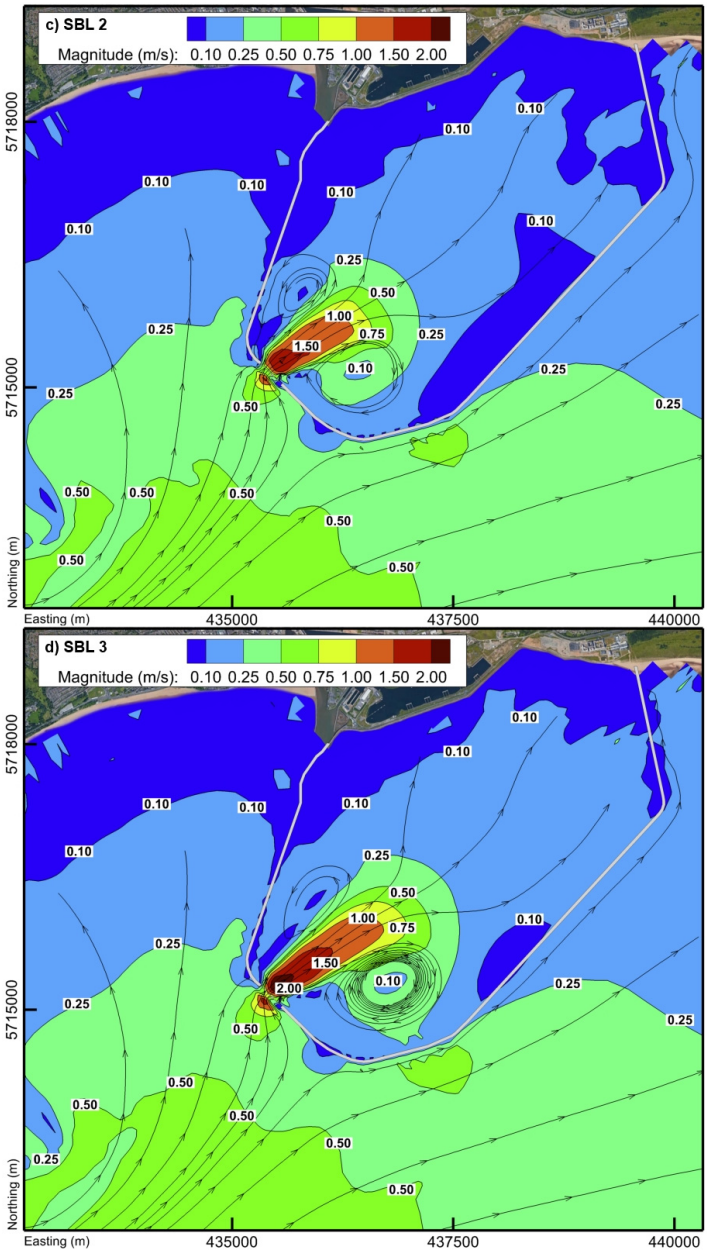

Figure 57: Continued – A comparison of velocity fields during the flood generation for a typical spring tidal cycle – (a) without lagoon, (b) SBL 1, (c) SBL 2, (d) SBL 3, (e) SBL 4, and (f) SBL 5.

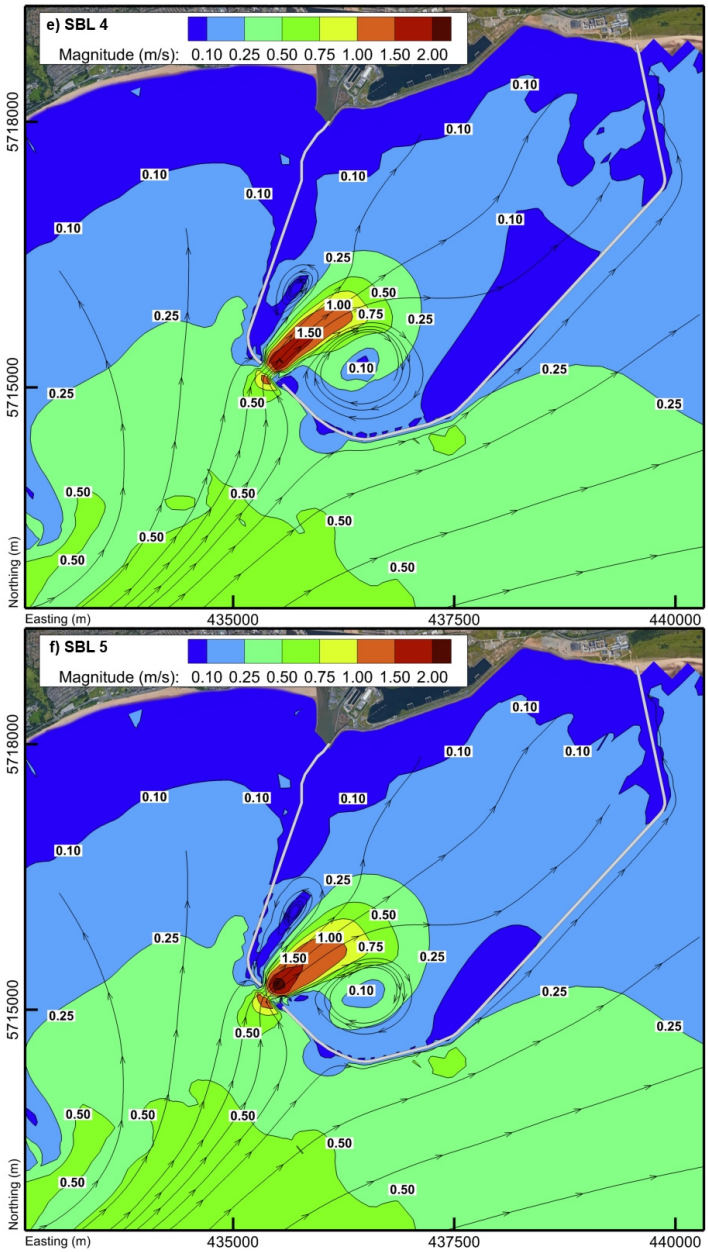

Figure 57: Continued – A comparison of velocity fields during the flood generation for a typical spring tidal cycle – (a) without lagoon, (b) SBL 1, (c) SBL 2, (d) SBL 3, (e) SBL 4, and (f) SBL 5.

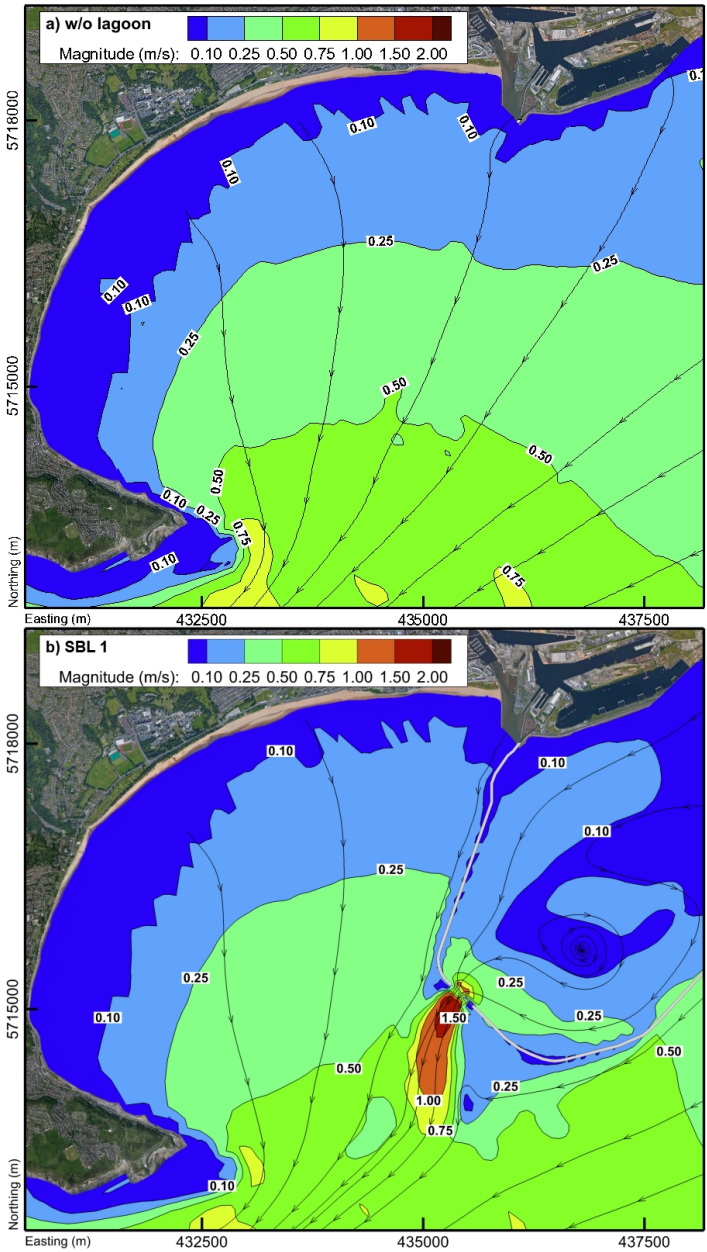

Figure 58: A comparison of velocity fields during the ebb generation for a typical spring tidal cycle – (a) without lagoon, (b) SBL 1, (c) SBL 2, (d) SBL 3, (e) SBL 4, and (f) SBL 5.

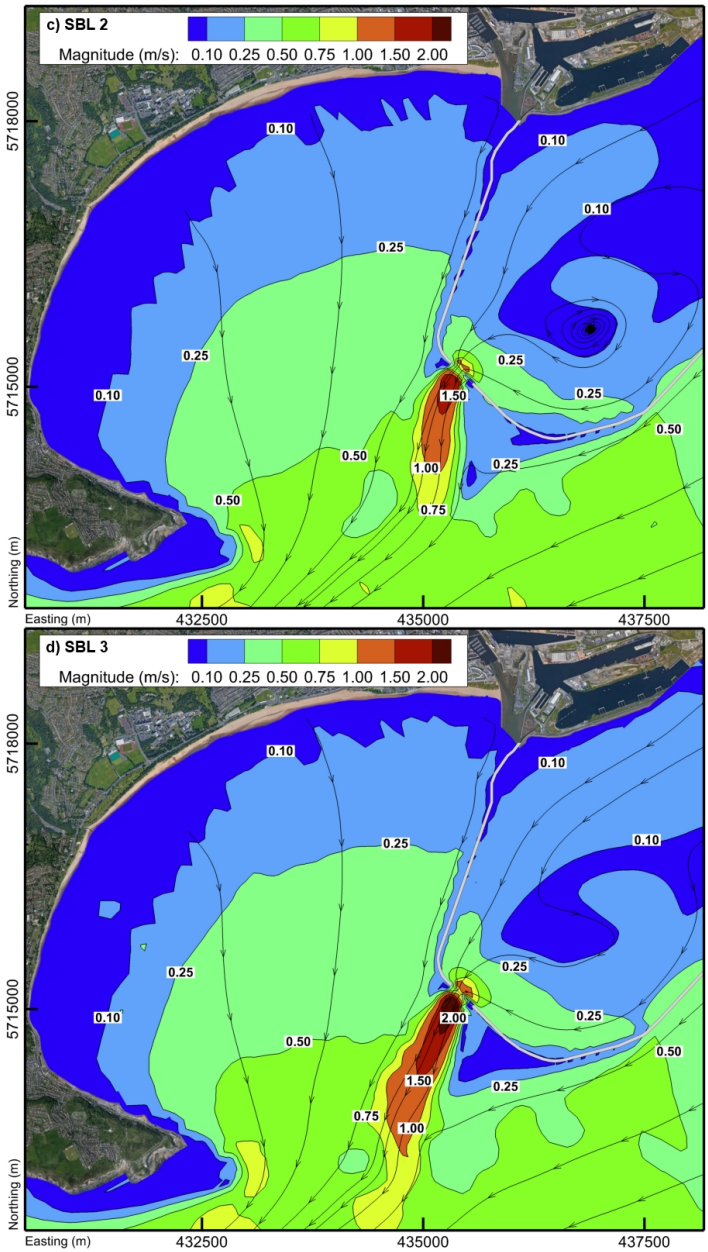

Figure 58: Continued – A comparison of velocity fields during the ebb generation for a typical spring tidal cycle – (a) without lagoon, (b) SBL 1, (c) SBL 2, (d) SBL 3, (e) SBL 4, and (f) SBL 5.

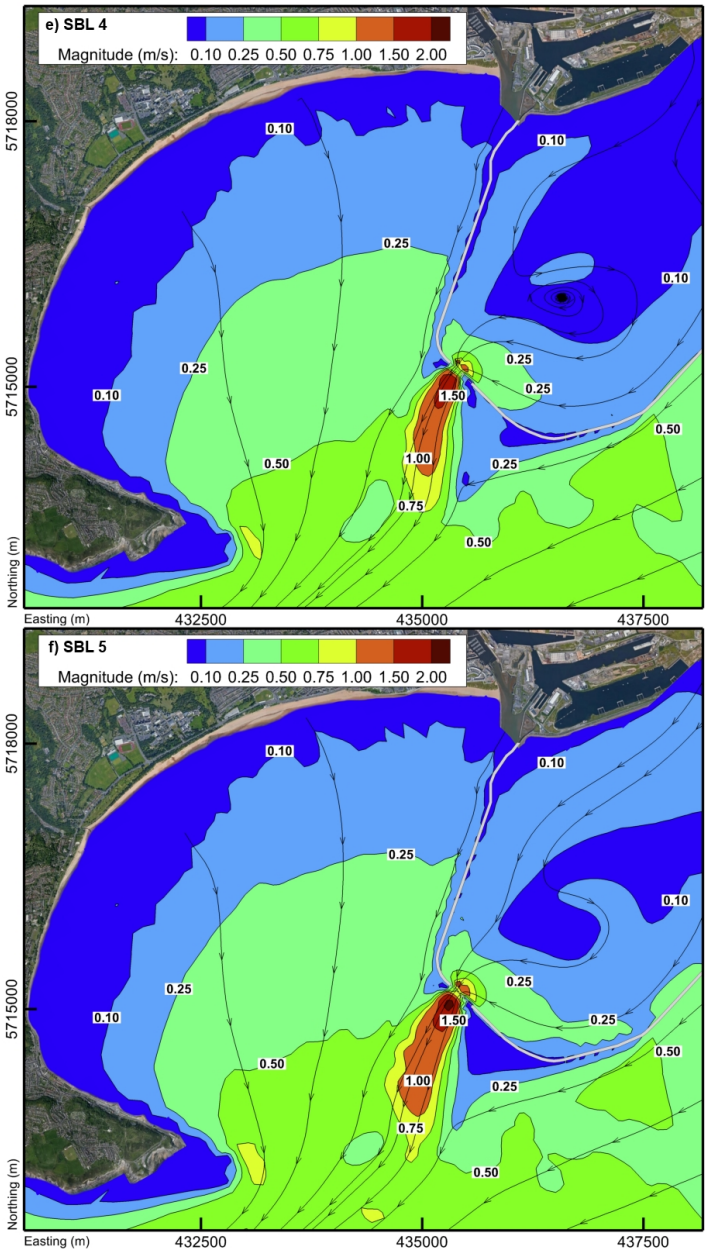

Figure 58: Continued – A comparison of velocity fields during the ebb generation for a typical spring tidal cycle – (a) without lagoon, (b) SBL 1, (c) SBL 2, (d) SBL 3, (e) SBL 4, and (f) SBL 5.

The 3D complexity of the velocity profile in scenarios SBL4 and SBL5 is highlighted in Figure 59. The predicted velocity profiles have been recorded at 50 m increments from the turbine exit at four locations. At 50 m and 100 m downstream of the turbine, the higher velocity in the middle layers is still clear. However, the jet completely dissipates by the distance of 150 m, where velocity profile transitions to a conventional logarithmic shape of free surface flow. This observation is consistent with the findings of Jeffcoate et al. (Jeffcoate et al. 2013). Even though the effects of the jet were lost after this distance, a direct comparison between the two scenarios indicated a clear difference between simplified and realistic velocity distribution. Scenario SBL5 still retains a higher depth-averaged velocity compared to SBL4. An evident increase in the flow velocity could be observed in all cases with the refined momentum treatment.

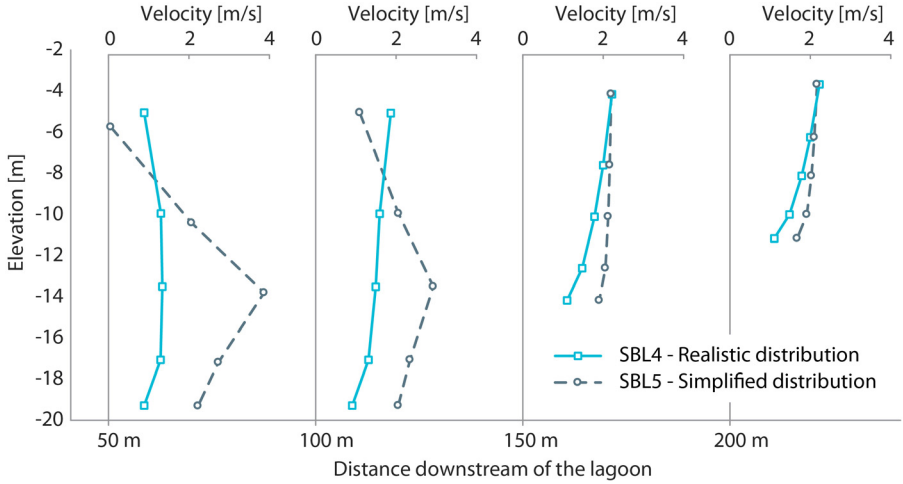

Figure 59: Representative 3D velocity profiles for SBL4 and SBL5 during the ebb generation in four locations downstream of the turbine.

5.3.3. Bed shear stress

In general, sediment transport is governed by several factors, including sediment type, salinity, biological interactions and most importantly hydrodynamic conditions in the region (X. H. Wang and Aandutta 2013). Bristol Channel and Severn Estuary are covered by a diverse bed morphology, including bare rock, gravel, sand and mud. Off the Welsh coast, the estuary bed consists predominantly of sand banks with an isolated muddy zone occurring inside the Swansea Bay (Dyer 1984).

Previous studies have shown that general distribution of the sediments across the estuary correlates well with the maximum bed shear stress from numerical predictions (Warwick and Uncles 1980). The threshold values for the initiation of erosion and deposition are commonly represented by critical shear stress for erosion (τ_{ce}) and deposition (τ_{cd}) respectively. Shi et al. (2015) investigated the erosion and deposition processes in estuarine environments and proposed threshold values of τ_{ce} = 0.14 N/m^2 and τ_{cd} = 0.08 N/m^2 for erosion and deposition respectively. The study employed several different empirical equations for calculating the bed shear stress in the Yangtze River estuary in China, including the combined current-wave action based on the models of Soulsby (1995) and van Rijn (1993). The maximum values of the combined current-wave action in the study rose up to 0.446 N/m^2, from which the currents alone contributed to only 0.224 N/m^2. Similar values were predicted in the Swansea Bay by the Delft3D simulation prior to the construction of the lagoon, where bed shear never exceeded 0.3 N/m^2 (Figure 60).

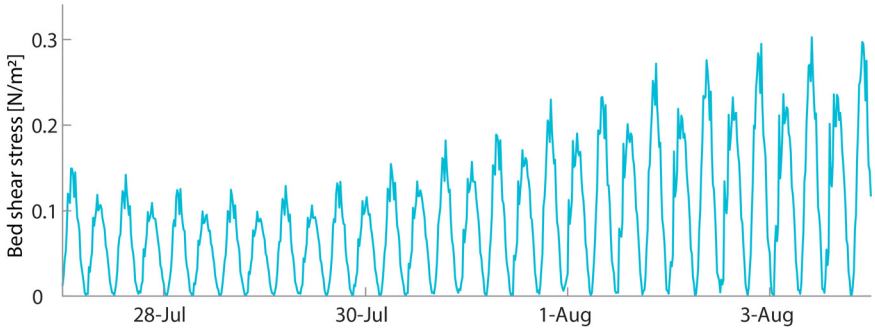

Figure 60: Prediction of bed shear stress in Swansea Bay prior to construction of the lagoon.

The construction of the lagoon would mean a significant disruption to the natural sediment transport processes, with maximum bed shear stress multiplied by several orders of magnitude compared to natural conditions. Even though the affected regions are relatively small, the erosion could lead to disastrous consequences to the environment and structural stability of the lagoon if not addressed before the lagoon is constructed.

Bed shear stress is difficult to measure directly, particularly in turbulent flows, however, there is a way to estimate it from near-bed velocity profiles (Jeffcoate et al. 2017). In the 2D simulations, the local shear stress is assumed to be given by a quadratic friction law including the magnitude of the depth-averaged horizontal velocity (Equation (27)). For the 3D simulations, the same equation is used, but

instead of a depth-averaged velocity, the magnitude of the horizontal velocity in the first layer just above the bed is used (Equation (28)):

$$\overrightarrow{\tau_b} = \frac{\rho_0 g \vec{U}|\vec{U}|}{C_{2D}^2} \tag{27}$$

$$\overrightarrow{\tau_{b_{3D}}} = \frac{\rho_0 g \overrightarrow{u_b}|\overrightarrow{u_b}|}{C_{3D}^2} \tag{28}$$

where ρ_0 is reference density of water, g is acceleration due to gravity, U is the depth-averaged velocity, u_b is the horizontal velocity in the first layer just above the bed, and C_{2D}^2 and C_{3D}^2 are the 2D- and 3D-Chézy coefficients.

Bed shear stress was calculated at the time of maximum flow velocity upstream and downstream of the turbines. Figures 61 and 62 respectively show the results during the flood and ebb generation stage, corresponding to velocity results in Figures 57 and 58. Because bed shear stress is directly related to the velocity field, the impact of the tidal lagoon on the results showed similar patterns as the impact of the lagoon on the velocity field. The changes in bed shear stress were the most prominent locally around the lagoon, coinciding with the position of the jets on both sides of the lagoon. The area further away from the site was left largely unaffected by the operation of the lagoon.

Both flood and ebb cycles produced similar results, with the flood cycle affecting the bed shear stress inside the lagoon and ebb cycle affecting it outside, just downstream of the turbine housing block. There was little difference in the bed shear stress between the baseline run (SBL 1) and the 2D run with a realistic velocity distribution (SBL 2). The extent of the area affected was similar, however, SBL 2 case showed a slightly higher value of maximum shear stress with 17.2 N/m^2, compared to 15.8 N/m^2 in SBL 1. Similarly, the 3D simulation with the same distribution (SBL 4) with 16.9 N/m^2 resulted in only a slight increase from SBL 1. This shows that if the design of the draft tube manages to efficiently dissipate the velocity profile evenly across the diffusor exit, the shear stress imposed on the bottom surface would not be too dissimilar to the one predicted by the baseline scenario. The results also indicate that under this assumption, where velocity is more evenly distributed across the depth, 2D simulation is sufficient for assessing the bed shear stress, with a 3D model predicting very similar results.

When velocity distribution was simplified the bed shear stress increased dramatically. In the 2D case (SBL 3) the maximum value rose to 29 N/m^2, while the 3D case produced even higher shear stress, with a maximum value of 50 N/m^2. The area of impact has noticeably increased in the 2D case (SBL 3), extending further away

from the turbines in the shape of the jet. In the 3D case (SBL 5) the affected area stayed roughly the same, but with a much higher concentration of the higher values close to turbines, which then dissipated relatively quickly. This shows that in the case with the simplified velocity distribution, where the jet is assumed to be much more concentrated, a 3D simulation with momentum conservation is essential for providing more accurate results.

The increased bed shear stress caused by the exiting jet indicates extensive erosion on both sides of the lagoon. This is particularly problematic on the inside of the lagoon, where eroded sediment is most likely to be deposited in the lower velocity regions closer to the coast and in the centre of the vortices forming on both sides of the jet (Figure 57). In contrast to high-velocity current during the flood generation, velocity magnitude on the inside during the emptying of the lagoon was consistently weaker, resulting in almost insignificant bed shear stress (Figure 62). Therefore, it is likely that ebb currents will not be able to flush out sediments accumulated during the filling of the lagoon, inhibiting the long-term performance of the scheme and incurring additional operational costs for dredging. This effect was present even during the baseline scenario (SBL 1) but was further amplified in simulations with conserved momentum. Increased bed shear stress in these cases would result in a higher rate of erosion under the jets and a higher rate of deposition in low velocity regions during the filling stage. The bed shear stress during the emptying stage has remained low even when momentum conservation was considered (Figure 62c-f).

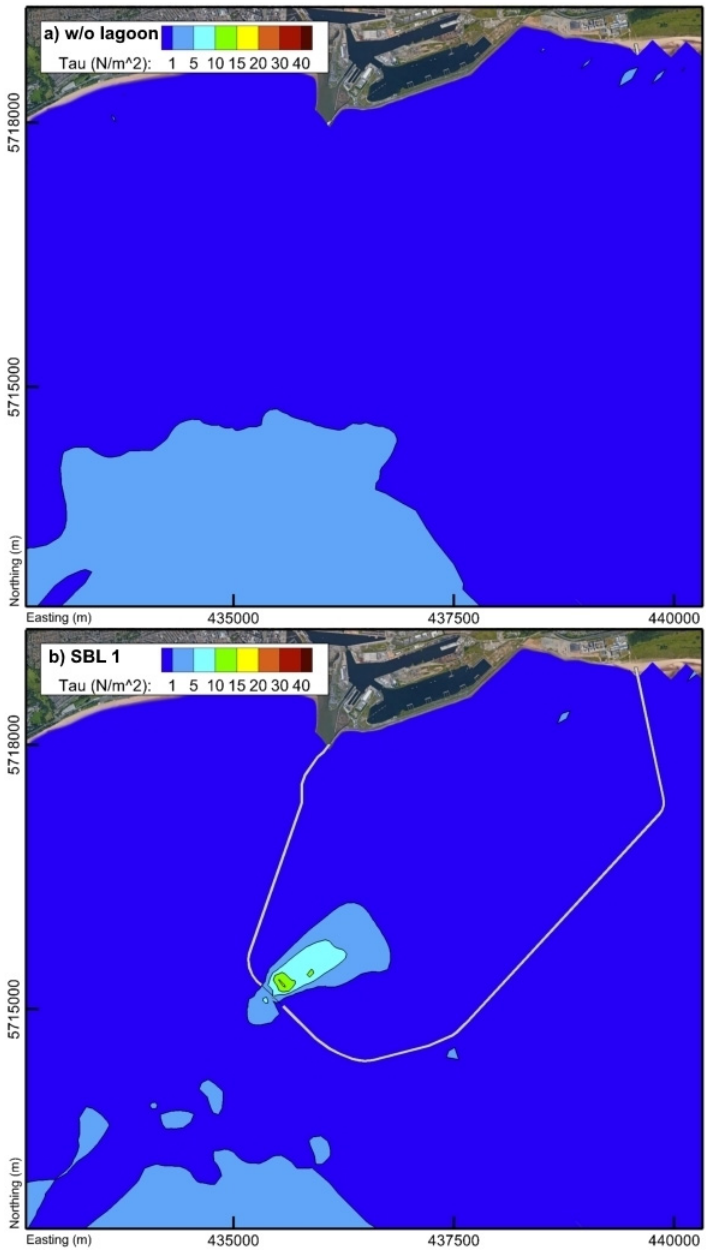

Figure 61: Bed shear stress during the flood generation – (a) without lagoon, (b) SBL 1, (c) SBL 2, (d) SBL 3, (e) SBL 4, and (f) SBL 5.

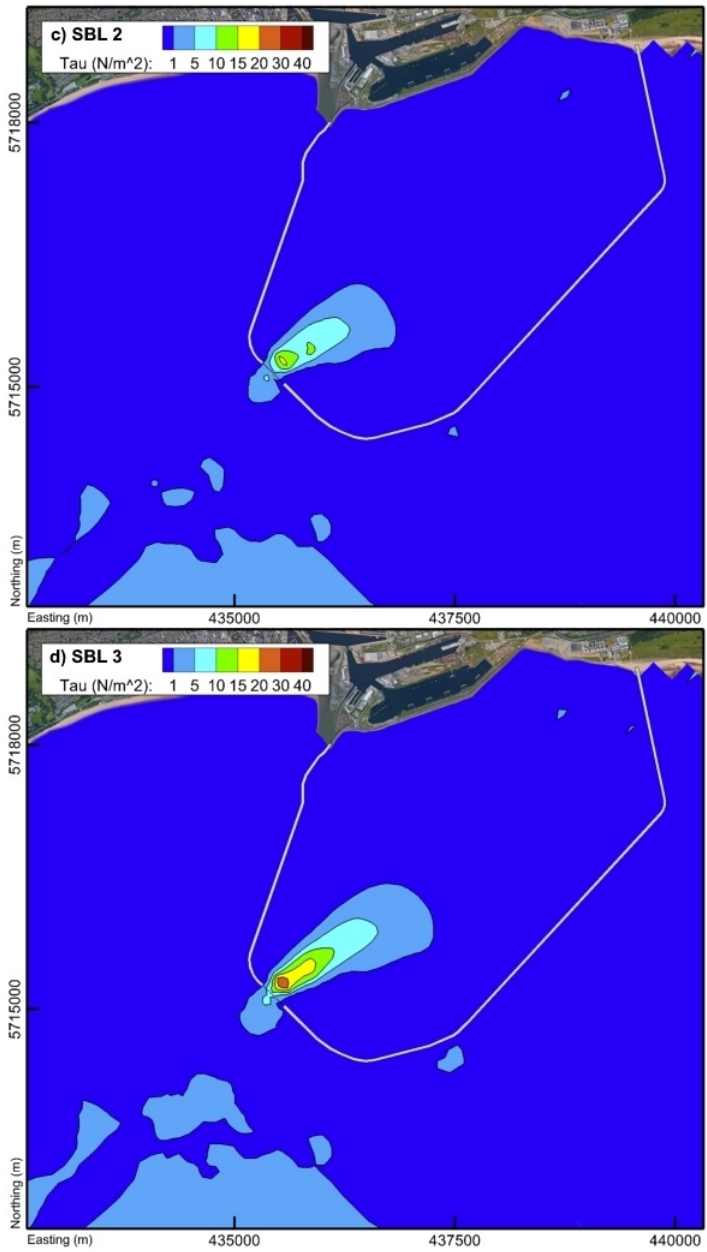

Figure 61: Continued – Bed shear stress during the flood generation – (a) without lagoon, (b) SBL 1, (c) SBL 2, (d) SBL 3, (e) SBL 4, and (f) SBL 5.

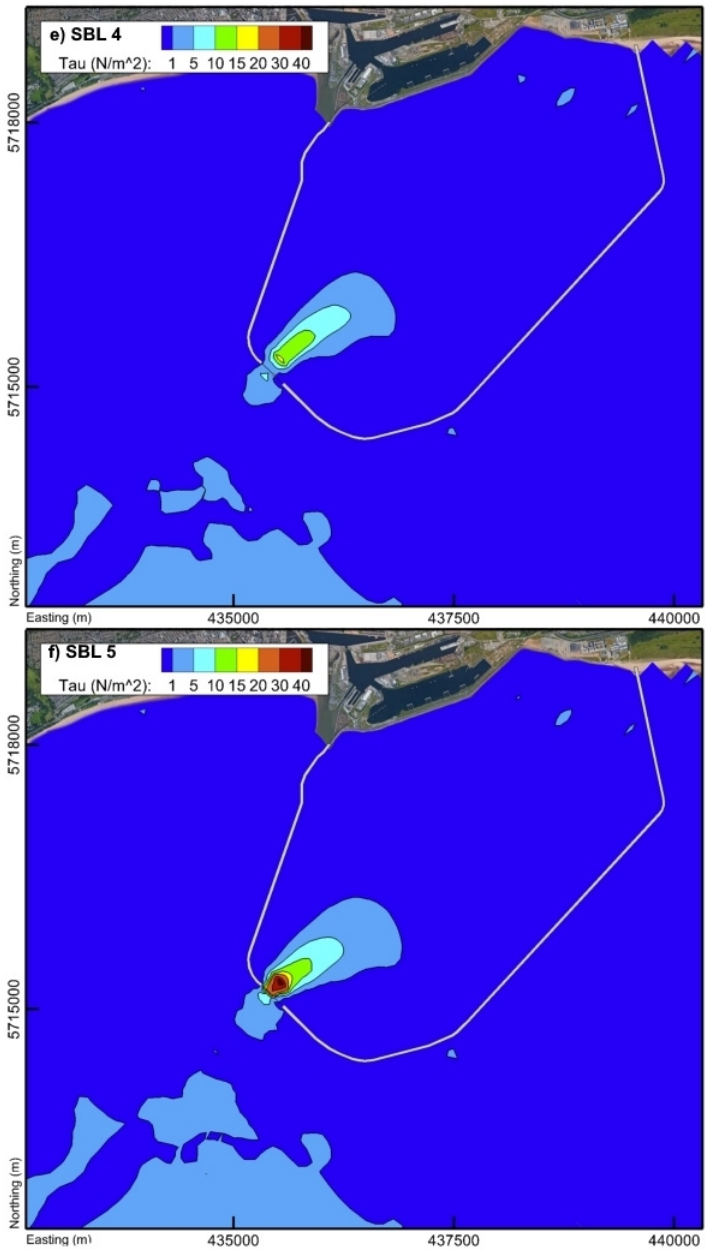

Figure 61: Continued – Bed shear stress during the flood generation – (a) without lagoon, (b) SBL 1, (c) SBL 2, (d) SBL 3, (e) SBL 4, and (f) SBL 5.

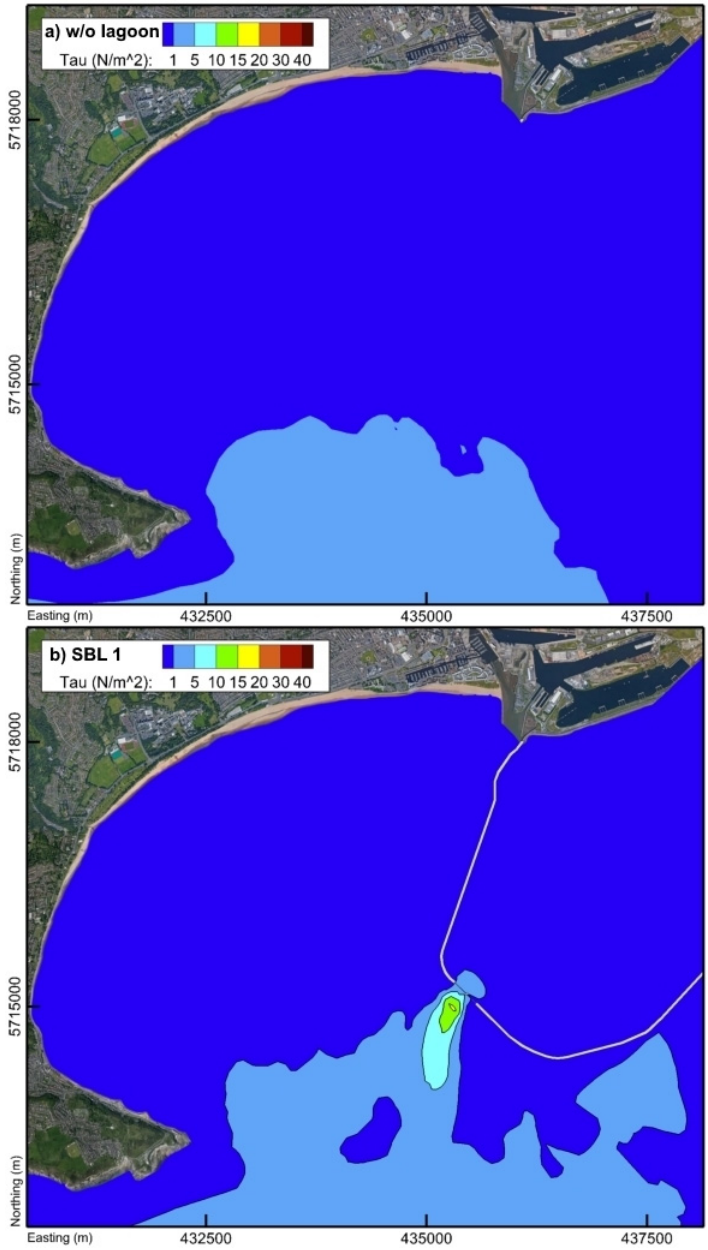

Figure 62: Bed shear stress during the ebb generation – (a) without lagoon, (b) SBL 1, (c) SBL 2, (d) SBL 3, (e) SBL 4, and (f) SBL 5.

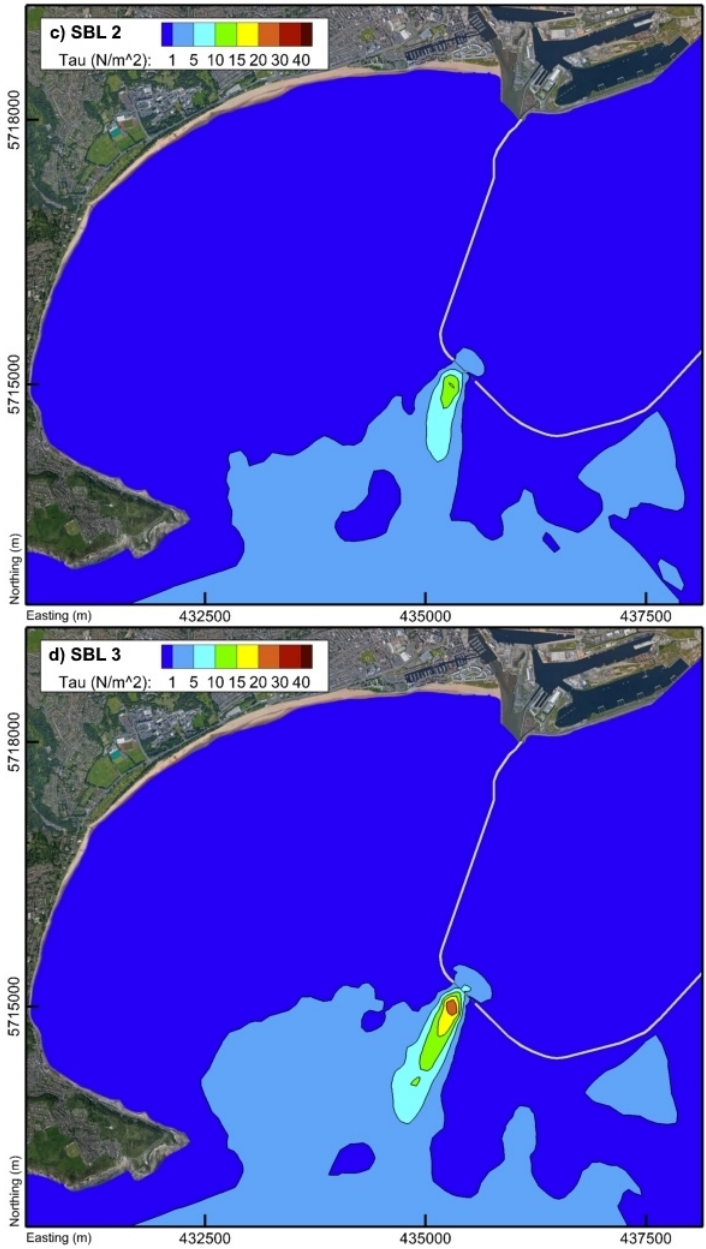

Figure 62: Continued – Bed shear stress during the ebb generation – (a) without lagoon, (b) SBL 1, (c) SBL 2, (d) SBL 3, (e) SBL 4, and (f) SBL 5.

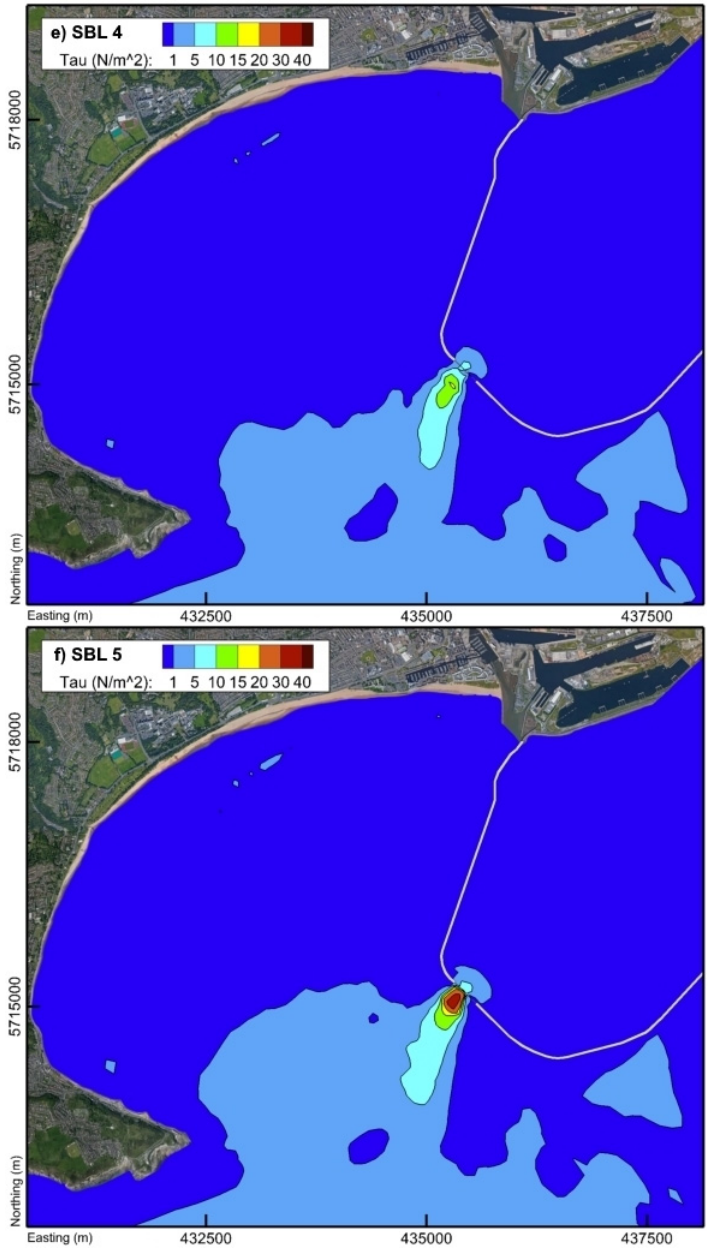

Figure 62: Continued – Bed shear stress during the ebb generation – (a) without lagoon, (b) SBL 1, (c) SBL 2, (d) SBL 3, (e) SBL 4, and (f) SBL 5.

5.3.4. Water levels

A comparison between the model predictions for the different scenarios highlighted that the treatment of the momentum had little influence on water surface elevations outside of the lagoon, where both high and low tide water levels were practically unaffected throughout the domain. However, there was a noticeable difference in the water levels inside the lagoon as illustrated in Figure 63 and Tables 21 and 22. The figure shows the water level time series for a typical tidal cycle during a spring tide, with the same trend being observed for the complete 14-day neap-spring tidal cycle.

Table 21: Maximum water level values in meters recorded during a typical spring tide, illustrated in Figure 63.

	Scenario	Max out [m]	% of SBL1	Max in [m]	% of SBL1
2D, only mass transfer	SBL1	4.24	-	2.80	-
2D, w/ mom. transfer	SBL2	4.24	0.0%	2.83	1.1%
	SBL3	4.25	0.1%	3.24	16.0%
3D, w/ mom. transfer	SBL4	4.22	-0.6%	2.80	0.2%
	SBL5	4.22	-0.5%	3.09	10.6%

Table 22: Minimum water level values in meters recorded during a typical spring tide, illustrated in Figure 63.

	Scenario	Min out [m]	% of SBL1	Min in [m]	% of SBL1
2D, only mass transfer	SBL1	-4.05	-	-2.72	-
2D, w/ mom. transfer	SBL2	-4.05	0.0%	-2.74	0.8%
	SBL3	-4.05	-0.1%	-3.17	16.8%
3D, w/ mom. transfer	SBL4	-4.04	-0.1%	-2.73	0.4%
	SBL5	-4.05	0.2%	-3.03	11.6%

The most noticeable difference in the water elevations inside the lagoon occurred for the scenarios with the simplified velocity distribution (SBL3 and SBL5). Compared to SBL1 the maximum expected water level for the two scenarios had increased by 0.44 m and 0.29 m, respectively, and predictions of the lowest water levels had fallen by roughly the same amount. Both runs with the realistic velocity distribution (SBL2 and SBL4) did not result in any significant change of the water levels inside the lagoon. In both cases, the differences were limited to less than 1 per cent compared to the mass conservation only, namely SBL1 scenario.

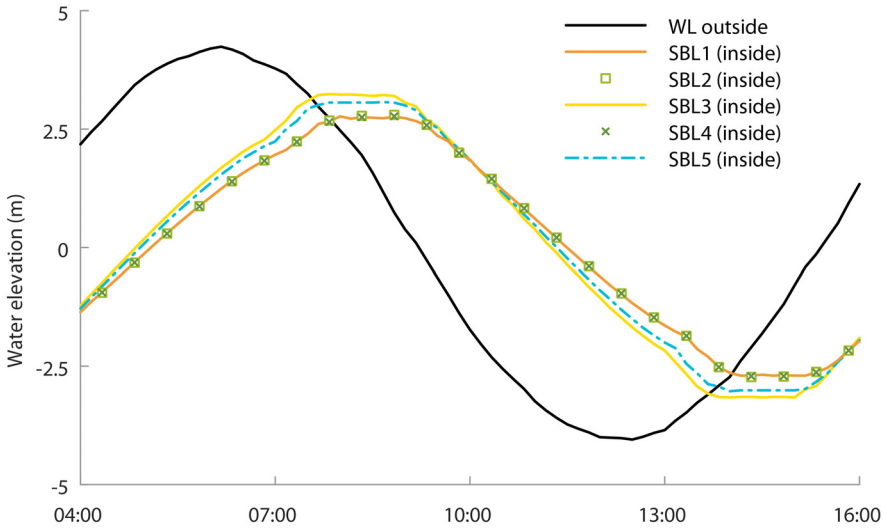

Figure 63: Comparison of water elevations inside the lagoon for the five different cases on 23.1.2012.

5.3.5. Power output

Predicted annual energy potential is a critical factor when considering the construction of a tidal power plant. The instantaneous power production was calculated at each timestep using the power-head relationship (Figure 21) and then integrated over the time interval of the simulation to obtain total electricity generated in that period. The simulation time was carefully selected to cover a typical neap-spring tidal cycle spanning over 14 days and taking into account the neap-spring variation in power production. The lagoon operation during this cycle for the baseline scenario (SBL 1) is illustrated in Figure 64. Neglecting any tidal variations that could develop over the rest of the year, this neap-spring tidal cycle was presumed to be sufficient for this assessment. The estimated annual (neap-spring averaged) energy was then calculated by extrapolating the simulation results over the period of one year (Xue et al. 2019). The total electricity generated for the baseline scenario (SBL1) was estimated to be about 578 GWh/year, which was consistent with predictions from past studies (Angeloudis et al. 2016b; Angeloudis et al. 2018; Angeloudis and Falconer 2017).

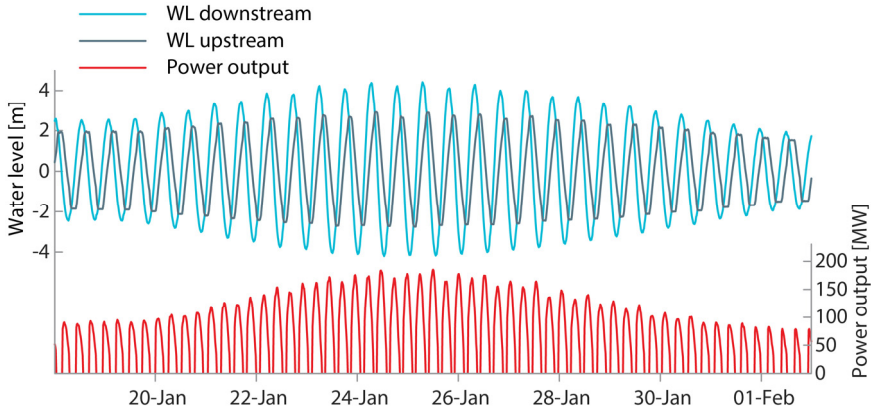

Figure 64: Predicted water levels on either side of the Severn Barrage and the corresponding power output over a typical neap-spring tidal cycle for the SBL 1 case.

Table 23: Typical annual energy prediction extrapolated from a characteristic neap-spring tidal cycle for the five different cases.

	Scenario	Annual Energy [GWh]	% of SBL1
2D, only mass transfer	SBL1	578.39	-
2D, w/ mom. transfer	SBL2	584.98	1.1 %
	SBL3	515.36	-10.9 %
3D, w/ mom. transfer	SBL4	578.63	0.0 %
	SBL5	532.85	-7.9 %

Unlike the local hydrodynamic conditions, the annual energy potential, which is mainly governed by the water level difference across the lagoon, was less sensitive to including momentum conservation in the numerical model. Predictions from all five simulations are summarised in Table 23. The values ranged from 515 GWh/year to 585 GWh/year.

In scenarios SBL2 and SBL4, where a more realistic distribution of the velocity was predicted, the impact on the estimated power output was practically negligible with 1.1 per cent and less than 0.05 per cent increase respectively. The predicted power output for scenarios SBL3 and SBL5, with the simplified implementation of the jet, has decreased by 10.9 per cent and 7.9 per cent respectively.

This is almost counter-intuitive since we would expect a higher energy output due to the higher water level amplitudes observed inside the lagoon (Figure 63). However, this resulted in the lagoon operating at higher heads and generating over shorter time intervals, which considerably decreased its efficiency (Figure 21). This re-

emphasises the importance of accurate modelling of the discharged jets. By just including the momentum conservation, without careful consideration for the appropriate distribution of the velocity profile, the model may produce inaccurate predictions for power output.

5.4. Summary

This case study demonstrated how the modified Delft3D model can be used for the assessment of impacts on the hydrodynamic conditions due to the operation of a tidal range energy power plant. The momentum conservation of the turbine discharge was achieved by adding an extra term to the momentum equations, representing an equivalent external force acting on the volume of the computational cell across the turbine infrastructure. The calculation of the force is highly sensitive to the assumption of the outlet velocity distribution and choosing the most realistic velocity profile is of utmost significance. As was demonstrated for scenarios SBL3 and SBL5, a simplified velocity distribution concentrated over a small flow-through will result in a highly sophisticated 3D velocity field locally. The results showed that it had a noticeable effect on the velocity magnitude of the jet and on the tidal amplitude inside the lagoon, which negatively affected the estimated power output. The realistic distribution, that can be attributed to the flow exiting a diffuser (SBL2 and SBL4), still showed an increase in velocity magnitude, but did not show any drastic changes to the water levels and power estimation.

Regardless of the assumption of the structure of the velocity distribution, it was observed that 2D models generally predict a larger water level amplitude inside the lagoon compared to 3D models. Similar observations were found in literature, where depth-averaging failed to capture the higher complexities of the flow exiting the turbines, thereby affecting water levels in the proximity of the hydraulic structures (Jeffcoate et al. 2013). The differences between the 2D and 3D model in the case of realistic distribution were much closer than those of the simplified velocity distribution. The diffusor-induced flow from the case with the realistic distribution better matched the 2D nature of the tidal hydrodynamics. With larger computational costs of the 3D model, this indicated that depth-average models can be sufficient for preforming hydrodynamic simulations, unless the study is concerned specifically about the vertical velocity profile of the jet.

The effects of the correct momentum transfer on the hydrodynamics were constrained to a relatively local area. As observed in Figure 59, there was very little

change in the hydrodynamics at a distance of about 20 times the turbine diameter downstream of the turbines. However, this could still have a significant impact on solute transport modelling and sediment fluxes, particularly in the vicinity of the turbines. Unbalanced erosion and deposition inside the lagoon, coupled with low velocities during the emptying stage, suggests that lagoon could be prone to silting. This would lead to a decrease in volume of the impoundment, which could significantly inhibit the performance of the power production, as well as incur additional operational costs for regular dredging of the basin. A downside of such regional-scale models is that they fail to include the rotational velocity of the flow exiting the turbines, which could have a further impact on sediment transport processes. To include such level of detail, it would be necessary to model the hydrodynamics at a much higher grid resolution, which is unnecessary for simulating the hydrodynamics characteristics at the regional scale.

The estimated power production indicated that just including the momentum conservation, without considering the appropriate assumptions, can have a negative effect on the accuracy of the power output predictions. While the momentum treatment is important from the erosion and sediment transport point of view, the results showed that power output was not as affected. Including the momentum, conservation contributed to only about 1 per cent change in the annual energy output for the cases with the realistic velocity distribution (SBL 2 and SBL 4). However, when assuming a simplified velocity distribution at the turbine exit (SBL 3 and SBL 5), the predicted energy output fell by as much as 10 per cent. The higher discharge rates in the case of simplified distribution meant that turbines operated under lower head difference towards the end of the generation cycle, which resulted in a reduced power output. This illustrated the sensitivity of power output to the assumption of the velocity distribution.

This study showed that modifications introduced to the Delft3D software transformed it into a model that is well capable of simulating the operation of any TRS in the estuarine environment. The model was used to assess the changes to the hydrodynamic conditions across the whole domain, including:

- changes in water levels
- impact on the velocity field,
- magnification of bed shear stress, and
- estimation of power production.

This was achieved through both 2D and 3D simulations. The 3D model showed to be particularly important for the predictions of the maximum water levels inside the

lagoon and estimation of bed shear stress, as 2D model failed to capture flow complexities of the discharged jets due to depth-averaging. Conservation of momentum was proved to be very important for correct predictions of hydrodynamics, however, it showed to be very sensitive to assumptions of the velocity distribution.

6
CONCLUSIONS

6.1. General conclusions

The research presented in this book has been directed towards improving hydrodynamic modelling tools for simulation of TRS, and thus improving the reliability of the model for assessing hydrodynamic impacts originating from the operation of TRS.

Hydrodynamic simulations can be used to analyse water level change, velocity patterns and sediment transport – results which are fundamental in assessing environmental impacts. They can also be employed to predict power output, which is essential for assessing the efficiency and profitability of a TRS. They can be used before, during and after the TRS design process and can be refined to focus on just specific aspects of TRS operation, making them a versatile tool which can be very useful for informing decision makers. Accurate and efficient hydrodynamic models are therefore paramount for increasing the chance for future deployment of the technology.

One of the research objectives was to assess the current methodologies for simulation of TRS in hydrodynamic models and implement the numerical techniques into the Delft3D software. The required numerical techniques were identified through an extensive review of the literature. The study clearly presented their theoretical background and demonstrated their implementation into the source code of Delft3D model. In order to reach this objective, the proposed STPG Severn Barrage scheme was used as a case study throughout the development process. The scheme has already been investigated in many studies in the past, employing several different hydrodynamic models and numerical techniques, thereby making it an

ideal case study for validation and benchmarking of the routines developed for the Delft3D model.

The TRS module contained four major additions to the source code:

- hydraulic structures modelled as coupled sink and source term in the continuity equation,
- an algorithm for determining the operational stages of the TRS operation,
- hill chart for modelling discharge through turbines, and
- orifice equation governing the discharge through sluices.

The impacts of the barrage operation were assessed by analysing the differences between simulation runs with and without the barrage in place.

It was shown that modelling the Severn Barrage requires the extension of the domain to the continental shelf to prevent the scheme to affect open boundary conditions. The estimated annual energy production of an ebb-only generation scheme was predicted to be in the same range as the most recent published predictions (Angeloudis et al. 2016b). There is, however, some measure of uncertainty when it comes to annual power estimations because results are highly sensitive to the turbine manufacturing characteristics. Even though the study herein employed an industry-provided hill chart for the type of turbines intended for deployment in the STPG proposal, it should be acknowledged that actual characteristics are not publicly available and the energy estimation should be considered only as an indicator of the scheme's power generation potential.

Also important is the appropriate selection of the representative tidal interval, which should cover the mean neap-spring tidal cycle for the estimation of the annual power production. The near-field impacts were assessed by analysing the changes in hydrodynamics on an estuary-scale. It was shown that ebb-only operation had both positive and negative impacts on the coastal flood risk. The maximum water levels upstream of the barrage (inside the impoundment) fell by more than 1 m, significantly reducing the risk of flooding due to storm surges for communities in the upper reaches of the estuary. On the other side of the barrage (seaward side) the effect was reversed, with higher maximum water levels which resulted in higher flood risk. With 0.3 m rise just downstream of the barrage and gradually dropping towards the open boundary, the change on the seaward side was not as significant as inside the impoundment, however, it affected a substantially larger region, with impacts observed as far away as Cardigan Bay and the Irish Sea. The operation of the barrage significantly changed the entire tidal amplitude inside the impoundment,

also affecting the minimum water elevations, resulting in permanently flooding of intertidal mudflats.

The results showed a significant reduction on maximum current velocities domain-wide and increase in maximum flow velocity at the exit from turbines and sluice gates, substantially altering the sediment transport processes in the estuary. Direct comparisons with the past studies showed that Delft3D performed well in simulating impacts on the tidal regime due to the TRS operation, indicating that that the modifications included in the TRS module are appropriate for modelling the hydrodynamics of tidal range projects in the Severn Estuary and Bristol Channel. The results also showed the importance of hydrodynamic modelling when designing TRSs, as they are fundamental for determining the environmental impacts of the scheme and its power production potential.

The second research objective was to develop an improved method for numerical modelling of the momentum transfer through a TRS that can be applied to the finite-difference numerical models, such as Delft3D. The literature review showed the disregard for momentum conservation as one of the more significant shortcomings of existing TRS models. At the time of this writing, the only published example that has addressed the issue was found to be a study by Angeloudis et al. (2016b), where a momentum conservation technique involved artificially changing the water depth of the internal boundary in a finite-volume model. Delft3D is a finite-difference model, where hydraulic structures are instead represented through a coupled sink and source terms in the continuity equation. Thus, to model the momentum conservation, a novel technique was proposed, that parametrised the induced momentum as an external force acting on the computational cell. This force was included in the computation through a new term added to the momentum equations. The appropriateness of the developed method was first tested on an experimental study involving a tidal barrage, followed by its application to a case study of Swansea Bay lagoon to investigate its impacts on a regional-scale hydrodynamic model.

The new routines were applied to a regional-scale TRS model in order to assess the impacts of the developed method on the performance of the hydraulic model. The proposed Swansea Bay lagoon scheme was used as a case study, which is deployed in an estuary-scale domain. While the model allowed for a full assessment of hydrodynamic impacts due to the TRS operation, the main focus was on the treatment of momentum and its effects on the results. The study combined the TRS module, developed through the first objective, with the momentum conservation

technique, developed and validated through the second and third research objectives. To assess the contribution of momentum treatment, five different simulation scenarios were considered, the first one being the baseline scenario – a 2D simulation without momentum conservation. This was followed by two 2D simulation runs with momentum conservation, one assuming a realistic and the other assuming a simplified distribution of vertical velocity profile. Finally, a pair of 3D runs with momentum conservation was performed with both types of vertical distributions.

Simulation results showed that the developed momentum conservation affected only a relatively local area around the lagoon, constrained to the zone dominated by the jets exiting the TRS. In general, including the momentum conservation has visibly enlarged the length and magnitude of the jets. However, no changes to the hydrodynamics were observed beyond the point where the jets have completely dissipated. The results showed to be sensitive to the assumption of vertical velocity distribution. The simplified velocity distribution had a bigger impact on the hydrodynamics and power output estimation than the realistic distribution, emphasising the importance of selecting an appropriate vertical velocity profile for the discharged jet. Comparing the 2D and 3D simulations for the same type of vertical velocity distribution, showed very little change to the hydrodynamic predictions and power output estimations. There was, however, a clear increase in local bed shear stress from 2D to 3D model results. The magnification of bed shear stress was again much more prominent with the simplified vertical velocity distribution and less so with the realistic distribution. In general, these results indicate that 2D hydraulic models with momentum conservation are sufficient for analysing hydrodynamic impacts of TRS on a regional scale. However, the 3D model has proved to be indispensable for accurate predictions of local-scale impacts, especially in an around the lagoon.

The main finding of this research can be summarised as follows:

- It was shown that ignoring momentum conservation leads to significantly underestimated predictions of bed shear stress in the region just downstream of the turbines. Results showed that correct momentum treatment is essential for accurate predictions of sediment transport processes in the vicinity of a TRS.
- The effects of the momentum conservation were limited to the area in the vicinity of the Swansea Bay lagoon and had no visible impact on the far-field conditions. While a simplified model might be sufficient for assessment of

the regional-scale impacts, the momentum conservation method proved to be essential for accurate assessment of local conditions, such as the increased velocity of the discharged jet, estimation of power production and magnified bed shear stress, associated with increased erosion and changes to the sediment transport patterns.

- Delft3D showed to be a reliable tool for simulation of the TRSs. Based on the benchmarking results, it performed on par with other established models, such as EFDC and DIVAST. This includes:
    - assessment of water level changes due to the TRS operation,
    - impact of the TRS operation on the velocity field,
    - magnification of local bed shear stress,
    - estimation of instantaneous and annual power output,
    - modelling the impacts on the open boundary by the use of the extended domain (to the continental shelf), and
    - expanding the depth-averaged model to 3D.

  The model was further improved with the addition of the technique for momentum conservation of flow through the hydraulic structures. This qualified the model to be used as a multi-scale tool, that can simultaneously produce satisfactory results on the global, regional, and local scales.

6.2. Recommendations for further study

Even though this study addressed several topics on tidal range modelling, some areas of interest were left unexplored due to lack of data availability and time constraints. Therefore, a number of considerations are recommended for further research.

To date, most TRS studies have focused on a single tidal range scheme, with some limited studies involving the operation of two or three schemes simultaneously. However, there have been various proposals for a number of different tidal range schemes across the region, including a fleet of 6 tidal lagoons, proposed by Tidal Lagoon Power (2016). To assess such networks of TRS schemes, a multi-scale modelling approach is needed, that includes:

- assessment of potential far-field impacts due to the cumulative effect,
- investigation of potential interactions between the individual schemes and
- analysis of impact of those interactions on the combined capacity for power production.

The TRS schemes could be further improved by optimising the operation parameters to maximise the power production and to minimize the environmental impacts. These two factors are usually mutually exclusive, which means that the problem could be further expanded to a multi-objective optimisation study, looking for the best trade-off between the two. In the first instance, the optimisation can be performed in combination with simplified formulations, such as 0D models, and using state of the art techniques, such as genetic algorithms. Once the best trade-off is determined, the resulting parameters could be fed back to the Delft3D model to perform a full analysis of power production and impacts on the environment of the selected parameters.

The results of this study demonstrated the importance of the momentum conservation of the flow through hydraulic structures on predictions of local bed shear stress. The results indicated that the lagoon could be prone to silting due to the large recirculation effects that occur during the filling of the impoundment and low velocities during releasing. Further study on sediment and solutes transport, including the momentum conservation technique, is required to get a better impact of such schemes and importance of the modifications carried out in this study.

This study has shown that momentum treatment is sensitive to the assumption of the vertical velocity distribution in the jets exiting the TRS. Actual velocity profiles are usually hard to obtain because they rely on detail turbine characteristics, which manufacturing companies are often reluctant to share. Obtaining such velocity profiles requires either measuring flow from a laboratory-scale model of a turbine or use of sophisticated CFD models for turbomachinery design. Either way, obtaining such data would considerably reduce the uncertainty associated with the assumption of how the discharge is represented in the simulation.

Vertical velocity profile will also change through the different periods of the operation cycle. The turbines, together with the diffusor, will perform with variable efficiency during different periods of the generation stage. With ever-changing head difference and depth of tailwater, the vertical velocity profile can change significantly over time. Because of the unavailability of data, the current model assumes a constant velocity distribution throughout the simulation. Acquiring those changes through physical experiments or CFD simulations of the turbines and implementing a routine that could vary the velocity distribution over time could even further increase the accuracy of the model, particularly with the 3D simulations.

Finally, the computational efficiency of the model could be significantly enhanced by high-performance computing (HPC). Even though Delft3D already has

capabilities for parallel computations, the technique is not fully operational when TRS module is included in the simulation. Full parallelization of the TRS module would significantly reduce the required computation time, while also enabling the use of more complex model setups, with even larger domains, high-resolution grids and 3D models with a greater number of vertical layers.

7
BIBLIOGRAPHY AND FURTHER READING

Adcock, T. A. A., A. G. L. Borthwick and G. T. Houlsby. 2011. The Open Boundary Problem in Tidal Basin Modelling with Energy Extraction. Proceedings of the 9th European Wave and Tidal Energy Conference. Southampton, UK: 1–7.

Adcock, T. A. A., S. Draper and T. Nishino. 2015. Tidal power generation – A review of hydrodynamic modelling. *Proceedings of the Institution of Mechanical Engineers, Part A: Journal of Power and Energy* 229 (7): 755–771. http://journals.sagepub.com/doi/10.1177/0957650915570349.

Aggidis, G. A. and D. S. Benzon. 2013. Operational optimisation of a tidal barrage across the Mersey estuary using 0-D modelling. *Ocean Engineering* 66: 69–81. http://dx.doi.org/10.1016/j.oceaneng.2013.03.019.

Aggidis, G. A. and O. Feather. 2012. Tidal range turbines and generation on the Solway Firth. *Renewable Energy* 43: 9–17.

Ahmadian, R., R. A. Falconer and B. Bockelmann-Evans. 2014a. Comparison of hydro-environmental impacts for ebb-only and two-way generation for a Severn Barrage. *Computers & Geosciences* 71: 11–19. http://dx.doi.org/10.1016/j.cageo.2014.05.006.

Ahmadian, R., R. A. Falconer and B. N. Bockelmann-Evans. 2012. Far-field modelling of the hydro-environmental impact of tidal stream turbines. *Renewable Energy* 38 (1): 107–116. http://dx.doi.org/10.1016/j.renene.2011.07.005.

Ahmadian, R., R. A. Falconer and B. Lin. 2010a. Hydro-environmental modeling of proposed Severn barrage, UK. *Proceedings of the Institution of Civil Engineers - Energy* 163 (3): 107–117. http://www.icevirtuallibrary.com/doi/10.1680/ener.2010.163.3.107.

Ahmadian, R., C. Morris and R. A. Falconer. 2010b. Hydro-environmental modelling of off-shore and coastally attached impoundments of The North Wales coast. In *Proceedings of the 1st European IAHR Congress*. Edinburgh. http://orca.cf.ac.uk/id/eprint/7601.

Ahmadian, R., A. I. Olbert, m. Hartnett and R. A. Falconer. 2014b. Sea level rise in the Severn Estuary and Bristol Channel and impacts of a Severn Barrage. *Computers & Geosciences* 66: 94–105. http://dx.doi.org/10.1016/j.cageo.2013.12.011.

Alcrudo, F. 2004. A state of the art review on mathematical modelling of flood propagation. *IMPACT project*: 1–22.

Andre, H. 1976. Operating experience with bulb units at the Rance tidal power plant and other French hydro-power sites. *IEEE Transactions on Power Apparatus and Systems* 95 (4): 1038–1044.

———. 1978. Ten Years of Experience at the "La Rance" Tidal Power Plant. *Ocean Management* 4: 165–178.

Andritz Hydro. 2016. Technology Fit for the Future. *Hydro News* (29): 18–21.

Angeloudis, A., R. Ahmadian, R. A. Falconer and B. N. Bockelmann-Evans. 2016a. Numerical model simulations for optimisation of tidal lagoon schemes. *Applied Energy* 165: 522–536.

Angeloudis, A. and R. A. Falconer. 2017. Sensitivity of tidal lagoon and barrage hydrodynamic impacts and energy outputs to operational characteristics. *Renewable Energy* 114: 337–351. http://www.sciencedirect.com/science/article/pii/S0960148116307340.

Angeloudis, A., R. A. Falconer, S. Bray and R. Ahmadian. 2016b. Representation and operation of tidal energy impoundments in a coastal hydrodynamic model. *Renewable Energy* 99: 1103–1115. http://www.sciencedirect.com/science/article/pii/S0960148116307042.

Angeloudis, A., S. C. Kramer, A. Avdis and m. D. Piggott. 2018. Optimising tidal range power plant operation. *Applied Energy* 212 (November 2017): 680–690. https://doi.org/10.1016/j.apenergy.2017.12.052.

Atkins and Rolls-Royce. 2010. Severn Embryonic Technologies Scheme - Concept design of a very-low head dual generation tidal scheme for the severn estuary. Vol. 1.

Atlantis Resources Limited. 2018. MeyGen, Tidal Projects, Atlantis Resources. https://www.atlantisresourcesltd.com/projects/meygen/ 2018.

Bae, Y. H., K. O. Kim and B. H. Choi. 2010. Lake Sihwa tidal power plant project. *Ocean Engineering* 37 (5–6): 454–463. http://dx.doi.org/10.1016/j.oceaneng.2010.01.015.

Baker, A. C. 1991. *Tidal power*. IEE energy series 5. London: Peter Peregrinus Ltd. on behalf of the Institution of Electrical Engineers.

BEIS. 2016. Hinkley Point C. *Department for Business, Energy & Industrial Strategy*. https://www.gov.uk/government/collections/hinkley-point-c 2016.

———. 2018. DUKES 2018 Chapter 6: Renewable sources of energy. In *Digest of UK Energy Statistics (DUKES)*, 155–187. Department for Business, Energy & Industrial Strategy.

Bernshtein, L. B. 1972. Kislaya Guba Experimental Tidal Power Plant and Problem of the Use of Tidal Energy. In *Tidal Power*, 215–238. Boston, MA: Springer US. http://link.springer.com/10.1007/978-1-4613-4592-3_6.

Boccard, N. 2009. Capacity factor of wind power realized values vs. estimates. *Energy Policy*.

BODC. 2017. Download UK Tide Gauge Network data from BODC. https://www.bodc.ac.uk/data/hosted_data_systems/sea_level/uk_tide_gauge_network/ 2017.

Bourban, S. E., S. J. Couch, A. Baldock and S. Cheeseman. 2014. Coastal shelf model of northern European waters to inform tidal power industry decisions: SMARTtide. *Underwater Technology* 32 (1): 15–26.

Brammer, J., R. A. Falconer, C. Ellis and R. Ahmadian. 2014. Physical and numerical modelling of the Severn Barrage. *Science China Technological Sciences* 57 (8): 1471–1481.

Bray, S., R. Ahmadian and R. A. Falconer. 2016. Impact of representation of hydraulic structures in modelling a Severn barrage. *Computers & Geosciences* 89: 96–106. http://linkinghub.elsevier.com/retrieve/pii/S0098300416300206.

Carne, B. G. 1995. Thomas Fulljames, 1808-74: Surveyor, Architect, and Civil Engineer. *Transactions of the Bristol and Gloucestershire Archaeological Society* 113: 7–20.

Casulli, V. and G. S. Stelling. 1998. Numerical Simulation of 3D Quasi-Hydrostatic, Free-Surface Flows. *Journal of Hydraulic Engineering* 124 (7): 678–686. https://ascelibrary.org/doi/abs/10.1061/%28ASCE%290733-9429%281998%29124%3A7%28678%29.

Cebr. 2014. The Economic Case for a Tidal Lagoon Industry in the UK. *Report for Tidal Lagoon Power Ltd*. Vol. 2. London.

Chaineux, m. C. and R. H. Charlier. 2008. Women's tidal power plant Forty candles for Kislaya Guba TPP. *Renewable and Sustainable Energy Reviews* 12 (9): 2508–2517.

Charlier, R. H. 2007. Forty candles for the Rance River TPP tides provide renewable and

sustainable power generation. *Renewable and Sustainable Energy Reviews* 11 (9): 2032–2057.

Charlier, R. H. and L. Menanteau. 1997. The saga of tide mills. *Renewable and Sustainable Energy Reviews* 1 (3): 171–207.

Cho, Y. S., J. W. Lee and W. Jeong. 2012. The construction of a tidal power plant at Sihwa Lake, Korea. *Energy Sources, Part A: Recovery, Utilization and Environmental Effects* 34 (14): 1280–1287.

Clarke, J. A., G. Connor, A. D. Grant and C. m. Johnstone. 2006. Regulating the output characteristics of tidal current power stations to facilitate better base load matching over the lunar cycle. *Renewable Energy* 31 (2): 173–180. https://linkinghub.elsevier.com/retrieve/pii/S0960148105002247.

Cornett, A., J. Cousineau and I. Nistor. 2013. Assessment of hydrodynamic impacts from tidal power lagoons in the Bay of Fundy. *International Journal of Marine Energy* 1: 33–54. http://dx.doi.org/10.1016/j.ijome.2013.05.006.

Crown Estates. 2016. Severn Estuary Long Term Morphology. The Crown Estate.

Dadswell, m. J. and R. A. Rulifson. 1994. Macrotidal estuaries: a region of collision between migratory marine animals and tidal power development. *Biological Journal of the Linnean Society* 51 (1–2): 93–113. https://academic.oup.com/biolinnean/article-lookup/doi/10.1111/j.1095-8312.1994.tb00947.x.

DECC. 2008. Analysis of Options for Tidal Power Development in the Severn Estuary. *Interim Options Analysis Report*. Vol. 1–2.

———. 2010. Severn Tidal Power - Feasibility Study: Conclusions and Summary Report. *Feasibility Study Conclusions and Summary Report*. https://www.gov.uk/government/publications/1-severn-tidal-power-feasibility-study-conclusions-and-summary-report 2010.

Deltares. 2014. Delft3D-FLOW User Manual Hydro-Morphodynamics, Version 3.15. Delft Hydraulics, Delft, The Netherlands. https://oss.deltares.nl/documents/183920/185723/Delft3D-FLOW_User_Manual.pdf 2014.

Dincer, I. 2000. Renewable energy and sustainable development: a crucial review. *Renewable and Sustainable Energy Reviews* 4 (2): 157–175. http://linkinghub.elsevier.com/retrieve/pii/S1364032199000118.

DTI. 2003. Our energy future - creating a low carbon economy. *Command Paper*.

Du, m., H. Wu, H. Yu, T. Lv, J. Li and Y. Yu. 2017. Assessment of tidal range energy resources based on flux conservation in Jiantiao Bay, China. *Journal of Ocean University of China* 16 (6): 1090–1096. http://link.springer.com/10.1007/s11802-017-3247-2.

Dyer, K. R. 1984. Sedimentation processes in the Bristol Channel/Severn Estuary. *Marine Pollution Bulletin* 15 (2): 53–57. https://linkinghub.elsevier.com/retrieve/pii/0025326X84904624.

Ellabban, O., H. Abu-Rub and F. Blaabjerg. 2014. Renewable energy resources: Current status, future prospects and their enabling technology. *Renewable and Sustainable Energy Reviews* 39: 748–764. http://dx.doi.org/10.1016/j.rser.2014.07.113.

EMU Limited. 2012. Report for Centre for Research into Environment and Health (CREH) – Aberystwyth University, Swansea Bay Current Monitoring – Operational Report. Southampton.

Falconer, R. A., J. Xia, B. Lin and R. Ahmadian. 2009. The Severn Barrage and other tidal energy options: Hydrodynamic and power output modeling. *Science in China, Series E: Technological Sciences* 52 (11): 3413–3424.

Fulton, S. R. 2004. Semi-Implicit Time Differencing. Potsdam, New York, USA.

Gao, C. and T. A. A. Adcock. 2015. Numerical Investigation of Resonance in the Bristol Channel.

Guardian Media Group. 2018. Government rejects plan for £1.3bn tidal lagoon in Swansea. *The Guardian*. https://www.theguardian.com/business/2018/jun/25/government-rejects-plan-for-tidal-lagoon-in-swansea 2018.

Gubin, m. F. 1973. *Draft tubes of hydro-electric stations*. Published for the Bureau of Reclamation, U.S. Dept. of the Interior and

National Science Foundation, Washington, D.C. by Amerind Pub. Co. https://books.google.co.uk/books?id=ex3dAAAAIAAJ.

Hammons, T. J. 1993. Tidal power. *Proceedings of the IEEE* 81 (3): 419–433. http://ieeexplore.ieee.org/document/241486/.

Hamrick, J. m. 1992. A Three-Dimensional Environmental Fluid Dynamics Computer Code: Theoretical and Computational Aspects. *The College of William and Mary, Virginia Institute of Marine Science. Special Report 317, 63 pp.* (317).

Hendry, C. 2016. The role of tidal lagoons. https://hendryreview.files.wordpress.com/2016/08/hendry-review-final-report-english-version.pdf 2016.

Hinson, S. 2018. Tidal lagoons. *BRIEFING PAPER* (7940): 25. researchbriefings.files.parliament.uk/documents/CBP-7940/CBP-7940.pdf.

Hooper, T. and m. Austen. 2013. Tidal barrages in the UK: Ecological and social impacts, potential mitigation, and tools to support barrage planning. *Renewable and Sustainable Energy Reviews* 23: 289–298. http://dx.doi.org/10.1016/j.rser.2013.03.001.

Hulsbergen, K., R. Steijn, G. van Banning, G. Klopman and A. Fröhlich. 2008. Dynamic Tidal Power (DTP) – A new approach to exploit tides. *Proceedings of the 2nd International Conference on Ocean Energy* (October): 1–10.

Hunter, N. m., P. D. Bates, m. S. Horritt and m. D. Wilson. 2007. Simple spatially-distributed models for predicting flood inundation : A review. *Geomorphology* 90: 208–225.

IRENA. 2018a. Ocean energy. *International Renewable Agency website*. https://www.irena.org/ocean 2018.

———. 2018b. Hydropower. *International Renewable Energy Agency*. https://www.irena.org/hydropower 2018.

Jeffcoate, P., P. K. Stansby and D. Apsley. 2013. Flow Due to Multiple Jets Downstream of a Barrage: Experiments, 3D Computational Fluid Dynamics, and Depth-Averaged Modeling. *Journal of Hydraulic Engineering* 139 (7): 754–762. http://ascelibrary.org/doi/10.1061/%28ASCE%29HY.1943-7900.0000729.

———. 2017. Flow and bed-shear magnification downstream of a barrage with swirl generated in ducts by stators and rotors. *Journal of Hydraulic Engineering* 143 (2): 1–8.

Kadiri, m., R. Ahmadian, B. N. Bockelmann-Evans, W. Rauen and R. A. Falconer. 2012. A review of the potential water quality impacts of tidal renewable energy systems. *Renewable and Sustainable Energy Reviews* 16 (1): 329–341. http://dx.doi.org/10.1016/j.rser.2011.07.160.

Kelly, K. A., m. C. McManus and G. P. Hammond. 2012. An energy and carbon life cycle assessment of tidal power case study: The proposed Cardiff-Weston severn barrage scheme. *Energy* 44 (1): 692–701. http://dx.doi.org/10.1016/j.energy.2012.05.023.

Kirby, R. and C. Retière. 2009. Comparing environmental effects of Rance and Severn barrages. *Proceedings of the Institution of Civil Engineers - Maritime Engineering* 162 (MA1): 11–26. http://www.icevirtuallibrary.com/doi/10.1680/maen.2009.162.4.155.

Launder, B. E. and D. B. Spalding. 1974. The numerical computation of turbulent flows. *Computer Methods in Applied Mechanics and Engineering* 3 (2): 269–289.

Lee, D. S., S. H. Oh, J. H. Yi, W. S. Park, H. S. Cho, D. G. Kim, H. m. Eom and S. J. Ahn. 2010. Experimental investigation on the relationship between sluice caisson shape of tidal power plant and the water discharge capability. *Renewable Energy* 35 (10): 2243–2256. http://dx.doi.org/10.1016/j.renene.2010.02.018.

Lee, H. S. 2011. Ocean renewable energy: Tidal power in the Yellow Sea. *Journal of International Development and Cooperation* 17 (3): 29–44.

Lesser, G. R., J. A. Roelvink, J. A. T. m. van Kester and G. S. Stelling. 2004. Development and validation of a three-dimensional morphological model. *Coastal Engineering* 51 (8–9): 883–915.

Li, Y. and D.-Z. Pan. 2017. The ebb and flow of tidal barrage development in Zhejiang Province, China. *Renewable and Sustainable Energy*

Reviews 80: 380–389. http://www.sciencedirect.com/science/article/pii/S1364032117307578.

Liang, D., J. Xia, R. A. Falconer and J. Zhang. 2014. Study on Tidal Resonance in Severn Estuary and Bristol Channel. *Coastal Engineering Journal* 56 (1): 1450002-1-1450002–18. http://www.worldscientific.com/doi/abs/10.1142/S0578563414500028.

Lin, J., S. Jian, L. Liu, Y. Chen and B. Lin. 2015. Refined representation of turbines using a 3D SWE model for predicting distributions of velocity deficit and tidal energy density. *International journal of energy research* 39 (13): 1828–1842.

Marshall, J., C. Hill, L. Perelman and A. Adcroft. 1997. Hydrostatic, quasi-hydrostatic, and nonhydrostatic ocean modeling. *Journal of Geophysical Research: Oceans* 102 (C3): 5733–5752. https://agupubs.onlinelibrary.wiley.com/doi/abs/10.1029/96JC02776.

Nash, J. E. and J. V. Sutcliffe. 1970. River Flow Forecasting Through Conceptual Models Part I-a Discussion of Principles. *Journal of Hydrology* 10: 282–290.

Neelz, S. and G. Pender. 2009. Desktop review of 2D hydraulic modelling packages. Bristol.

Neill, S. P., A. Angeloudis, P. E. Robins, I. Walkington, S. L. Ward, I. Masters, m. J. Lewis, m. Piano, A. Avdis, m. D. Piggott, G. A. Aggidis, P. Evans, T. A. A. Adcock, A. Židonis, R. Ahmadian and R. A. Falconer. 2018. Tidal range energy resource and optimization – Past perspectives and future challenges. *Renewable Energy* 127: 763–778. https://doi.org/10.1016/j.renene.2018.05.007.

Neill, S. P. and m. R. Hashemi. 2018. Tidal Energy. In *Fundamentals of Ocean Renewable Energy*, 47–81. Elsevier. https://linkinghub.elsevier.com/retrieve/pii/B9780128104484000033.

Neill, S. P., P. E. Robins and I. Fairley. 2017. The Impact of Marine Renewable Energy Extraction on Sediment Dynamics. In *Marine Renewable Energy*, edited by Z. Yang and A. Copping, 279–304. Springer International Publishing. https://doi.org/10.1007/978-3-319-53536-4_12.

Nova Innovation. 2019. Bluemull Sound, Shetland. *Nova Innovation Website*. https://www.novainnovation.com/bluemull-sound 2019.

Oh, S. H., K. S. Lee and W. m. Jeong. 2016. Three-dimensional experiment and numerical simulation of the discharge performance of sluice passageway for tidal power plant. *Renewable Energy* 92: 462–473. http://dx.doi.org/10.1016/j.renene.2016.02.023.

Parker, B. B. 2007. *Tidal analysis and prediction*. *Sea-Level Science*. Silver Spring, Maryland: NOAA, NOS Center for Operational Oceanographic Products and Services. https://tidesandcurrents.noaa.gov/publications/Tidal_Analysis_and_Predictions.pdf.

Petley, S. and G. A. Aggidis. 2016. Swansea Bay tidal lagoon annual energy estimation. *Ocean Engineering* 111: 348–357. http://dx.doi.org/10.1016/j.oceaneng.2015.11.022.

Prandle, D. 1984. Simple theory for designing tidal power schemes. *Advances in Water Resources* 7 (1): 21–27.

Rahman, A. and V. Venugopal. 2015. Inter-Comparison of 3D Tidal Flow Models Applied To Orkney Islands and Pentland Firth. *11th European Wave and Tidal Energy Conference (EWTEC 2015)* (September): 1–10.

Rajar, R. 1997. *Hidromehanika*. Hydromecha. Ljubljana: University of Ljubljana, Faculty of Civil and Geodetic Engineering.

Reddy, J. N. 1993. An introduction to the finite element method. McGraw-Hill New York.

REN21. 2018. Renewables 2018 Global Status Report. Paris.

Retiere, C. 1994. Tidal power and the aquatic environment of La Rance. *Biological Journal of the Linnean Society* 51 (1–2): 25–36. http://linkinghub.elsevier.com/retrieve/doi/10.1006/bijl.1994.1004.

Rijkswaterstaat. 2016. WAQUA/TRIWAQ - two- and three-dimensional shallow water flow model. Technical documentation. http://simona.deltares.nl/release/doc/techdoc/waquapublic/sim1999-01.pdf.

Roberts, A., B. Thomas, P. Sewell, Z. Khan, S. Balmain and J. Gillman. 2016. Current tidal

power technologies and their suitability for applications in coastal and marine areas. *Journal of Ocean Engineering and Marine Energy* 2 (2): 227–245.

Rosatti, G., L. Bonaventura, A. Deponti and G. Garegnani. 2011. An accurate and efficient semi-implicit method for section-averaged free-surface flow modelling. *International Journal for Numerical Methods in Fluids* 65 (4): 448–473. http://doi.wiley.com/10.1002/fld.2191.

Rourke, F. O., F. Boyle and A. Reynolds. 2010. Tidal energy update 2009. *Applied Energy* 87 (2): 398–409. http://dx.doi.org/10.1016/j.apenergy.2009.08.014.

Seazone. 2013. 1 Arcsecond Gridded Bathymetry [ASC geospatial data]. *EDINA Marine Digimap Service*. http://digimap.edina.ac.uk 2013.

Shi, B., Y. P. Wang, Y. Yang, m. Li, P. Li, W. Ni and J. Gao. 2015. Determination of Critical Shear Stresses for Erosion and Deposition Based on In Situ Measurements of Currents and Waves over an Intertidal Mudflat. *Journal of Coastal Research* 316 (November): 1344–1356. http://www.bioone.org/doi/10.2112/JCOASTRES-D-14-00239.1.

Soulsby, R. L. 1995. Bed shear-stresses due to combined waves and currents. In *Advances in Coastal Morphodynamics*, edited by C. T. and m.J.F. Stive, H.J. de Vriend, J. Fredsøe, L. Hamm, R.L. Soulsby and J. C. Winterwerp, 4–20 to 4–23. Delft Hydraulics, The Netherlands.

Stansby, P. K., N. Chini and P. Lloyd. 2016. Oscillatory flows around a headland by 3D modelling with hydrostatic pressure and implicit bed shear stress comparing with experiment and depth-averaged modelling. *Coastal Engineering* 116: 1–14. http://dx.doi.org/10.1016/j.coastaleng.2016.05.008.

Stelling, G. S. and J. A. T. m. Van Kester. 1994. On the approximation of horizontal gradients in sigma co-ordinates for bathymetry with steep bottom slopes. *International Journal for Numerical Methods in Fluids* 18 (10): 915–935. https://onlinelibrary.wiley.com/doi/abs/10.1002/fld.1650181003.

STPG. 1989. The Severn Barrage Project : general report. *Energy Paper Number 57*.

The National Oceanography Centre. 2018. Continental Shelf Model (CS3 and CS3-3D). *National Oceanography Centre website*. https://www.noc.ac.uk/ 2018.

The Planning Inspectorate. 2015. Tidal Lagoon Swansea Bay. *National Infrastructure Planning*. https://infrastructure.planninginspectorate.gov.uk/projects/wales/tidal-lagoon-swansea-bay/ 2015.

Tidal Lagoon Plc. 2016. Key Statistics - Tidal Lagoon. *Tidal Lagoon Power website*. http://www.tidallagoonpower.com/projects/swansea-bay/key-statistics/ 2016.

———. 2017. Environmental Statement Chapter 4. Project Description. *Application for Developmnet Consent*. http://www.tidallagoonpower.com/wp-content/uploads/2017/05/DCO-Application-ES-4.0-project-description.pdf 2017.

———. 2018. Swansea Bay - Tidal Lagoon. *Tidal Lagoon Power website*. http://www.tidallagoonpower.com/projects/swansea-bay/ 2018.

Tidal Lagoon Power. 2016. Ours to Own - Building a new British industry from our natural advantage. *TLP Publication* (October). http://www.calvertfoundation.org/initiatives/oto.

Uncles, R. J. 1984. Hydrodynamics of the Bristol Channel. *Marine Pollution Bulletin* 15 (2): 47–53.

———. 2010. Physical properties and processes in the Bristol Channel and Severn Estuary. *Marine Pollution Bulletin* 61 (1–3): 5–20. http://dx.doi.org/10.1016/j.marpolbul.2009.12.010.

United Nations. 2016a. Paris Agreement Signature Ceremony. *UNFCC* (April): 1–6. http://newsroom.unfccc.int/media/632121/list-of-representatives-to-high-level-signature-ceremony.pdf.

———. 2016b. Paris Agreement - Status of Treaties XXVII.7.d. *United Nations Treaty Collection* 21 (December 2015): 1–7. https://treaties.un.org/pages/ViewDetails.aspx?src=TREATY&mtdsg_no=XXVII-7-d&chapter=27&clang=_en.

Uqaili, m. A. and K. Harijan. 2012. Energy, environment and sustainable development.

Energy, Environment and Sustainable Development 12: 1–349.

van Rijn, L. C. 1993. Principles of sediment transport in rivers, estuaries and coastal seas. Aqua Publications: Amsterdam.

Wang, S., P. Yuan, D. Li and Y. Jiao. 2011. An overview of ocean renewable energy in China. *Renewable and Sustainable Energy Reviews* 15 (1): 91–111. http://dx.doi.org/10.1016/j.rser.2010.09.040.

Wang, X. H. and F. P. Aandutta. 2013. Sediment Transport Dynamics in Ports, Estuaries and Other Coastal Environments. In *Sediment Transport Processes and Their Modelling Applications*, 13. InTech. https://www.intechopen.com/books/advanced-biometric-technologies/liveness-detection-in-biometrics.

Warren, I. R. and H. K. Bach. 1992. MIKE 21: a modelling system for estuaries, coastal waters and seas. *Environmental Software* 7 (4): 229–240. https://linkinghub.elsevier.com/retrieve/pii/026698389290006P.

Warwick, R. and R. Uncles. 1980. Distribution of Benthic Macrofauna Associations in the Bristol Channel in Relation to Tidal Stress. *Marine Ecology Progress Series* 3: 97–103.

Waters, S. and G. A. Aggidis. 2016a. A world first: Swansea Bay tidal lagoon in review. *Renewable and Sustainable Energy Reviews*. http://www.sciencedirect.com/science/article/pii/S1364032115013945.

———. 2016b. Tidal range technologies and state of the art in review. *Renewable and Sustainable Energy Reviews* 59: 514–529. http://dx.doi.org/10.1016/j.rser.2015.12.347.

Wilhelm, S., G. Balarac, O. Métais and C. Ségoufin. 2016a. Head losses prediction and analysis in a bulb turbine draft tube under different operating conditions using unsteady simulations. *28th AHR Symposium on Hydraulic Machinery and Systems, Grenoble, July 4-8*: 839–848.

———. 2016b. Analysis of Head Losses in a Turbine Draft Tube by Means of 3D Unsteady Simulations. *Flow, Turbulence and Combustion* 97 (4): 1255–1280.

Wolanski, E. and m. Elliott. 2016. Estuarine water circulation. In *Estuarine Ecohydrology*.

Wolf, J., I. A. Walkington, J. Holt and R. Burrows. 2009. Environmental impacts of tidal power schemes. *Proceedings of the Institution of Civil Engineers - Maritime Engineering* 162 (4): 165–177. http://www.icevirtuallibrary.com/doi/10.1680/maen.2009.162.4.165.

Xia, J., R. A. Falconer and B. Lin. 2008. Impact of the barrage construction on the hydrodynamic process in the Severn Estuary using a 2D finite volume model. *Flood Risk Management: Research and Practice* Extended A: 8.

———. 2010a. Impact of different operating modes for a Severn Barrage on the tidal power and flood inundation in the Severn Estuary, UK. *Applied Energy* 87 (7): 2374–2391. http://dx.doi.org/10.1016/j.apenergy.2009.11.024.

———. 2010b. Impact of different tidal renewable energy projects on the hydrodynamic processes in the Severn Estuary, UK. *Ocean Modelling* 32 (1–2): 86–104. http://dx.doi.org/10.1016/j.ocemod.2009.11.002.

———. 2010c. Hydrodynamic impact of a tidal barrage in the Severn Estuary, UK. *Renewable Energy* 35 (7): 1455–1468. http://dx.doi.org/10.1016/j.renene.2009.12.009.

Xia, J., R. A. Falconer, B. Lin and G. Tan. 2011. Estimation of future coastal flood risk in the Severn Estuary due to a barrage. *Journal of Flood Risk Management* 4 (3): 247–259. http://doi.wiley.com/10.1111/j.1753-318X.2011.01106.x.

———. 2012. Estimation of annual energy output from a tidal barrage using two different methods. *Applied Energy* 93: 327–336. http://dx.doi.org/10.1016/j.apenergy.2011.12.049.

Xue, J., R. Ahmadian and R. Falconer. 2019. Optimising the Operation of Tidal Range Schemes. *Energies* 12 (15): 2870. https://www.mdpi.com/1996-1073/12/15/2870.

Zhou, J., R. A. Falconer and B. Lin. 2014a. Refinements to the EFDC model for predicting the hydro-environmental impacts of a barrage

across the Severn Estuary. *Renewable Energy* 62: 490–505. http://dx.doi.org/10.1016/j.renene.2013.08.012.

Zhou, J., S. Pan and R. A. Falconer. 2014b. Optimization modelling of the impacts of a Severn Barrage for a two-way generation scheme using a Continental Shelf model. *Renewable Energy* 72: 415–427. http://dx.doi.org/10.1016/j.renene.2014.07.036.

———. 2014c. Effects of open boundary location on the far-field hydrodynamics of a Severn Barrage. *Ocean Modelling* 73: 19–29. http://www.sciencedirect.com/science/article/pii/S146350031300187X.

Zienkiewicz, O. C. and R. L. Taylor. 2000. *The finite element method*. 5th ed. Oxford Butterworth-Heinemann. http://openlibrary.org/books/OL6900453M.

8
LIST OF FIGURES AND TABLES

List of figures

List of tables

Prostor
kraj
čas
20

The series *Prostor, kraj, čas* (Space, Place, Time) publishes shorter, thematically rounded studies on various aspects of the study of space and time based on geographical information systems and remote sensing, as well as their social and cultural constructs: how people of different eras and landscapes think, live, feel, use and change space and time.

Nejc Čož was born in Ljubljana in 1989. During his studies he was fascinated by the impact of technology on the environment, which led him on the path of environmental engineering. After graduating in Civil Engineering from the University of Ljubljana in 2013, he went to the UK to do his PhD and study the environmental impact of renewable energy projects. In 2019, he completed his PhD on the hydrodynamic impacts of tidal power plants. His enthusiasm for environmental research has also extended to the field of remote sensing, where he now works at the Institute for Anthropological and Spatial Studies of the Research Centre of the Slovenian Academy of Sciences and Arts.

Založba ZRC

http:\\zalozba.zrc-sazu.si

ISBN 978-961-05-0710-9

9 789610 507109

https://doi.org/10.3986/9789610507109